KfK 3738
November 1984

Liquid Metal Tribology in Fast Breeder Reactors

E. Wild, K. J. Mack, M. Gegenheimer
Institut für Reaktorbauelemente
Projekt Schneller Brüter

Kernforschungszentrum Karlsruhe

KERNFORSCHUNGSZENTRUM KARLSRUHE
INSTITUT FÜR REAKTORBAUELEMENTE
PROJEKT SCHNELLER BRÜTER

KfK 3738

LIQUID METAL TRIBOLOGY IN FAST BREEDER REACTORS

E. Wild; K.J. Mack; M. Gegenheimer

Kernforschungszentrum Karlsruhe GmbH., Karlsruhe

Kernforschungszentrum Karlsruhe GmbH
ISSN 0303-4003

LIQUID METAL TRIBOLOGY IN FAST BREEDER REACTORS

ABSTRACT:

Liquid Metal Cooled Fast Breeder Reactors (LMFBR) require mechanisms operating in various sodium liquid and sodium vapor environments for extended periods of time up to temperatures of 900 K under different chemical properties of the fluid.

The design of tribological systems in those reactors cannot be based on data and past experience of so-called conventional tribology. Although basic tribological phenomena and their scientific interpretation apply in this field, operating conditions specific to nuclear reactors and prevailing especially in the nuclear part of such facilities pose special problems.

Therefore, in the framework of the R&D-program accompanying the construction phase of SNR 300 experiments were carried out to provide data and knowledge necessary for the lay-out of friction systems between mating surfaces of contacting components.

Initially, screening tests isolated material pairs with good slipping properties and maximum wear resistance. Those materials were subjected to comprehensive parameter investigations. A multitude of laboratory scale tests have been performed under largely reactor specific conditions. Unusual superimpositions of parameters were analyzed and separated to find their individual influence on the friction process.

The results of these experiments were made available to the reactor industry as well as to factories producing special tribo-materials.

TRIBOLOGIE IN FLÜSSIGMETALLEN FÜR SCHNELLE BRUTREAKTOREN

INHALT:

Schnelle Reaktoren werden mit flüssigem Natrium gekühlt. Sie enthalten Bauelemente, die in Flüssigmetall bei Temperaturen bis zu 900 K sowie bei unterschiedlichsten chemischen Eigenschaften und Aggregatzuständen des Natriums über lange Zeiten betrieben werden.

Die Auslegung reib- und verschleißbeanspruchter Bauteile, die in Flüssigmetallumgebung sicher arbeiten sollen, ist auf der Basis der konventionellen tribologischen Kenntnisse allein nicht möglich. Vielmehr ergeben sich spezielle Probleme aus den reaktorspezifischen Forderungen für den nuklearen Teil einer derartigen Anlage.

Daher wurden im Rahmen des baubegleitenden F+E-Programmes für den Schnellen Natriumgekühlten Reaktor SNR-300 tribologische Untersuchungen in Natrium durchgeführt.

In Auswahlversuchen wurden zunächst Materialpaarungen ermittelt, welche gute Gleiteigenschaften und hohe Verschleißresistenz aufwiesen. Diese Materialpaarungen wurden sodann umfangreichen Parameteruntersuchungen unterworfen. Die zahlreichen Laborexperimente wurden an Modellgeometrien unter weitgehender Annäherung an reaktorspezifische Betriebsbedingungen durchgeführt. Dabei mußte auch das gleichzeitige Auftreten und Zusammenwirken mehrerer Einflußparameter analysiert und nach Einzeleffekten separiert werden.

Sämtliche Ergebnisse wurden der Reaktorindustrie sowie den Werkstoffherstellern verfügbar gemacht.

CONTENT

LIST OF FIGURES

1. INTRODUCTION

The design of tribological systems in sodium-cooled reactors can not be based on the data and past experience obtained with conventional tribology. Although basic tribological phenomena and their scientific interpretation apply in this field, the operating conditions specific to nuclear reactors and prevailing especially in the nuclear components of such facilities pose special problems /1, 2, 3/. As shown in Fig. 1 distinction is made between the conventional and non-conventional plant sections from the tribological point of view. The conventional section includes the turbine-generator unit, and the non-conventional section includes the nuclear reactor core and the primary and secondary cooling systems.

Friction, wear and lubrication problems in the conventional part have largely been solved, or at least their nature is known and understood. Therefore the preconditions for establishing reliable and stable lubricating systems can be determined. In this part of the plant it is possible to use oils or greases with sufficiently high viscosity in friction or roller bearings and sufficiently high circumferential speeds will generally be encountered.

In the non-conventional section basic tribological phenomena and their scientific interpretation do not apply. The reactor core, coolant pipes and heat exchangers, apart from the sodium pump, can be regarded as relatively rigid structures. However, the structure consists of many tens of thousands of different components which in operation move relative to each other owing to differential thermal expansion or flow-induced vibration or during loading and unloading events.

In all these cases reactor-specific operating conditions are extremely unfavourable from the tribological point of view. Table I shows these parameters which are known as the collective stress pattern in more detail. The most important locations of rubbing contact are summarized in Table II and some discussed in the following:

Figure 2 shows a section of core structure which in the Sodium Cooled Fast Reactor SNR 300 consists of some 500 core elements. They are all centered in the bottom plate and supported against each other by distance pads in support or restraint planes above and below the fuel zone indicated. The whole struc-

ture is restrained by an upper and a lower ferritic clamping ring. The fundamental hexagonal form of the fuel elements results in a honeycomb system in which each element must be able to self-orient (Fig. 3). This is only possible if the coefficient of friction of the system between the adjacent elements is not greater than 0.57. A relative radial movement of this type caused by rod bowing can be superimposed on an axial movement brought about by differential temperatures. In addition fuel elements must be able to move axially even after prolonged periods of operation, especially for loading and unloading.

Various friction contacts exist inside each fuel element, both in the area of each fuel rod suspension and in the spacer region as shown in Fig. 4. There may be relative movements between the individual spacers or between the spacers and the cladding tubes. If the coefficients of friction are too high (following swelling) grid-type spacers may be deformed or even destroyed. In adhesive wear with material displacement there may be local blockages in the cooling channels. Abrasive wear may weaken the wall of the cladding tube involved /4/.

The application of centering systems in various components shows Figure 5, namely (A) a thermoshock shield or concentric heat exchanger tubes; (B) heat exchanger pipe penetrations with unfinned and finned contact areas, respectively. In typical straight tube heat exchangers (Fig. 6) the mounting of the grid spacers is comparable with that in fuel rod bundles.

Despite all these adverse preconditions it is necessary to guarantee safe functioning of these complicated tribological systems over prolonged periods of time. For this purpose the tribological behavior of all components in contact and moving relative to each other must be known.

After intensive studies of literature tribological experiments have been carried out over a number of years to elucidate the associated problems. First, a number of commercially available materials were selected for screening tests. These revealed metallurgical, physical and mechanical properties which indicated good tribological behavior and above average wear resistance.

Screening studies were carried out under standard conditions (e.g. constant Na-temperature, specimen geometry, load, velocity) and the materials with the

best tribological properties in sodium were determined /5, 6,/. These materials were then subjected to parameter studies in which the specific tribological load limits were of special interest.

In a multitude of experiments the tribological behavior was measured from specimens of original component geometry and the results compared with those obtained from simplified model geometries.

The work has been realized as a part of the R&D program accompanying the construction phase of the Sodium Cooled Fast Breeder Reactor SNR 300.

2. LITERATURE SURVEY

Basic studies on the frictional and wear behavior of materials in liquid sodium were performed as early as in the fifties and sixties at various research establishments. Whilst in the early days material combinations were discussed involving tool steels and, generally, "hard on soft" pairings, the "hard on hard" combination grew in importance at a later stage. Until that time cobalt-base welded-on alloys as well as precipitation-hardened nickel-base alloys had proved their worth.

In experimental work conducted in the UK /7/ the influence of different types of boundary lubrication has been found. One of those was rather the effect of adsorption whilst another type is achieved by complex Na-Cr compounds as a surface layer. The sodium temperatures and the oxide content are of special importance in this context.

Also studies were made on austenitic steels in liquid sodium and sodium aerosols /8/. In the sodium aerosol atmosphere lower wear rates were measured than in sodium. The lower overall wear is explained by boundary lubrication effects through complex oxides. The influence of varied oxygen concentration in sodium is described. Moreover, friction and wear processes are explained under thermodynamics aspects. On precorroded specimens friction coefficients are measured of e.g. $\mu < 0.2$ which did not undergo major variations.

In the Netherlands studies on wear involving potential structural and cladding materials have been performed /9-12/. According to the test results available it was found that

- work performed with the objective of finding suitable bearing materials allow an evaluation in relative terms
- the dynamic friction coefficient of several material couples under investigation depends on the temperature to a limited extent.
- in general, static friction is only slightly higher than dynamic friction.
- with the experimental parameters initially used the results obtained can be applied under certain conditions only to the problem under consideration.

At different research establishments in the U.S.A. studies on wear and welding behavior have been made on a relatively broad basis involving a large spectrum of materials in various liquid metal environments.The test temperatures ranged from 520 to 900 K and the surface pressure stresses from 0.2 to 0.9 MPa /13/. The test results, however, exhibit hardly a clear tendency. The report /14/ gives guidelines for designers concerning the application of the test results to real cases. These guidelines are based on the discussion of the theories of wear whose principles are explained. The quantitative data suggest that the resistance to wear is high for material pairs consisting of hard metals and cobalt-base coatings. The most favorable friction coefficients ($\mu < 0.1$) were found for pairs of Hastelloy C on hard metal K-95.

Since the work published in /13/ and /14/ quite a number of friction tests have been made in support of development work con-ducted on FFTF. Its main goal has been to determine suitable pad materials. Within the framework of a small test series friction problems were studied in connection with the fuel element wire spacers. For steel on steel pairs (AISI 304 and 316) high wear rates were found.

In a recent publication /15/ experiments are reported with chromium plated and aluminized Inconel 718, Stellite and chromium carbide coatings. The friction tests have shown that carbides make up the only group within the spectrum of materials studied which permanently show favorable friction values in sodium. The advantages indicated for chromium carbide are its chemical stability and its favorable thermal dilatation. Also titanium carbide coatings were investigated. However, they were eliminated from the program when their low chemical stability in sodium was detected.

In other experiments /16/ special material properties were found to be of importance for frictional pairs in sodium environments:

- differing cristalline structures
- greatly differing lattice parameters
- differing electrochemical potentials.

Additional reports are given of extensive tribological experimental work /17-21/. The objective of that study is:
- to determine suitable pad materials for the FFTF core,
- to improve the resistance to wear of structural materials by suitable surface treatment or coating,
- to find bearing materials with a low potential towards change in surface composition under the influence of corrosion or mass transport,
- to investigate the statistic reliability of the friction coefficients of selected materials.

According to the test results available favorable friction coefficient were found for several material pairs in the temperature range up to 750 K. Good results have been obtained for Tribaloy 700 and aluminized Hastelloy C (like on like). Also for sliding pairs made of dissimilar materials (Tribaloy 700 - Aluminis; Inconel 718 or A-286 borated - Aluminis; Inconel 718) mean and maximum kinetic friction values were measured which do not exceed acceptable values in the temperature range tested. By contrast, the adhesive forces (breakaway) measured after standstills are relatively high.

Experiments with various sliding pairs made of cobalt-base, nickel-base and tungsten hard metals were performed in France /22,23/. The most important findings are:
- In case one partner of a sliding pair consists of austenitic steel, the result is always unsatisfactory.
- The results obtained in tests with chromium carbides are unsatisfactory. Above all, an irregular and high friction coefficient is always manifest.
- Tungsten carbides (WC) materials have a high resistance to wear. Above 580 K friction coefficients of 1 to 1.3 were measured.
- Likewise low wear and high friction coefficients were found in pairs consisting of cobalt-base materials (Stellites).
- The nickel-base alloys Adnic and Colmonoy exhibited friction coefficients below 0.55.

For Titanium carbide, nickel, cobalt and tantalum alloys particular attention was paid to the time of pre-corrosion. The tests were started after various durations of dwell of the material specimens in sodium. Both the wear rates and the friction coefficients attained a maximum after about two hours of dwell-time. After 10 - 12 hours the measured values were generally lower by a factor of 10.

In the U.S.S.R the temperature dependence of the friction coefficients of some carbide materials is examined /24/. The maximum test temperatures in vacuum or air were 2000 K. The friction values of all pairs investigated ranged from 0.4 to 0.8 up to approximately 200 ^{o}C, with a decreasing tendency up to approx. 1100 K. Above 1200 K the values rose up to $\mu = 1$. No difference was found in the friction behavior between pairs made of like alloys and pairs made of unlike alloys.

Summary: The material pairs Inconel 718 - Inconel 718 and Stellite 6 - Stellite 6 discussed for use in SNR 300 were subjected to friction tests at several laboratories but for different operating conditions.

With the comparatively great number of test results available the following picture could be traced for Inconel 718:

- The friction coefficient shows a high dependency on the friction path. In the majority of experiments the initial value attains about 0.2 and the final value clearly more than 0.5.
- The temperature parameter is obviously superimposed by the sliding path parameter so that an unambiguous assignment is not possible.
- The tests reveal an influence of the amplitude of motion and the sliding velocity. For small amplitudes and low velocities higher friction coefficients were obtained than for larger amplitudes and higher sliding velocities.
- An influence of loading and surface pressure stress, respectively, seems to be exerted mainly in the initial phase of sliding in case the existence or conservation of an oxide layer depends on it. After run-in the friction force, in case of purely metallic contact, appears to be largely proportional to the load applied.
- Following a dwell time of about one week at 863 K the surface oxidation (also at a relatively low O_2-content) leads to a substantial drop in the

friction coefficient. However, at lower temperatures but higher O_2-content similar values are measured. On the whole, a great number of all measured data for Inconel 718 exceed considerably the specified value of 0.5 (max. acceptable for SNR 300).

Experiments involving Stellite 6 H and 6 B showed:

- The friction coefficients measured at constant temperature (923 K) are very dissimilar.
- In case of oscillating movement with the sodium temperature subjected to variations, the initial values at 500 K amount to approx. 0.33. With the increase of sodium temperature the measured friction coefficients rise up to about 0.6 at 873 K.
- The startup friction (breakaway) occurring in these experiments attains values up to 0.99.

Conclusion: According to the literature available up to this time:

- Materials were found with favourable wear resistance and (in the U.S.A.) acceptable friction coefficients.
- Some experience was gained about the influence of chemical surface processes on the tribological behavior of material couples.
- The meaning of Na-temperature, normal load, sliding velocity or rubbing distance as parameters was studied (more or less occasionally).
- Most of the experimental results are in an unsatisfactory agreement.
- Very different specime geometries and various O_2-contents in Na were used in the experiments.
- There were basic measuring problems concerning wear volume and O_2-content in the sodium.
- A very small margin of safety between measured and maximum acceptable friction coefficients was found with respect to SNR 300 load pad requirements.

For this reason more intensive experimental work was necessary to provide both data and experience for the proper tribological lay-out of the SNR 300.

3. EQUIPMENT

3.1 Sodium Loops

Sophisticated experimental facilities were built to carry out the necessary experiments under extreme operating conditions:.

- First, the "Sodium Wear- and Selfwelding Loop" NVP I has been constructed with only one test vessel to install test sections of various design. Pipework and components were fabricated of stainless steel. The sodium flow rate of 300 kg/h led to a flow velocity of ≈ 0.45 m/sec in the pipes. A 10 %-bypass flow was continuouly purified in a filter mesh cold trap. The O_2-content in the sodium being also continuously measured by an oxigenmeter.
  But, at an early stage the loop capacity was found to be insufficient. Therefore, three additional test vessels were installed, allowing parallel performance of wear- and selfwelding experiments /Fig. 7/.

- "Sodium Wear Loop" NVP II has been provided /5/ owing four test vessels /Fig. 8,9/. The facility consists of a sodium supply and purification circuit and its different components. Pipework and components were fabricated of stainless steel. The sodium flow rate was up to 3000 kg/h according to a maximum sodium flow velocity in the pipes of 1.6 m/sec. Also in this loop a 10 %-bypass flow running continuously through the filter-mesh cold trap. So, due to surface corrosion problems on structural materials the oxygen content of the sodium was maintained at ≈ 5 ppm throughout the test program.

The loop could be operated isothermal at temperatures up to 500 °C. An intermediate heat exchanger enabled the loop to supply test section through-flow at 600 °C whilst the sodium temperatures at all other components (except heater) did not exceed 500 °C.

In the experiments performed over many years conventional plugging meters and/or in-line-oxygen-meters (solid electrolytes) were used to measure the oxygen content in the sodium. Also sodium samples were taken to be analyzed after destillation /25-27/. When, in a later stage, the O_2-content became an important parameter, an additional device has been installed to contain

vanadium foil samples (for equilibration analysis after dismanteling) /28,29/.

3.2 Test Sections

Various experimental facilities which could be connected to the sodium supply and clean-up system were used to move pairs of materials relative to each other under loads in various geometries. The test sections were designed to detect errors caused by malfunction of any test section component or by condensation of sodium vapor in the cover gas seals.

Test Section I

A pin-on-disk configuration (Fig. 10) was constructed for rotating or intermittent relative motion. In addition to the genuine elasticity of the drive mechanism, a varying combination of the friction force detector cells can maintain different stages of elasticity of these systems (Fig. 11).

Test Section Ia: The upper material specimen A (3 pins) loaded by the deadweight is driven by the shaft W. The support B with the lower specimen (disk) has been fixed by an axial bearing C so that it will pivot freely. It is prevented from simultaneous rotation by the bending lever D. The latter will be bent by the friction force applied and its deflection is measured by strain gauges. In addition a torsion cell E measuring the torque of the driving shaft has been installed to measure friction forces in two lines simultaneously.

Test Section Ib: The lower specimen support has been attached to the bottom of the test section. The friction force is recorded only by the torsion cell E in the driving shaft.

Test Section Ic: The lower specimen support has been fixed so that it too is allowed to pivot freely. The friction force is measured by the bending rod D.

Test Section Id: Again the specimen support B has been locked in position. The bending rod and the torsion cell are removed. A quartz force link Q has been installed into the driving system above the test section.

Test Section II

This test section is designed as plate-on-plate configuration. It is implemented in the test section shown in Fig. 12 and allows translatory relativ motions.

Test Section IIa: In a clamping system, two flat specimens are pressed against a central plate oscillating vertically. The reciprocating motion of the vertical shaft and attached specimen is generated by a driving system outside the test chamber. The forces required to drive the shaft up and down are continuously measured by an installed quartz crystal. The weight of the shaft is compensated for by a defined cover gas pressure inside the test vessel.

Test Section IIb: It represents a configuration with a modification of the specimen support system to realize a higher overall rigidity.

Test Section IIc: In a special version of this test section (Fig. 13) a micro- hydraulic cylinder C has been installed in the shaft D in which the central specimen A oscillates at a low frequency (0.12 Hz) upward and downward (± 5 mm) between the external specimens B. The top part of the shaft (D_1) is driven by the excenter E (primary movement). C receives from a commanding cylinder higher frequency pulses so that the relative movement between the specimens A and B is composed of the basic movement of D_1 and the superimposed vibration of D_2. In the pressure cylinder G the normal load to be set on the specimens is applied (as a constant or cycling load).

Test Section III

Additionally, a new system with a tilting plane was developed and put into operation with liquid sodium (Fig. 14). This system has been used so far only with other media /30, 31/. From this new design considerably reduced equipment influence was expected on the friction process as well as on the signal transfer.
The relative movement between the material specimens (rider A/lower specimen) is effected by tilting the whole test section and hence the slipping plane. Beginning of sliding of the rider A is recorded and assigned to the slope of the sliding plane.

4. TEST SPECIMEN GEOMETRIES

For screening as well as parameter tests with variable material combinations two specimen configurations were used in a simplified standard geometry (Fig. 15). In test section I there was the "pin- and disk"-system installed, moving either oscillating or continuously rotating. For especially translatory relative motion in test section II the "plate on plate"-configuration has been realized.
To substitute the original systems the following specimens were manufactured:

- Fuel pin - wire spacer system: Two versions of specimen geometry were fabricated. Fig. 16 exhibits the couple for test section I and Fig. 17 for test section II, respectively.
- Fuel pin - grid spacer system (Fig. 18)
- Heat exchanger tube - tube support systems (Fig. 19),
- Spacers of concentric heat exchanger tubes (Fig. 20),
- Centering knobs of the type used between the wall of the vessel and the thermoshock plate of a reactor.

5. MEASURING

5.1 Material Wear

Concerning the evaluation of quantitative material wear some different methodes are discussed in Refs. /32 - 36/. A most suitable process was applied in the experiments described here:

Modifications in material specimens resulting from wear essentially relate to
- change in length of the cylindrical pins,
- surface roughening of the annular disk,
- change in weight of both sliding partners.

Positive or negative changes in length of the pins are recorded by ultra-fine micrometers and by use of a micro-scale weight assays are possible with sufficient accuracy up to 0.1 mg.

On the annular disks wear profile measurements have been carried out. The procedure is shown in Fig. 21. The mean depth of penetration E_m of the wear

surfaces is determined. This is the mean distance determined from several measurements made at different locations between the reference profile (original surface) of the work piece and plane a in Fig. 21 characteristic of the arithmetic centre line average height. By means of a micro-scanning system six radial traces per sliding path are recorded. The area confined in the individual case by the reference profile (over the initial area of the envelope) and the curve traced is recorded by means of a planimeter. The division of the surface area by the width (W) of the sliding area gives the dimension E_m. If pure asperities or flattenings of the surfaces of Rt $\lesssim$ 1 μm are encountered, the measured value is indicated as the surface roughness Rt together with the arithmetic centre line average height /37/.

At the early stage of run in wear is frequently noticed from the fact that some of the micro-asperities characterizing the specimen surface are abrased. This abrasion is determined via the bearing area at various depths of the sectional lines (Fig. 22).

Besides these processes which are assessable in quantitative terms, changes in shape or mutual material transfers occasionally occur without actually changing the volume or the weight. These quantitative values, which are not less important in the evaluation of the material pairs, are recorded on photographic pictures when the surface is viewed.

To determine the effect of wear on tubular specimens with respect to wall weakening three profile sections each running normal to the wear track were recorded at the minimum (Fig. 23).

5.2 Friction Coefficients

The friction coefficients μ were evaluated from the friction forces measured tangential to the contact area F_T and related to the normal load F_N, hence $\mu = F_T/F_N$. Sparious influences caused by the equipment were eliminated by calibration experiments. A distinction was made (shown in Fig. 24) among:

- breakaway friction coefficients, μ_b, measured in the first onset of a movement after standstill,
- dynamic friction coefficient, μ_d, measured as an average during continuous movement

- static friction coefficients, μ_s, as a maximum value in continuous and intermittent movement.

6. TEST MATERIAL SELECTION

In high-temperature environments characterized by lack of lubricating media and contact with active chemical agents, conventional bearing materials have not been adequate /38-40/. Resistance to wear and galling are not fixed properties of a material and no arrangement of formulae have been developed to predict these satisfactorily. When the requirement of operation with high-temperature sodium environment as the lubricant is superimposed on the design, the relative importance of the characteristics may be changed significantly from their importance in conventionally lubricated elements. The many characteristics commonly considered in selection of bearing materials are discussed more in detail in /13/ and /1/. For the experiments carried out at KfK both, a literature survey as well as an expective tender of the material producing industry led to the choice of the materials listed in Tab. III.

Some materials were subjected to friction tests in cold worked or annealed conditions, respectively (austenitic steels, nickel base alloys). Inconel 718 has been available in an annealed and in a heat-treated version.

Various coatings were applied by flame- or plasma spray, whilst Cr_3C_2 and Tribaloy 700 coatings were realized by D-gun deposition. The advantages of the detonation-gun plating include low heat input to the base material. This is of special importance for thin walled (sheet) components as duct load pads, separating fuel element wrapper tubes. As an alternative methode to some wear specimens Tribaloy 700 has been applied as coating also by plasma arc equipment. But obviously thermal expansion led to partial loosening of the layer. For the candidate materials being under examination in screening tests, chemical compositions and hardness are given in the appendix, Tab. A1.

The screening tests revealed a group of material pairs with qualified tribological behavior:

- Inconel 718
- Stellite 6
- Tribaloy 700
- LC-1C; LC-1H (Cr_3C_2)
- Inconel 718 A (aluminized)

In parameter tests they were always in couples "like on like". Their various characterization data is given more detailed with supplementary tables and figures in the appendix.

7. TEST PROCEDURE

The general test specimen handling program is given in Tab. IV. It describes the procedure from the specimen preparation to the documentation of the results.

7.1 Screening Tests

From the materials selected (according to 6) whose corrosion behavior in sodium had led to positive results or for which above average resistance to wear could be expected from their properties, the most favorable sliding partners were determined in preselection experiments. Under tribology aspects /34 - 36/ a generally more favorable friction and wear behavior could be expected from "unlike" pairs (hybrid pairings) than from "like on like" pairs. This more advantageous tribological behavior is essentially due to

- differing lattice parameters,
- the most dissimilar positions possible of the dominant alloy constituents in the galvanic contact series,
- the lowest tendency possible of alloys to get dissolved in each other /13/.

The first approximately 100 experiments were therefore performed with the hybrid combinations entered in Table V-IX.

To reduce the number of pieces kept on store, to streamline processing steps and to give due consideration to novel material developments, but also with the objective in mind that the amounts of wear should be better categorized and interpreted, respectively, all later screening tests were performed with "like on like" pairings (Tab. X and XII). One exception was made due to the instrument panel, Test Nr. 118-132, Tab. XI. Later, in connection with a program to investigate the tribological behavior of original reactor components, also ferritic hybrid pairings were tested under standard conditions due to Tab. XIII and XIV. Co-free material pairings were tested as long term

alternatives for the Mark I pad materials Stellite and Inconel (Tab. XV, Test matrix 11).
Considering the movements to be expected at the SNR 300 control rods, an oscillating relative movement was chosen. The specimen loading and the sliding path were so defined that within well defined testing periods measurable results could be expected. Fig. 25 and Table XVI show the "standard" test program according to which almost all tests had been performed.In this way the testing schedules of KfK and INTERATOM were brought to agree with each other (KfK-IA standard program). After each new assembling of the test specimens the loop was heated up to test temperature. During this time (3-5 h) as well as during intermediate dwell times, the specimens were not in contact under load. Consequently, the surfaces were completely flashed by the sodium flow. For intercomparison tests (test No.356-375) by US ARD and KfK (involving differing test section systems as parameters) the temperature plot was reproduced of the scheme applied in the USA (Fig. 26).

7.2 Parameter Investigation

With the most favored material couples an extensive parameter test program has been realized. The parameters of interest were subjected to variations, whilst the rest of operating conditions were kept constant in conformity with the standard program. For most of the "parameter experiments" the development of temperature according to Fig. 25 had been fixed. The parameters were:

- contact pressure
- sodium temperature
- surface-macro roughness
- rubbing velocity
- rubbing distance
- O_2-content in Na

Also the influence of various kinds of movements on the behavior of friction systems was studied. The amplitude and frequency of both the primary movement and of the superimposed (higher frequency) vibration were considered as parameters.

The diagrams in Fig. 27 show three characteristic types of cycling relative movements in the experiments:

a) Relative velocity of oscillating primary movement (standard movement).
b) Relative velocity of the lower frequency vibration superimposed on the standard movement.

c) High frequency vibration superimposed on the standard movement.

To investigate the influence of nonstatic pressure on the tribological behavior, a load variation of ± 10 % and ± 80 %, respectively, with a constant frequency (10 Hz) was superimposed to the static basic load of 200 and 1000 N, respectively. The cycling normal load for one amplitude each of the movement has been shown graphically as an example in Fig. 28. Other operating conditions during the experiments were kept constant.

All parameter tests are shown in chronological order in Tabs. XVII through XXVIII, grouped with respect to the parameters under investigation.

8. TEST RESULTS

8.1 Screening Tests

8.1.1. Wear Behavior of Hybrid Pairings (Tests No. 1-99)

With the development of control rods as the background, material pairings having a high wear resistance had to be determind. Since the possibility existed of contamination of the reactor cooling circuit, the abrased amounts resulting from wear should be kept as low as possible. By a minimum tendency of self-welding (breakaway friction coefficient) the safe mobility of the control rods should be guaranteed even after extended down times. By analogy with the requirements made, only the amounts of wear were measured initially and later-on the friction coefficients as well. In the representation of results the pins and disks of standard specimen geometry have been entered as bars. Pin shortening caused by wear and the depth of penetration of the wear tracks in the disks have been indicated as bars reduced in size relative to each other. In some cases cross shading suggests material transfers to the sliding partner (Figs. 29a-d). However, it is difficult to establish from this chronological representation an intentional order or ranking of the material pairings by their respective wear resistance.

To allow a reliable interpretation to be made, some of them were combined into groups in which either like pin materials had been combined with differing disks or differing pin materials with similar disks. Figure 30 shows the difference in wear behavior of various Colmonoy and Stellite alloys,

respectively, with respect to austenitic steel AISI 1.4981. On account of the considerable differences in hardness between the steel involved and the wear resistant alloys, a distinct abrasion of material had been expected to occur on the steel side. According to expectations, it attained the same order of magnitude in all cases. Except in the case of Stellite 6H more or less intensive material transfers may take place everywhere with the consequence that a real "steel on steel" material couple is obtained. Therefore, independent of the amount of wear, a better mark must be given to Stellite 6H as the sliding partner for AISI 1.4981.

If one studies the materials used on Inconel 718 (Fig. 31) a similarly good resistance to wear is found for Stellite 6H, Colmonoy 56 and FeCr 50. The wear was maximum on the Inconel side with FeCr 50 as partner, whilst it was smaller by one order of magnitude with Stellite 6 as partner.
Tungsten carbide WC (Ni) showed a high wear resistance to Stellite 1 and Colmonoy 6. The sliding surfaces of these pairings got increasingly smoothed with the friction path becoming longer. These smooth surfaces led to significantly increasing friction coefficients ($\mu >> 1$) which was primarily due to the total displacement of sodium.

8.1.2 Wear and Friction Behavior of Like Materials (Tests No. 100-125; 170-250)

To reduce the materials kept on store to a reasonable number and to simplify the technology in the application of wear resistant coatings, the reactor manufacturer (INTERATOM) indicated more interest for the use of "like on like" material pairings. The parameters were kept constant which had previously been used for pairings consisting of unlike materials. Moreover, evaluation of the wear behavior of such combinations proved to be less complicated and more reliable. Whilst in the comparative presentation in Fig. 29 the effect of wear has been plotted as the changes in length of the pins and penetration depth of the wear tracks in the disks, respectively, the representation chosen in Fig. 32 for the calculated amount of wear proved to be more suitable. The vertical bars above the contact line K are indicative of the material at the pin specimens. The bars below the contact line show the wear rate of the disk material. These are average values of several experiments. Among the material combinations examined under standard conditions. The austenitic steels and the TZM molybdenum alloy exhibited unsatisfactory

resistance to wear. Slightly better, but still unacceptable for the planned uses, was the wear rate of FeCr 50. Tantalum and Ferro TiC turned out to have insufficient resistance against the chemical aggressiveness of sodium. The WC(Ni) hard alloy had to be removed from the program because of excessive inclination to fracture, while the Colmonoys were rejected because of their insufficient binding power to the substrate material. (But this has been remarkably improved in the meantime).

Towards the end of the screening tests described, the tasks set had been slightly modified. On the basis of previously evaluated wear tests, the production of rather high amounts of abrased material, which could lead to a contamination of the sodium loop had not to be expected. At the same time, the request was more and more urgently expressed to have safely moving control rods and to provide the fuel elements with the possibility of becoming largely self-orientating in the composite core structure.
So, in the tribological experiments, static and dynamic friction behavior had become the more significant criterion.

In accordance with the sequence of optimum wear resistance apparent from these experiments, the following pairs of materials were selected for subsequent friction tests:

Inconel 718 / Inconel 718 (tests No. 264/266/267)
Stellit 6H / Stellite 6H (tests No. 265/268/269).

In the first test series three Inconel pairs (annealed) were used, two of them (tests No. 264 and 266) with flat and one (test No. 267) with spherical specimens. While all parameters were kept constant, these tests were then repeated with Stellite 6H (tests No. 265 and 268, flat specimens, test No. 269 spherical specimens).

Figures 33 and 34 are graphical representations of the results.

For annealed Inconel 718 (an) the friction coefficients would only approximately fulfill the expectations concerning $\mu \leq 0.5$. Moreover, lower friction coefficients were measured for Stellite 6H.

The results of subsequent tests involving heat treated Inconel 718 (ht) "like

on like" as well as combined with the sheet material Stellite 6B are shown in Figs. 35 and 36, respectively.

Comparison of the results for the two Inconel versions (an, ht) shows lower friction coefficients for the annealed material. For the hybrid pairing Inconel 718 (ht)/Stellite 6B most favourable values were obtained as a proof for tribological advantages of unlike materials. From corresponding experiments carried out at INTERATOM at this time, results were available in a good agreement with KfK /41,42/.

Since Stellite 6 and Inconel 718 yielded favorable results also in parameter tests (Section 8.2), they were specified inter alia as reference duct load pad materials for the Mark I core of SNR 300. For their application in a number of other friction systems (especially in control rod guides) with relative movement alternating with considerable down times static friction coefficients μ_s or break-away friction μ_b may be of special interest. For this reason in Fig. 37 the friction force diagrams of two tests (No. 266 and 268) are given more detailed. Break-away friction at the onset of movement has been registered only sporadically, about 10-20 % higher than average dynamic friction. Static friction coefficients μ_s being slightly higher than dynamic mean values. This has been taken into account with the upper limitation of the scattering bands of all respective diagrams.

Due to the high co-content of Stellite 6 Co-free alternative materials having at least the same or even better tribological features must be found.

First, the SNR 300 instrumentation panel to be made of Stellite 6 according to the existing concept, was to be fabricated from a Co-free material. Inconel 718 was proposed as candidate material. For this material, the friction behavior had to be determined with respect to the austenitic steel of the measuring probes at handling temperature (520 K). To gain a paramount picture of the sliding behavior of the material pairings to be compared, i.e.Inconel-Steel, Stellite-Steel, Steel-Steel, supplementing tests were performed also at temperatures of 725 and 873 K (Tab. XI, Test matrix No. 7).

For the nickel and cobalt base alloys increasing friction values were obtained with rising temperatures, for the austenitic steel 1.4961 falling friction values. The results have been represented in Fig. 38 as an example

for the handling temperature of 520 K. From the whole number of tests (9) carried out for comparison, it was found that friction coefficients of the Inconel 718/Steel-pairing were in general rather slightly lower than those of the Stellite 6/Steel-pairing. With these results there is no satisfactory agreement to former experiments, but only at handling temperature (520 K). Nevertheless, Inconel 718 could be accepted as instrumentation panel alternative material.

Several novel developments were offered by various material manufacturers as cobalt-free alternative to Stellite 6 and Inconel 718, respectively. Preliminary studies on the compatibility with liquid sodium and first experience already gathered in the U.S.A. led to a preselection of three potential candidates:

- Inconel 718 A (alitized),
- LC-1H (Cr_3C_2 D-gun coated),
- Tribaloy 700 (Ni-base + 35 % Mo).

With these materials experiments were performed in "like on like" pairings and "hybrid pairings". Since the results were comparable with that of Stellite 6 and Inconel 718, the tests were performed under the IA-KfK program with all parameters kept constant (ground surfaces, Rt < 5 µm).

The result for five tests carried out with LC-1C (tests No. 293 - 295, 304) are presented in Fig. 39. The friction values on an average were rather less favourable than for the previously tested reference materials (Inconel 718, Stellite 6).

Lower friction coefficients were obtained for Tribaloy 700 like on like (Tests No. 311-314). Even the highest value (temperature range 523 K) is giving a satisfactory margin of safety to the 0.5 -maximum. On the other hand, different contact pressure (8 MPa, 20 MPa) didn't cause clear different friction coefficients (Fig. 40).

A very similar situation is presented by the scattering band of friction coefficients for Inconel 718A as shown in Fig. 41 (tests No. 323-326). In this case the higher contact pressure led to slightly lower friction

coefficients on an average. Also increasing temperature caused rather decreasing friction factors. Very similar results were obtained for this materials in three additional experiments (tests No. 327-329) with a contact pressure of 20 MPa.

With the recommendation of conventional tribology in mind to prefer unlike material couples the hybrid pairing Inconel 718 A/Tribaloy 700 has been tested (tests No. 434-439). However, as can be seen in Fig. 42 friction coefficients of these couples were relative favourable and more constant over the total cumulative rubbing distance. Only very little influence from temperature variation was found.

8.1.3 Interim Program

The material specified as the duct load pad material for the mechanical reflector elements was Inconel 718. This implies that at least in one area there is frictional contact with respect to the Stellite duct load pads of the fuel element. To obtain validating data for this special case, further frictional tests were performed under an interim program with the material pairing Inconel 718 on Stellite 6 B (Figs. 43 and 44). In the tests No. 306 and 309, the internal specimen (see Fig. 15B) was made from Inconel 718, the two external specimens were made from Stellite 6B. In the tests No. 307 and 308 the external specimens were made from Inconel 718 and the internal specimens from Stellite 6B. The sodium temperatures 523 and 673 K were selected as parameters. For comparison, these tests were likewise reproduced with two pairings Stellite 6B on Stellite 6B (tests No. 305 and 310). The results indicate:

- The friction coefficient of the pairing Inconel 718 on Stellite 6B is on an average higher than that of the pairing Stellite 6B on Stellite 6.
- A major dependence on temperature cannot be recognized for the two pairings.
- During startup following 16 hours of standstill under load the initial friction coefficient is relatively low ($\mu_d < 0.3$), above all for Stellite 6B. But it gradually increases to attain the mean value of 0.4.
- The maximum values exceeded the mean values indicated by an extremely smalll amount only.

- Increased startup friction (adhesive forces) at the beginning of the individual partial tests were not measured.

8.1.4 Ferritic Heat Exchanger Materials

On account of the swelling behavior of austenitic structural materials exposed to irradiation, ferritic steels were discussed as alternatives, on the tribological behavior of which no data whatsoever were available.

With the specified materials steel AISI 6770 and 90 MnV8, respectively, (tests No. 403 - 414) first the friction and wear coefficients were determined with the sodium temperature as the parameter. To permit comparisons to be made, these tests were first carried out with specimens in standard geometry (Fig. 15a) and according to the standard test program (Fig. 25). The wear rates measured are shown in Fig. 45. The vertical bars indicate the average material abrasion from the pins. The abscissa shows the used material combinations and the sodium temperatures. The AISI 6770 -6770 pairs exhibited wear rates seveal orders of magnitude higher than those shown by the "wear resistant" hard facing alloys (righthand side of Fig. 45). At high sodium temperatures of 823 K the material abrasion was less than at a temperature of 523 K. However, increased ductility resulted in pronounced deformation of the specimens. At 523 K major loss of material occured as macro particles. The wear rate of the hardenable tool steel 90 MnV8 shows a clear dependence on temperature. At the temperature range 523 K - 673 K, it retains its original hardness (approximately 65 HRc) and is very resistant to wear. At higher temperatures its hardness rapidly decreases, and the wear level is similar to that of the 6770 - 6770 - pairings.

In the combination with the Colmonoy 5 the wear behavior of the different steels was improved considerably. At the higher test temperatures slight steel wipping on the Colmonoy specimens was found.

The friction coefficients measured in these experiments are plotted as a function of temperatures for different material combinations in Fig. 46. The differences between the values shown by the steel-on-steel pairs and those shown by the steel-on-hard facing pairs are rather significant especially at higher temperatures. In both cases the curve of the friction coefficients

correspond to the related severity of surface deterioration.

8.1.5 Ferritic Cladding Materials

Within the framework of the general program conducted at SCK-CEN on the characterization of ferritic cladding materials, tribological studies had to be made with two novel materials. They have been called DTO_2 and B3. Their alloy constituents and the results of structural analyses are summarized in Table AX.

To allow comparisons to be made with previously studied austenitic materials, the tribological behavior had to be determined of the two steels in "like on like" pairs and relative to "wear resistant coatings". The wear partners selected were Colmonoy 56 and the Cr_2C_3 coating LC-1H. The tests were first performed in test section I with specimens of the pin-disk system (tests No. 440-463). Further tests had to be made with specimens in original geometry (cladding tube relative to wire spacers) (tests No. 464-477). In test section I the specimens were used as shown in Fig. 15a, in test section II as shown in Fig. 15b. The test parameters to be studied had been harmonized with SCK/CEN. They are summarized in Table XXXI.

The friction coefficients recorded for DTO_2 (tests No. 440-451) in standard geometry are represented as a scattering field in Fig. 47. Considering the test temperatures of 653-873 K the width of the scattering band seems to be relatively narrow. The mean value is 0.5 which means that it is advantageous as compared with the values measured for some austenitic steels.

For B3 on B3 pairings (tests No. 452-455) and the B3 on LC-1H pairings (tests No. 456-459) nearly equivalent friction coefficients were measured. They are slightly less favorable than that of DTO_2 and are (comprised in Figs. 48 and 49) within the same limits of the scattering band. The fact that on an average the same values were obtained for the B3/LC-1H pairs as for the B3/B3 pairs can be explained by smearing of B3 onto the CrC partner taking place in all cases. In this way a B3/B3 pair was in fact obtained also here after some time of operation.

With B3 on Colmonoy 56 pairs (tests No. 460-463) comparable tests were performed while the relative movement was varied in addition. The values mea-

sured in continuous rotating movement (Fig. 50) likewise correspond to those of the pairs B3/B3 and B3/LC-1H, respectively. But in case of oscillating movement and lower speed the friction coefficients attain values $\mu < 1$.

For the different material couples in "pin-disk"-geometry the wear effect (shortening of pin specimens) is shown in Fig. 51. Wear rates calculated after these measurements are 3×10^{-8} cm^3/cm Kgf.

8.2 Parameter Investigation

8.2.1 Chemical Reaction of Na with the Materials under Consideration

Influence of precorroded or newly machined probes:

Some tests could not be started immediately after installation in the test section, because of operating failures in the sodium circulation in the test facility. Testing with these materials started only after quite a long dwell time in sodium. The results subsequently exhibited a clearly different wear behavior. Therefore, particular attention was paid to the influence of the dwell of specimens in sodium.

With the material couples Stellite 6H (Pin)/Steel 1.4961 (Disk) and Inconel 750 (Pin)/1.4981 (Disk) experiments were carried out under standard load F_N = 8 MPa and continuously rotating movement. The time of precorrosion (specimen surfaces not in contact) has been the parameter of interest. The material worn away by wear could be measured only at the stainless steel disks whilst very little reduction of pin length has been superimposed by adhesion of steel wear particles. The specific wear coefficient (K) calculated for this materials are shown in Fig. 52. A nearly identical wear behavior was evident for both steels with minimum wear after four hours of precorrosion.

To take into account the largely intermittent movements both at the control rods and at the fuel element load duct pads, accompanied by partly extended standstills, tests were performed by which the materials were precorroded for a rather long period.

Precorrosion of materials was originally intended to take place in a corrosion test bench. Before the determination of the sliding behavior in the wear

test bench this would have automatically required cooling down, withdrawal and insertion as well as purification of the specimens so that falsifying influences on the test result obtained had to be expected. Therefore, in these tests precorrosion was performed in the wear test bench proper.

The material pairing Stellite 6H/Stellite 6H was used for these experiments. Three specimens in total were exposed for 1800 hours in the test sections of the wear test facility (tests No. 282 and 283 with the specimen couples in contact under load, test No. 284 with the probes not contacting). Then the trial runs were directly performed in three test sections, i.e. without previous modification of the specimens.

The startup friction coefficients μ_b measured in the three tests and furtheron μ_d measured along a sliding path of about 100 cm have been plotted in Fig. 53. In two cases an adhesion effect can be recognized significantly exceeding average dynamic friction coefficients. In test No. 284, however, μ_b lies below the mean value established later. For comparison the friction curve for newly machined Stellite 6H is appended in the diagram.

In test section III (Section 3.2, Fig. 14) the influence was investigated of long-term surface corrosion (6500 hours) on the friction behavior of Stellite 6. To be able to record in an optimum way the change of surface as a function of friction loading, small friction paths were first selected with low contact pressure applied. The test section was tilted about four times every minute so that the duration of static contact between each movement was ca. 14 sec. After 15 and 33 strokes respectively there was a dwell time of 15 h with the specimens in contact under load. By this way static friction coefficients (μ_s) were measured in test No. 320 up to 62 cycles as shown in Fig. 54 ($0.4 < \mu_s < 0.53$). Start up friction (break-away) after dwell (μ_b) was but unessentially higher than μ_s.

Test No. 321 was then carried out over 1000 cycles in total. The first 420 cycles (cumulative rubbing distance S_c = 12.6 m) with a stroke length of $\pm$ 15 mm each, the next 580 cycles (9.28 m) with a stroke of $\pm$ 8 mm. The stroke was reduced on one side only. In this way it was possible to measure the first of the wear track after 400 cycles, the other at the end of the whole test. Dwell times for testing the break-away friction coefficient were interpolated after 210, 560 and 860 cycles respectively. Figure 55 shows the static fric-

tion coefficients (μ_s) recorded in these tests. Most of the values are below 0.5. Break away coefficients above 0.5 (in one case 0.76) were measured after the various dwell times which are evident from the diagram. These measured static friction coefficients have to be seen in close connection with the specimen surfaces after 6500 h of precorrosion (Fig. 56). The contact areas are grainy in their structure. The grains have a high Fe-content and are therefore relatively ductile, especially at the test temperatures selected. They are initially leveled out by the friction loading without material abrasion taking place (Fig. 57). When the specimens were weighted no loss in weight was found.

Test No. 322 has been realized with newly machined surfaces on similar material specimens. The friction diagram obtained in this case is also represented in Fig. 54 for comparison. Its values are somewhat lower than those of the precorroded material and fit very well in the scattering bands gained from experiments under standard conditions.

Influence of environmental conditions

In reactors friction systems operate under very dissimilar environmental conditions:
- in liquid sodium,
- in dry cover gas (Ar),
- in cover gas saturated with sodium aerosol (Ar + Na).

It had to be expected that this would lead to different chemical surface reactions with the resulting impact on the friction behavior of the materials. These questions were clarified in a test series involving LC-1H specimens with brushed surfaces.

At constant temperature (873 K) three test runs each were performed in Na, Ar and Ar + Na, the sliding path attaining 100 m. The scattering fields of the measured friction coefficients have been plotted in Fig. 58 for comparison.

In liquid sodium there was a distinct rise in the friction coefficients along the sliding path ($0.12 < \mu_d < 0.7$) with a slight decrease at the end of each dwell time (tests No. 393-395).

In dry argon (see analysis in Table A II) higher but constant values ($0.4 \leq \mu_d \leq 0.5$) are obtained after a run-in period (S_R = 20 m) (Tests No. 390-392 and 396-398).

Nearly constant, low values μ_d = 0.2 up to 0.25 were obtained in argon saturated with sodium (tests No. 399-401).

To elucidate the extent to which these differing values can be ascribed to the reaction of the material with sodium, detailed surface analyses were performed /43/. Figure A 22 shows the measured proportions of material specimen compositions prior to their use in the various atmospheres. Their changes get apparent in the comparison with Fig. 59.

Initially, some few oxygen containing chromium compounds appear on the surfaces exposed to liquid sodium which had obviously been abrased by friction. This may be the main cause for the rise in the friction coefficients.

On the surfaces surrounded by argon saturated with sodium, sodium-chromium-oxygen compounds formed which exert a lubricating effect. They are not removed by the flow medium during the test. In dry argon the oxygen offer was too low for an oxide film to be formed. The sodium was lacking so that complex oxides were not formed. The relatively low measured value $0.4 \leq \mu_d \leq 0.5$ for the dry solid friction can be attributed only to the surface quality already existing before the test and which was largely maintained also during the friction process.

Influence of oxygen content:

Considerations might be of interest which have been directed toward a reduction of the O_2-content in the sodium of the SNR 300. In a special test series (tests No. 274-280; 330) the question had to be clarified to which extent the experimental results obtained earlier with a higher O_2 content (10 ppm) are still valid for an O_2 content of approx. 1 ppm.

For this reason experiments were carried out under standard conditions with the exception of the O_2-content in the sodium as the variable (10 and 1 ppm). For the SNR 300 fuel element duct load pad reference materials Inconel 718 and Stellite 6H results were obtained as shown in Fig. 60. A comparison of

the friction factors plotted for both 1 ppm and 10 ppm shows that lowering the O_2-content in sodium does not result in a general deterioration of the friction coefficient. A decreasing tendency of the friction coefficient as a function of increasing O_2-content in the sodium is recognizable. However, for Stellite 6H there is still an acceptable margin of safety to the given maximum ($\mu < 0.5$). Some results from earlier experiments fit well into the diagram as a proof of newly obtained data.

8.2.2 Influence of normal load

Also in this case little orientation was to be found in the literature /44/. Therefore, some tests were realized under variation of load
$0 < F_N < 150$ Kpf.

With the materials Inconel 718 - Inconel 718
Steel 1.4961 - Steel 1.4961
WC (CrNi) - WC (CrNi)
Colmonoy 4 - Colmonoy 4
Stellite 6H - Stellite 6H

studies were made in which both the friction coefficients of the different pairings were compared and the influence of varied loadings on the friction behavior was determined. The movement was a translatory oscillating one with an amplitude of $\pm$ 5 mm.

The greatest surface pressure stress applied was 75 MPa with the normal component of force acting on the specimens being 150 kgf at the maximum. During the entire test the sodium temperature was kept constant at 673 K and the O_2-content at about 5 ppm. The test result is shown in Fig. 61. Accordingly, the friction force plots for all materials investigated run directly proportional to the normal force in the lower load range up to about 50 Kgf (25 MPa). For the austenitic steel and the nickel alloy Inconel 718 this tendency continued until the end of the respective test.

By contrast, for Colmonoy 4, Stellite 6H and hard metal WC (CrNi) a lower rise in the friction force plot can be recognized. This development obviously starts at a later time with the hardness of the material getting stronger, i.e. in case of higher loading (transition from elastic to plastic contact).

8.2.3 Influence of Sodium Temperature

Some interesting hints are given in the literature /45-47/ about friction data as a function of ambient temperature. But those figures were found under different operating conditions and for other materials.

Beginning with Inconel 718, the sodium temperature was studied as a parameter. To allow comparisons to be made with results supplied by TNO, a surface loading of 8 MPa was set in the first test (test No. 256). The relative movement was oscillating (± 5 mm). The start occurred after a short warmup period at a sodium temperature of 473 K. The wetting temperature was intentionally not attained and a corrosion influence was excluded as far as possible. The development of temperature over the whole test duration with the related values of the friction coefficient are shown in Fig. 62. The individual partial tests are separated by heatup and cooling down intervals of about one hour each. During these intervals the material specimens were at standstill under load. In the present diagram (and partly also in the following ones) a longer standstill will be expressly indicated. The development of the friction curve shows the tendency to fall up to 673 K and then rises up to 873 K to attain its original value of about 0.5. Following a standstill of ten hours at 873 K, the plot starts below its last end value, but exhibits for the first time a slightly increased startup friction. In case of a temperature course decreasing stepwise the friction coefficient μ_d = 0.55 is more or less maintained.

In the following test (No. 257) the load was increased to such an extent for a constant sliding surface (25 mm^2) that a contact pressure of 50 MPa was obtained. Up to 5 m sliding path lower friction coefficients were measured (up to 873 K). However, after standstill the measured friction force was slightly higher than before and in the following individual tests it showed the tendency to rise. This led to the assumption that, in general, a gradual rise in the friction coefficient must be anticipated for a longer sliding path.

This was investigated more thoroughly in the following test (No. 258) in which the temperature upon attainment of 873 K was kept constant over several partial tests with 100 cm sliding path each. In fact, the friction coefficient approximates in this case the value of 0.7 which is maintained also

after rather long standstill (Fig. 63).

In a further test (No. 259) the temperature course was so chosen that the material specimens were initially kept in sodium at 873 K for one night (Fig. 64). During the subsequent start the breakaway friction coefficient was slightly higher than in the preceding tests. The subsequent development of the friction curve is a bit irregular but with increasing temperature (after dwell time) it shows a significant rise which is more a function of temperature than of sliding distance.

Comparable tests performed with Stellite 6H followed (tests No. 260 and 261, Fig. 65). Both with a contact pressure of 2 MPa and 5 MPa the friction coefficients determined are lower than for Inconel 718. Moreover, they suggest a lower dependency on the temperature.

In the following test run (No. 262) finalizing this series (Stellite 6 H) the temperature was likewise varied stepwise from 473 K to 873 K, but then kept constant until the end of the test. With the value μ_d = 0.3 to 0.45 the friction coefficient is relatively advantageous over the whole duration of the test. This is shown for comparison with the Inconel 718 material couple in Fig. 63 over an identical temperature distribution.

From other experiments with the oxygen content in the sodium as the variable also an influence of temperature was found. Comparison was made of friction diagrams obtained at different temperatures (523, 673 and 873 K) but for similar oxyde levels (Fig. 66).

For Inconel 718(an) slightly increasing friction coefficients were measured in 1 ppm as well as in 10 ppm oxyde content as a function of increasing ambient temperature. An approximating tendency was registered also for Stellite 6.

8.2.4 Influence of Test Section Elasticity

Tribological properties of material combinations in liquid metal have been investigated experimentally for many years at various research establishments. However, the comparison of results derived from such experiments often entailed difficulties because they had been obtained with a different

target in mind, with different parameters and above all in various test section systems. The target of tribological experiments in sodium mainly determines the design features of the test sections to be used. On the one hand, the material specimens are placed in sodium heated up to 900 K. On the other hand, shaft penetrations and bearings as well as connections of measuring devices can only be installed in areas subjected to substantially lower temperatures. This requires that specimen supports, guides and drive elements must be withdrawn from the zone of hot liquid metal via the cover gas, and flanges. For reasons of rigidity these mostly long vertical components have been designed with appropriate cross sections and consequently large masses to be moved. Their oscillation behavior may influence unfavorably both the friction behavior and the transfer of measuring signals in the respective test section. Consequently, work discussed here concentrated on the friction behaviour of materials, taking especially into account the equipment criteria characteristic of the friction systems.

Experiments were carried out with different test sections as shown in Figs. 11 and 12. In test sections I and II has been varied the system elasticity using different specimen supports and different measuring principles (Tab. XXII). In test section II the mass of the system has been changed by applying the load either through a prestressed spring or through weights.

To reduce the influence from mass acceleration forces in the pin-disk- and the plate-plate test section, low driving velocities of 0.25 and 2.5 mm/min were selected for the initial runs. They were subsequently increased to 25 and 150 mm/min. Afterwards the elasticities and masses of the test section systems were subjected to variation. All other parameters were kept constant. The materials used exclusively were Stellite 6 and Inconel 718. To exclude uncertainties the surface roughness of the probes was kept constant ($5\,\mu m \leq Rt \leq 10\,\mu m$).

To display the test results (tests No. 315-318) two typical friction force curves are shown in Fig. 67. Here, the static friction coefficients μ_s and the dynamic friction coefficients μ_d of Stellite 6 and Inconel 718 are plotted as a function of system elasticity (elasticity being defined as deviation μm per kg force). The cumulative rubbing distance of each run has been 10 m. For high system elasticity the friction values of both materials are greater than for low elasticity. In the more elastic system the static friction coef-

ficients are higher up to 20 % than the dynamic values wile this difference is substantially reduced with decreasing elasticity (increasing rigidity). Friction values of approximately identical magnitude were obtained from different test sections when their oscillation behaviour as a function of geometry, mass, and elasticity were similar. These results are shown for a mean drive velocity of 25 mm/min. Similar results are obtained with sliding velocities in the range of 0.25 to 150 mm/min /48/.

8.2.5 Influence of Sliding Velocity

Under varied sliding velocity friction and wear behavior has been tested for cermets, ceramics and high temperature alloys /49/. Most of the materials used in this program were standard commercial materials for which considerable properties information exists in the literature. But, as a matter of fact, ambient conditions and atmosphere were different from those in a Sodium Cooled Fast Breeder Reactor.

In specific areas in the reactor core relative movements are cyclic at very different time dependent relative rates. The simulation of such movements in test facilities is generally performed by means of excentrics or crankshafts. The experimental results obtained are assigned in general to "mean" velocities. This poses particular problems at high temperatures and low driving rates. At such conditions the friction movement is no longer continuous but intermittent (stick-slip) /35, 36, 50/.

The design and selection of materials for the fuel element duct load pads in fast reactors are of high interest. Static friction to be classified between static welding and dynamic friction plays a particular role in this context. Static friction is a variable with short-term occurrence at the beginning of each friction movement and it is not insignificant whether this friction movement takes place after extended dwell times or after only short-term interruption of the rubbing process in case of stick-slip. These important aspects for the design of tribological test sections and for comparison of results were investigated in numerous specific experiments /51/. First of all, slow movement has been analyzed for one single stroke of oscillating friction. A friction force plot has been traced (Fig. 68). It is characteristic in case of stick-slip. The movement carried out by the specimen in a number of individual steps is of intermittent characteristic. Between these

steps, the materials remain under static contact. Different velocities could be assigned to this friction diagram: An average drive velocity V_a or the instantaneous velocity V_d of the drive system. Both don't describe exactly the prevailing motion. During each individual friction step occur relative movements between the material pairs. Then one can assign the real rubbing velocity V_t wich is in general higher than the drive velocity.

Whilst Fig. 68 represents a more schematic description Fig. 69 shows the quantitative situation. The real rubbing velocity is plotted as a function of different average drive velocities V_a. The increasing average drive velocity is associated with a rise in the real rubbing velocity but between both is no proportionality. At very low driving rates (0.25 mm/min) one gets $V_t \approx 25 \times V_a$ and at the highest we obtained $V_t \approx 4 \times V_a$.

There is also no proportionality between the static friction coefficients and the real rubbing velocity. So far, the static friction coefficient is rather a function of the rest time of the specimens in static contact between the friction steps. Results of experiments from other test sections seem to sustain these results and showed a good agreement.

The influence of the average drive velocity V_a on static and dynamic friction coefficients of Stellite 6 and Inconel 718 shows Fig. 70. The static friction factors are again higher than the dynamic ones and the differences between them are reduced with increasing drive velocities. Most interesting are these results in the lower range of drive velocity $V_d \leq 2.5$ mm/min where the static friction coefficient is essentially higher (50 - 60 %) than the dynamic value.

8.2.6 Superimposed Oscillating Movement

This problem has been tackled /52, 53/ and certain different wear mechanisms were recognized. But relative movements between contacting components in the reactor core may take very different courses:

- Translatory movements at a low rate during replacement of fuel elements.
- Oscillating and intermittent movements, respectively, at a low rate due to thermal expansion.
- Higher frequency vibration caused by hydraulic influences from the cooling medium or by a special type of stick-slip-friction.

In most cases slow movements caused by thermal expansion and hydraulically induced vibrations occur at the same time (superimposed). Some important questions have arisen to this effect:

- Which evidence is provided by test results obtained for simple movements as regard the complicated movements to be expected in the reactor ?
- Do friction coefficients and wear rates undergo general variations in case a high frequency oscillation is superimposed on a lower frequency movement?
- Which influence is exerted by cycling load paralleling such movements on the behavior of friction systems ?

To answer these questions a series of representative experiments have been performed /54/ with two material pairs like on like:

- chromium carbide LC-1H,
- Tribaloy 700 (Ni-base, 35 % Mo).

The results from the tests with CrC (tests No. 330-335) in which the vibration-frequency was varied (at constant vibration amplitude of $\pm$ 0.1 mm) have been plotted in Fig. 71. The first part of the test up to a time of 1.5 h was conducted in the absence of superimposed vibration (vibration + 0) and with the standard movement applied in earlier tests ($\pm$ 5 mm, 0.12 Hz, approximative 145 mm/min). The expected friction factor values known from previous tests were obtained. In the subsequent test procedure the superimposed vibration frequency was varied from 2.5 to 40 Hz. This resulted in unessentially increasing friction coefficients with increasing frequencies up to 5 Hz. If there was only vibration without the primary movement ($\pm$ 0; 40 Hz), friction coefficients were registered slowly decreasing.

A similar picture was obtained when the amplitude of the movement was varied from 0.1 to 0.5 mm at a constant frequency of 10 Hz (Fig. 72). A slightly increasing tendency of the friction coefficients is exhibited, caused by increasing amplitudes. The mean values of the experimental results from each test step of constant parameters are nearly identical, if the product of amplitude and frequency, i.e. the mean friction velocities are equal.This is especially indicated for tests No. 336 through 341 with Tribaloy 700 in the diagrams (Figs. 73, 74). Columns with same symbols represent nearly identical friction factor scattering fields as a function of similar mean friction velocities.

For comparison in Figs. 71 and 72 the dynamic friction coefficients obtained from experiments at standard conditions are indicated in the diagrams. It can be seen that friction coefficients from the experiments under superimposition of movements at varying amplitudes are lower with respect to the standard experiments, even at comparable or longer cumulative rubbing distances.

As to wear measurement tests were made with newly treated specimens in each case. The tests were stopped and the specimens dismantled after cumulative rubbing distances of 115; 230; and 345 m, respectively. Than, using the Abott plot, the bearing area of the profile of surface was determined and the results compared with a weight assay each.

The wear rates volume measured in two experiments after constant rubbing distances are shown in Fig. 75 at equal cumulative rubbing distances. Higher wear values (about 30 %) were measured for high frequency movement as compared to the values obtained at lower frequencies.

8.2.7 Superimposed Cycling Normal Load

In the tests No. 342-355 /54/ first a static load of 200 N was applied to the specimens and a rubbing distance of 5 m was operated. Than the load was increased to 1000 N and another 5 m of rubbing took place. In the following test step and subsequently, a cycling load was superimposed to the static load and the test was conducted over a total rubbing distance of 50 m. As shown by the measuring results, Fig. 76, the friction forces were proportional to the load cycles independent of the respective amplitude. Accordingly, the mean friction coefficients are independent whether the load was statically applied or cycling.

The material wear caused by friction proves to be proportional to the maximum normal load $\bar{F}_N$. This applies likewise to small loads up to $F_N < 400$ N (20 MPa). With the load getting higher $F_N > 1000$ N, a greater increase in surface wear is observed (Table XXX).

8.2.8 Different Test Section Systems

When our test results were compared with the results supplied by other research establishments, problems occassionally arose because in most cases

dissimilar test parameters had been selected and different test section-systems used. To find a basis of comparison, above all between work performed at KfK and work performed at USARD, special tests were agreed. They were based on the test sequence previously used at USARD (Fig. 26). To be able to conduct the planned tests within a limited period of time, considering the test bench capacity available, slightly shortened precorrosion and interim corrosion times (dwell) were chosen at KfK. The friction tests proper were performed with LC-1C specimens in the same sequence and with the majority of test parameters being identical. Minor differences appear in the specimen diameters imposed by the test section systems and the resulting amplitudes of movements (on account of the requirement that amplitude A = specimen diameter d and A = d/4, respectively).

With the core clamping system in SNR 300 and the reference data supplied by USARD as the background, the interest concentrated on the friction coefficients in the tests performed.

The results from the tests No. 356-369 (dynamic friction coefficients, μ_d) have been summarized in Fig. 77.

For comparison, the scattering fields of the LC-1C data measured at USARD and determined at KfK are also indicated. It is evident that

- the USARD values on the whole are slightly more favorable than the KfK results;
- the USARD friction plots exhibit stronger fluctuation and a less pronouced tendency to increase, above all during the first 648 K phase (see Fig. 26);
- the KfK plots take a steadier course although the rise is almost uniform. This behavior can be ascribed to the wear induced change of surface (smoothing) and to the sodium storage capacity between the contact areas which diminishes in parallel;
- in both cases lower values are measured after the last dwell (39 hours) at lower sodium temperature as compared with the preceding test phase;
- the lowest static and kinetic friction coefficients were obtained in test section IIb having the lowest system elasticity;
- high values of breakaway were not measured in all cases in the KfK tests. Moreover, it seems important in this context whether dwell takes place under normal tension (standstill in the dead center of the system) or under

tangential tension (standstill in the middle of the stroke);
- the surface changes occurring during the tests are evident from a comparison of the profile diagrams. The plot A in Fig. 78 has been recorded prior, the plot B after the friction test. They are shown representative for all worn surfaces of this test series. The wear of the relatively hard material is mainly abrasive in its nature. The tips of the micro-asperities were abrased but not deformed. A smoothed real contact area (macro-profile bearing area) is spread like a network over the specimen surface (Fig. 79). The individual surfaces exhibit an extremely good smoothed appearance with nearly no friction grooves detectable in the direction of movement.

To be able to compare the greatest number of results, tests were also performed with Inconel 718 and Stellite 6, respectively, under USARD test conditions (tests No. 370 - 375). Results shown in Fig. 80 are in satisfactory agreement with friction coefficients obtained under KfK-IA standard test conditions.

8.2.9 Macro-Surface Roughness

When differing coating materials resistant to wear and the related differing processes of application are used /55/, the question arises of the optimum surface roughness. Tests were performed in which LC-1H specimens were used with three different roughness values:
- brushed surface, Rt < 30 µm;
- ground surface, Rt < 5 µm;
- lapped surface, Rt < 0.5 µm.

All tests were conducted over a total sliding path of 100 m. After 20 m of sliding path each a standstill of 16 h (dwell) followed when the specimens under load had established a static contact at the test temperature.

Figure 81 is a comparative summary of the dynamic friction coefficients measured for the three surface qualities under consideration (tests No. 376 - 389). The different friction coefficients for different surface roughness in sodium are shown in a first step to be dependent on the different volumina of the liquid medium stored between the contact areas. In a second step this sodium is responsible for the chemical reactions taking place on the surface or also for the adsorption effects with the associated decrease in surface energy.

- For the lapped specimens values up to $\mu_d \leq 1.2$ /56/ were measured. On account of excessively high mechanical stress of the test facility, experiments had to be discontinued before the end of the planned test duration.
- The friction coefficients were more favorable for specimens with ground surfaces ($\mu_d \leq 0.88$). However, for friction loaded components in the reactor these values are not acceptable.
- Only the friction coefficients of the brushed specimens - mainly at the onset of friction after standstill periods - comply with the requirements expressed by the reactor manufacturer. However, also in a continuous sequence of movements they attain $\mu_d \approx 0.65$.

In the tests No. 382-384 the specimens were withdrawn after 20 m sliding path each and measured in order to determine the wear rate. The change of surface caused by wear was determined by comparison of the surface bearing area prior to and after friction, respectively. The wear rate in this case was measured with $K = 6.10^{-11}$ $cm^3/cm.kgf$. After reinstallation of the test section friction coefficients were extremely low (Fig. 82). However, their difference as a function of different surface roughness is still evident. For these results one presumable reason might be seen in a extensive surface oxydation descented from the handling procedure.

The influence of the surface roughness on the friction behavior of LC-1C was likewise studied in dry Ar atmosphere, tests No. 390-392 (gas assay see Table A II). All operating parameters correspond to that in the preceding tests performed in sodium. Figure 83 shows the mean dynamic friction coefficients recorded. For all three surfaces they are clearly lower than in the preceding tests (0.13 up to 0.5). The originally differing values converge in the first test (run-in) phase into a very narrow scattering band. Also during the next four partial tests neither a rise nor a noticeable divergence of measured values is observed. Contrary to the tests in sodium, the most favorable values for lapped surfaces are partly measured in these latter tests.On all three surfaces similar wear mechanisms were effective. On ground and lapped specimens adhesive wear predominates, on brushed specimens abrasive wear. On the lapped and brushed specimens material transplantations (smearings of binder material) are clearly visible. On the other hand, the abrased particles were accommodated in the rather large cavities of the brushed specimens.

On the brushed surface (which offers the highest interest because of the

friction coefficients measured) a network shaped contact area develops while the macro-profile is leveled out. The micro- profile of each worn asperity is comparable with that of the ground and lapped versions, respectively.
The wear rate determined for brushed surfaces in several tests in sodium is 1.4×10^{-11} cm^3/cm Kgf (mean value). The wear rates in argon are higher by approximately a factor 10 than the values determined in sodium.

8.2.10 Formation of Particles

In all former friction experiments carried out under continuously rotating movement most of the wear particles were removed from the surfaces by the liquid sodium. In experiments under oscillating relative movement, particles remained between the surfaces and were found to be very different in shape and size. This caused a number of attempts to be made to find any connection between the frictional behavior of the material couples under investigation and the particles. Several models were discussed /57,58/ and special experiments have been carried out to support the models /59/.

With LC-1H material specimens eight tests (No. 342-347;402;421) were carried out with

- ground surfaces (Rt $\leq$ 5 µm) } in Ar
- brushed surfaces (Rt $\leq$ 40 µm) }
- ground surfaces (Rt $\leq$ 5 µm) } in Na
- brushed surfaces (Rt $\leq$ 40 µm) }

The sodium temperature was 773 K and the cumulative rubbing distance 40 m. Oscillating relative movement with a stroke length of $\pm$ 0.5 mm has been modified to $\pm$ 2.0 mm after 30 m of rubbing distance.

The diagram of measured friction coefficients is given in Fig. 84:

- With smooth surfaces and short stroke oscillation ($\pm$ 0.5 mm) high friction coefficients were measured in argon as well as in sodium. Even a change of the stroke length ($\pm$ 2 mm) at a rubbing distance of 30 m did not effect the friction coefficients.
- With rough surfaces the change of the stroke length led to a temporary change of the friction coefficient in both argon and sodium. At this time the particles were stripped off the surfaces disappearing in the macro cavities of the contact areas. This enables the rubbing components to get

back in a closer contact, a process in general accompanied by increasing friction coefficients. In sodium, the more remarkable ascent of the friction coefficient (at change of stroke) may be assigned additionally to the displacement of the liquid from the surfaces.

8.3 Special R&D-Work

8.3.1 Fuel Element Duct Load Pads

Stellite 6B (0.9 mm sheet material, spot welded on steel 1.4961) was discussed as a possible Duct Load Pad Material. Hence, respective friction experiments were carried out in test section I. The three pin specimens (of the "pin-disk system") were fabricated of Stellite 6H and the sheet material (Stellite 6B) has been spot-welded on the disk specimens (tests No. 296-300). Friction curves of these experiments are shown in Fig. 85 for comparison with the results obtained for Stellite 6H (Fig. 34). As a possible cause of the higher average friction forces with Stellite 6B, it was found that, sliding of the relative small pin specimen led to a wave of deformation on the sheet material. The respective front edge of the pins (in the direction of movement) had the same effect as a cone so that macro-grooves developed.

Tests dealing with Stellite 6B (sheet material) as duct load pads were no longer carried out in the "pin-disk" specimen configuration.

Dispensing with high surface contact pressure (obtained in test section I), one modified then the material specimens such that a contact area of 15 x 13 mm was available. This was at the same time an approximation to the actual operation conditions as regards the ratio of the amplitude of motion A to the length of the duct load pad in the direction of motion d($A/d \ll 1$). Just for comparison, tests No. 301-305;310 were conducted with Stellite 6B under standard operating conditions in test section II, but with the "sheet metal character" as the parameter of interest.Also in this case (Fig. 86) the measured friction coefficients fluctuated more and more with increasing rubbing distance. They were also higher than for Stellite 6H. But to a certain extend the measured apparent friction forces were rather mechanical forces partly caused by the surmounting of sheet deformation.

However, the specimen surfaces obtained by cup-and-cone grinding were not

satisfactory (difficulties during grinding). This prevented the sliding surfaces from uniform contacting. Figure 87 shows the wear tracks of the pairing No. 301. As the consequence, the test results were recorded for a non-defined and considerably higher surface contact pressure than had been assumed. In the zones of the wear track cleared alternately, a different degree of smoothing was attained whilst in the central area asperities and material displacement occurred.

8.3.2 Centring Knubs / Tank Wall Geometry

The phenomenon to be investigated was the maximum weakening that must be anticipated if approximately 250-300 movements occur after periods of dwell of different durations. Throughout 16 experimental runs 20 movement cycles (± 0.5 mm) each were carried out after dwell times ranging 0 up to 13 h. The material under investigation was steel 6770.

The following tribological values, which could be assessed by measurements, were determined in tests 415 and 416:
- Break-away at the onset of movement,
- The mean dynamic friction coefficient during cycling movement,
- The depth of surface lesions brought about by wear.

Fig. 88 shows the friction coefficient recorded as function of the dwell time. According to the diagram, break-away turns out to be a function of this parameter. Its level up to 4 h dwell clearly increased from 0.7 to 1.2 and subsequently stayed at a mean value of about 1.25. At the same time the mean dynamic friction coefficient was found to vary in a range between 0.65 and 0.85 with a small dependence on the previous dwell periods.

Surface wear resulted merely from deformation and material transplantation on both sides. The maximum depth of penetration of the wear marks was about 200 µm.

8.3.3 Heat Exchanger Tube Guidance

In the experiments described below, it had been determined
- the severity of wear on heat exchanger (HTX) tube walls both in concentric array and in tube support (tube plate) configuration,

- the static and dynamic friction coefficients with respect to the friction forces expected in a concentric pipe system or in a HTX-tube plate.

Therefore 1500 movement cycles of ± 5 mm were carried out in each test run (tests No. 417 and 418) with the material couple Colmonoy 5/6770.

The friction coefficients measured between the spacers and the pipe wall are plotted in Fig. 89 as a function of rubbing distance for 523 ad 823 K. No significant difference is recognizable between the values measured in these temperatures. However, the change in surface roughness brought about by wear between the spacers and the inner wall of the tubes is relatively slight. At 523 K the roughness left over from finishing of the pipe surface (Rt < 20 µm) was more or less smoothed out (Rt < 5 µm). At 823 K, major material deformation is evident, especially at the edges of the contact areas.

8.3.4 Heat Exchanger Tube - Tube Plate

The components taken into account and the specimen geometries considered differ merely in the smooth and finned outer tube surface. The friction coefficients measured in the two systems are shown in Fig. 90 as a function of rubbing distance and for two sodium temperatures of 523 and 823 K. (6770 - Colmonoy 5) tests No. 419 and 420.

For the smooth tube surface, the friction forces turn out to be a function of the temperature. However, in the finned tubes there is no major difference between the friction coefficients.

A corresponding difference was also found in the wear action. While, on the surface of the smooth tube, a depth of penetration of the wear mark of 80 µm was measured, the changes at the fins were comperatively slight (Fig. 91). In this case, there is abrasion and material displacement, respectively, at two diamtrically opposite points with a maximum depth of approximately 20 µm, measured from the originaly cylindrical surface of the shell.

8.3.5 Cladding Tube/Spacers (austenitic)

For the design of the KNK II carbide test element first a friction coefficient $\mu < 1$ was assumed between cladding tubes made from steel AISI 1.4970

and grid spacers made from steel AISI 1.4981. This important variable as regards axial loading of the structural rods and twist loading of the spacer grids, respectively, had to be supported by experimental results. Due to the far reaching importance of these studies, also with a view to fuel elements and helical spacers, the tests were performed with two different specimen shapes (tests No. 422 - 433). The specimens according to Fig. 18 simulate the cladding tube grid spacer system and had been used in test section II. The design according to Figs. 16(in test section I) and 17 (in test section II) realized the cladding tube wire spacer geometry. In test section II the relative movement was an oscillating one in the direction of the cladding tubes axis ($\pm$ 1 mm). In test section I oscillation led to a relative movement transverse to the cladding tube axis, (also $\pm$ 1 mm).

According to a given test program the friction test proper followed a precorrosion time (dwell) of six hours each. At the end of a friction path S_R = 160 mm (64 minutes) dwells of 16 and 6 hours, respectively, were observed. The temperature and the loading were varied as the test parameters. The grouping of specimen geometries and the temperature variation are evident from Table XXVII (Test matrix 22).

The friction coefficients measured for the same normal load (F_N) at three temperatures are compiled in Fig. 92 (for F_N = 8 N), Fig. 93 (for F_N = 15 N), and Fig. 94 (for F_N = 30 N). At F_N = 8 N and F_N = 15 N the maximum values attain $0.6 \leq \mu_d \leq 0.7$. At F_N = 30 N maximum values of $\mu = 0.9$ are attained in the least favorable case at 633 K. But also in this case the value $\mu \leq 1$ previously assumed is not exceeded.

Wall weakening on the cladding tubes caused by wear was measured and recorded at all loci of contact. The diagrams plotted in Fig. 95 for three loadings at 873 K are given as examples. Although the wear scars have a very irregular appearance (difficult to measure) some proportionality of wall weakening to the load applied is evident. At F_N = 30 N a material abrasion of 100 μm at the maximum is obtained.

8.3.6 Cladding Tube/Spacers (ferritic)

Very highly fluctuating friction coefficients were recorded in tests No. 464-477 for the DTO_2 cladding tube/helical wire system (Fig. 96). Also the mean

value, especially for low loads (F_N), is very high as compared with the friction forces in the pin-disk system (Fig. 47). This difference can be attributed largely to the different contact geometries but also to the different friction velocities /60,61/.

Material wear on the cladding tube specimens lead to weakening of the tube wall. To record this process quantitatively, the profiles of the wear tracks were recorded at least at three points transversally to the direction of movement (Fig. 23). In Figs. 97-99 representative diagrams have been plotted as an example of the wear scars produced under different loadings. Here and also in the following photographic picture (Fig. 100) the proportionality of the wear effect to the load applied (F_N) is clearly visible.

The transverse micrographs in Fig. 101 illustrate that the high ductility of this material is the cause for strong, mainly adhesive wear.
The results of these tests were made available to SCK-CEN where a decision will be taken about a further development of DTO_2 and B_3.

9. SUMMARY

9.1 Materials

In a multitude of screening and parameter tests some few materials in "like on like" pairings have produced to be of particular value. Since most of the materials investigated have relatively high wear resistances, mainly the friction coefficient was used as a criterion of their assessment in relative terms. Their grouping into the category of favored materials was based on results from own experiments and on reference data supplied by other research establishments. This gave the following detailed picture:

The evaluation of Inconel 718 is based on friction diagrams measured under comparable conditions. In Fig. 102 the solution annealed material is indicated together with the hardened material. Thereby lower friction coefficients are indicated in the average for the annealed version (718an).

The friction coefficients of Stellite 6 were more favorable on the whole than that of Inconel 718. In Fig. 103 the scatter band of the friction diagrams

has been represented for standard tests involving Stellite 6H. For comparison, up to a friction path of about 10 m measuring data from parameter tests have been added. The likewise represented scattering field concernes the sheet metal Stellite 6B.

Although under given conditions friction coefficients $\mu > 0.57$ were measured for some pairings, a portion ≈ 20 % of these higher friction values seemed to be admissible according to the statistical distribution with a view to their use as fuel element duct load pad materials (Fig. 104). In this diagram data was considered obtained from corresponding experiments realized in INTERATOM test facilities.

After these results have been obtained and compared with the friction and wear coefficients, respectively, of all the other materials investigated the

INCONEL 718 and STELLITE 6

were retained as reference duct load pad materials for the Mark I core of SNR 300.

On account of the Cobalt content of Stellite 6 and the partly higher friction values of Inconel 718, these two materials should be substituted in the long run by Cobald-free alternatives having the same or better tribological properties.

Promissory new developments recommended by industry were:

LC-1H (Cr_3C_2)
TRIBALOY 700
INCONEL 718 A (NiAl).

For comparison, they were tested under standard conditions; the friction coefficients obtained are represented in Fig. 105. Although the values measured for LC-1H (1C) exceed the specified upper limit, especially after a long friction path has been covered, the scattering field as a whole is identical to that of Inconel 718 (solution annealed and aged, respectively). The situation is a bit more favorable for short sliding paths ($S_c < 25$ m) or in case of intermittent movement with clear regeneration of the oxide layers

possibly present on the rubbing surfaces. Very positive results have been obtained both for Tribaloy 700 and for Inconel 718A. According to this data all three cobalt-free alternatives can be recommended as substitutes to Inconel 718 and Stellite 6 as duct load pad materials.

Their use in a number of other components is likewise conceivable, i.e. in

- control rod guide,
- fueling machines,
- fittings,
- core clamping system,
- tube centering (knubs),
- tube supports.

The decision in favor of one or the other of the three materials presented will be determined to a considerable extent by aspects of processing and machining techniques.

- diffusion (Inconel 718 A),
- D-gun (LC-1H),
- plasma or D-gun (Tribaloy 700).

The coating method to be selected can in its turn be determined by:

- the geometry of the respective component:
  . accessible to machining,
  . admissible temperature of machining
  (solid material/sheet metal),
- the type of loading
  (adhesive force of coating exposed to shocks or bending forces and thermal shocks, respectively).

9.2 Chemistry

Because of the relative movements which take place among contacting components typical of the reactor core, hydrodynamic lubrication through the flow medium is missing. It is partly replaced if due to the chemical reaction of the materials involved with the liquid sodium, oxide layers may be formed.

Sodiumchromite and/or complex (refractory-) metal-oxide films of different thickness and also wear debris are more or less stable at the different experimental conditions (sliding distance, interface loading, exposure time, temperature).

Besides the reaction temperature and the time, the O_2-content in sodium and the alloy constituents of the materials play an important role. This was confirmed by the test results obtained. Accordingly, above all chromium carbides as well as cobalt and nickel alloys with a Cr-content > 15 % exhibit lower friction coefficients at the end of dwell times (without friction movement). The duration of effectiveness of such layers obviously depends greatly on the friction load. This process has a positive effect above all in control rod guides where short-term intermittent movements alternate with relatively long standstill times.

However, there is in general no proportionality between the reaction time and the quality of the layer. It gets clear by the example of Stellite 6 that up to an exposure time of 100 hours a chromite layer is formed which favors friction. In case of longer test periods (> 6000 hours) mass transport causes morphological changes of the surfaces. Grown metallic crystallites (Fe and Co, respectively) are responsible for the loss of the originally favorable tribological properties present.

Also for Inconel 718 a similar influence of surface chemistry on the friction behavior was detected both in the solution annealed and in the hardened conditions. If one can select among several materials with similar tribological qualities, that with the highest Cr-content should be preferred.

The friction properties of material pairs in cover gas (Ar) saturated with sodium have proved to be more favorable than those in liquid sodium. On the other hand, surface deterioration as a function of material wear was rather more significant in this medium.

9.3 Normal load

The influence of load and the resulting contact pressure, respectively, on the friction and wear process may be very different:

- If two bodies with great surface roughnesses (detonation,-D-gun plated, brush finished) are moved relatively to each other, the asperities can be overcome only if the two bodies change their mutual mean distance in a very short rhythm. In every movement "away" from each other the direction of friction corresponds to the flank angle of asperities. In each case the forces acting normal to each other on the sliding surfaces must be overcome. As long as such a surface topography is maintained, this play of forces causes the friction coefficients specific for the material to be falsified.
- In most cases leveling out of the amorphous surfaces starts already in the "run-in phase". The asperities are sheared off in a "cutting" process whose development with the time is greatly determined by the forces applied normal to the movement. During this leveling out process a gradual transition takes place (above all in less hard materials) of friction under plastic contact to friction under elastic contact.
- The amount of contact pressure also determines the life of the oxide layers lowering friction coefficients.

As already indicated in the previous section chemistry oxide layers must be recognized as a welcomed aid in managing friction problems encountered in sodium cooled reactors. Wherever possible, surface pressure stresses should therefore be so chosen that existing or regenerating oxide films are maintained as long as possible. As in all processes of wear, the pressure stress and friction path are the decisive variables also for abrasion of the oxide layers. This is confirmed by a number of friction experiments. The low friction coefficient initially favored by an oxide layer increases at a flatter rate for lower contact pressure and at a steeper rate for higher pressure stresses to attain finally the values specific for the base material.

If friction systems have sheet metals on one side, the geometry of the opposed side must be chosen such that for the greatest possible contact area the smallest possible pressure stresses occur. In case that components with small contact areas are moved along sheet metals at excessively high pressure stress, sheet metal deformation cannot be ruled out. The consequences may be high edge pressure stresses with plowing and hence concentrated wear.

9.4 Temperature

The influence of temperature on the friction processes in liquid sodium is not a direct one. The temperature is rather responsible for an entire parameter field, each variable of which may exert a different influence on the friction process:

- O_2 activity in sodium,
- viscosity of sodium,
- surface tension,
- material hardness,
- self-welding tendency.

If refractory steels and other refractory materials are used, hardly any noticeable changes in hardness result from the influence of temperature. The tendency to self-welding increases to a limited extent with rising temperature.

The surface tension of sodium is so reduced at temperatures $T < 600$ K that wetting of most of the metallic materials is ensured. The penetration and the amount of sodium left between the contact areas are likewise determined by the surface tension.
The temperature determines the oxygen activity of sodium and hence the availability of O_2 for the formation of complex oxide layers.

The temperature is likewise responsible for the viscosity of sodium. It attains the order of magnitude of the viscosity of H_2O. It is too low to cause, together with the reactor typical slow relative movements, the formation of load bearing hydrodynamic lubrication layers. These aspects probably explain why it is so difficult to attribute friction and wear coefficients to a given temperature. Statistically speaking, a slightly increasing tendency of friction coefficients with rising temperature can be noticed.

9.5 Temperature/System Elasticity

In most friction processes ambient temperature, system elasticity and relative rubbing velocity are acting superimposed at very different rates.

As a result of numerous experiments it was found that a relative velocity of the order of cm/s does not significantly influence the friction coefficients. But slow movement (mm/min) accompanied by both high temperature and remarkable system elasticity may cause the friction forces to increase. To prevent stick-slip friction conditions it may be helpful to inrease the average rubbing velocity. This (trick) should be supplemented by an increased rigidity of the system.

The total elasticity of such a friction system is composed of the elasticity of

- the constructional elements,
- the measuring cells,
- the friction materials employed.

For designing a tribological test the criteria applicable to the original components in the reactor core should be known and simulated.

9.6 Superimposition of Movement

If in a friction process higher frequency vibrations are superimposed to low frequency basic movements or cycling loads are superimposed to a static load, this entails a modification of the tribological behavior. For the materials investigated the tendency of diminishing friction coefficients caused by superposition of movements is recognizable.

This means in practice: Vibration favors the slipping behavior between sliding componets in the reactor. This experience could be helpful in lowering or raising a subassembly in the charge chute. For instance, application of a vibromotive force to the gripper of the fuel handling device should be recommended. By this variation the friction forces for several types of interference and misalignment may drop to an acceptable value.

Parallel to the normally greater cumulative rubbing distance in case of vibration the amount of wear is increased. In a primary movement with a small amplitude this wear may be relatively high locally. However, in a long-stroke primary movement it may be spread over a wide zone of contacting surface. This essentially depends on the conditions prevailing in each individual case.

9.7 Surface Roughness/Particles

Machining and finishing processes, respectively, are most determinant regarding the macro-roughness of surfaces. Whilst smooth surfaces (lapped, polished) are necessary to establish hydrodynamic films in rotating bearings, rather rough surfaces would enable friction systems to operate reliably in the reactor core. An optimum surface topography is given by the D-gun plating of various coating materials accompanied by brush finishing. However, a run-in process of those surfaces led to the production and formation of wear particles affecting the wear and friction coefficients in an incalculable way. From the experiments carried out in the past it was found:

With the smooth surfaces (lapped; ground) only very few small particles are formed with sharp edges and hardened by corrosion and/or cold working. The particles modify their shape during frictional processes (forming needles or rolls) but they do not grow to a size causing the surfaces to separate. With rough surfaces (brushed) many more particles are produced during flattening of the macro-asperities. Their development in terms of hardness and shape seems to be similar and capable of separating the mating components in the contact area. Also an effect of rolling particles, acting as micro bearings, could be paralleled by more intensive wetting of the surfaces. Since this relatively uncertain mechanism does not favor frictional processes in all cases, a surface finish may be recommended to compensate the wear in process. By careful grinding only the peaks of the macro-asperities should be removed. So, a network-like smooth bearing area provides low pressure contact, whilst a sufficient number of cavities enables the sodium to remain between the mating surfaces.

9.8 Original Geometry

In tribological experiments involving original structural components and model geometries reduced in scale, respectively, a picture is best obtained of their actual in-pile behavior. However, the range of validity of the test results obtained is greatly limited to the component under consideration. An application to other components is only possible if very special prerequisites are fulfilled concerning transferability.

The experiments described in section 8.3.1 concerned components of given

geometries. The objective of the investigation was to answer the question connected to each individual case in order to clarify the functional behavior of the respective component under original conditions.

The test results were interpreted under this aspect:

- For the fuel element duct load pads sheet material (Stellite 6, Inconel 718) was selected for being spot welded to the rubber tube. This situation was exactly simulated for the experiments. Also the type of movement and normal load (F_n) approximated original reactor conditions. According to experimental results, a non-uniform contact area may be expected causing fluctuating friction during relative movement. But even maximum friction coefficients did not exceed the given limit $\mu_d \leq 0.57$.
- The knobs centering the thermal shock shield with respect to the tank wall do not cause significant weakening of the tank wall, not even after about 300 relative movements.
- If the concentric (heat exchanger) tube systems the centering knobs are coated with a material whose favorable tribological behavior with respect to the tube wall material had been confirmed in standard experiments, a reliable performance of the friction system can be expected also in the original geometry.
- The advantage of finned over smooth tubular surfaces is due to the fact that relatively much sodium can be left in the cavities between the fins. Thus, in case of axial relative movement the frictional surfaces are sufficiently wetted by the medium. Appropriate tests have shown that this reduces mainly the self-welding tendency of the contacting materials.
- For the austenitic cladding tubes contacting both grid and wire spacers (1.4970/1.4981) lower friction coefficients ($\mu_d \leq 1.0$) were found than initially assumed in the design work.
- The results for ferritic cladding tube spacer systems provided indications of the further development work concerning the materials under consideration.

A question not yet answered satisfactorily concerns the transferability of tribological test results both from simplified test geometries to components of the original geometry and their general validity for components of different shapes and sizes. However, it can be recognized without any doubt from the multitude of test results obtained:

- The judgement of the comparability of tribological systems concentrates on the (relative to the contacting components) often very small points of contact. They are mainly characterized by their contact geometry:
  - flat on flat (flat contacting),
  - cylinder on flat (line contacting),
  - sphere on flat (point contacting),
  - crossed cylinders (point contacting).

If such systems are simulated as precisely as possible in shaping friction pairs for test purposes, a major prerequisite is already fulfilled for the transferability and comparability of tribological data. Obviously, all the rest of operating parameters must be identical to the friction processes to be compared. Some difficulties are encountered here in the special case of system elasticity. It is determined mainly by the shape, mass and material specific elasticity of the components sliding against each other. For laboratory testing it is therefore recommended that the test section elasticity is kept variable and that it is adapted in the individual case to the original conditions.

Only if the said prerequisites are fulfilled, the transferability from one case to the other is permissible. In experimental systems set up to determine favorable material pairs the specimen geometry plays a minor role. However, if possible, it should be identical for all tests to be compared.

10. REFERENCES

/1/ W.A. Glaeser: "Survey and Analysis of Materials Wear and Friction in Sodium". BMI 1907, Batelle Columbus Lab. (1971)

/2/ K. Natesan, T.F. Kassner, Che-Yu-Lit: "Effects of Sodium on Mechanical Properties and Friction Wear Behavior of LMFBR Materials". Reactor Technology Vol. 15, No. 4 (1970)

/3/ P.H. Delves, W. Rodwell: "Mechanisms in Sodium", I.A.E.A. S.M. 130/14, Sodium-cooled Fast Reactor Engineering, Proceedings, Monaco 1970, p. 757-769

/4/ R.J. Jackson et. al.: "Experimental Fuel Subassembly Irradiation Experience in EBR-II", Int. Conf. on Fast Breeder Fuel Performance, Monterey, U.S.A., (1979), HEDL-SA-1518

/5/ E. Wild, K.J. Mack, G. Drechsler: "Das Verschleißverhalten von Werkstoffkombinationen in flüssigem Na. Versuchseinrichtungen und experimentelle Ergebnisse". KfK 1659 (1972)

/6/ E. Wild, K.J. Mack: "The Friction Characteristics of Steel and Alloys in Liquid Sodium". Proc. of the International Conference of Liquid Alkali Metals, Nottingham U.K. (1973), 4-6 April 1973, S. 191

/7/ H.W. Roberts: "Friction and Wear Behavior of Sliding Bearing Materials in Sodium Environments at Temperatures up to 600 ^{o}C". TRG Report 1269 (1966).

/8/ M.J. Todd, A.L. Garnham, S. Turner: "Tribology of Stainless Steel in Sodium Liquid and Vapour". Proc. Instn. Mech. Engrs (1968-69), Vol. 183, Pt. 3 I p. 61

/9/ A.W.J. de Gee, J.W. Tichler: "Wear under Fretting Conditions - Some Experimental Results". TNO-Report Apr. 1968

/10/ A.W.J. de Gee, C.P.L. Commisaris, E.G. Chirer, A. Bogers: "Equipment for the Study of Wear under Conditions of Oscillatory Relative Motion". TNO-Bericht Nr. 39 (1967)

/11/ E.G. Chirer, J. W. Tichler, C.F. Etienne, W. Dortland, E.C.J. Buys: "Sodium Technology Development". Program 1st Quarter 1970, TNO-Report Apr. 1970

/12/ J.W. Tichler: "Reibversuche an Inconel 718". TNO-Report M 73/06/04, (1973)

/13/ J.K. Balkwill: "Mechanical Elements Operating in Sodium and Other Alkali Metals". LMEC-68-5 (1968)

/14/ N.J. Hoffmann, D.E. Goggin, J.J. Droher: "Friction and Wear Screening Tests of Materials in Sodium". LMEC-70-10 (1970)

/15/ N.J. Hoffmann, J. J. Droher: "Materials Compatibility in Sodium". LMEC-74-1 (1974)

/16/ W.J. Freede, L. Newcomb, R.S. Kennedy: "Static and Sliding Contact Behavior of Materials in Sodium Environments at Elevated Temperatures". NAA - SR - 12446 (1968)

/17/ W.J. Kurzeka, et al. "FFTE Support Work - Friction Tests", Progr. rpt. on Fuels, Materials, Coolant Chemistry and Fuel Handling Programs, 10-12/1971, AI-AEC-13021 p. 33

/18/ W.J. Kurzeka, et al. "FFTE Support Work - Friction Tests", Progr. rpt.on Fuels, Materials, Coolant Chemistry and Fuel Handling Programs, 1-3/1972, AI-AEC-13030 p.25

/19/ W.J. Kurzeka, et al. "FFTE Support Work - Friction Tests", Progr. rpt. on Fuels, Materials, Coolant Chemistry and Fuel Handling Programs, GFY 1972, AI-AEC-13037 p. 59

/20/ W.J. Kurzeka, et al. "FFTE Support Work - Friction Tests", Progr. rpt. on Fuels, Materials, Coolant Chemistry and Fuel Handling Programs, GFY 1973, AI-AEC-13110 p. 79

/21/ R.M. Oliva, P. Horton, W.J. Kurzeka, et al. "FFTE Support Work - Friction Tests", Progr. rpt. on Fuels, Materials, Coolant Chemistry and Fuel Handling Programs, GFY 1974, AI-AEC-13125 p. 48

/22/ B. Morin: "Some Particular Aspects of Friction in Liquid Sodium". EURFNR-521 (1968)

/23/ J.P. Fontaine: "Quelques aspects des phenomenes de frottement et de fretting-corrosion en liquid sodium". Corrosion Traitements. Protection, Finition. Nov. 1971 Vol. 19 (7) p. 379-393

/24/ G.V. Samsonov, Yu. G. Tkaxhenko: "Temperature Dependence of the Coefficient of Friction of Some Refractory Carbides". Soviet Mat. Sic. 7/No. 3 (1962)

/25/ H.U. Borgstedt, G. Wittig, G. Frees, G. Drechsler: "Erfahrung mit elektrochemischen Sauerstoffsonden in Natrium-Kreisläufen", ATW 19 (1974) p. 357

/26/ N.P. Bhat, H.U. Borgstedt: "Elektrochemical Chaines to Measure the Oxygen Activity in Alkali Metals". Presented at the 18th Main Meeting of the Society of German Chemists. Berlin (September 1979).

/27/ J.F.M. Rohde, M. Hissink, L. Bos: "Equipment for Sampling Sodium". Journal of Nuclear Energy, Vol. 24, Pergamon Press (1970)

/28/ D.L. Smith: "An Equilibration Method for Measuring Low Oxygen Activities in Liquid Sodium". Nucl. Technol. 11, 115 (1971)

/29/ J.A.J. Walker et. al.: "Methods for the Analysis of Oxygen, Hydrogen and Carbon in Sodium".The Alkali Metals Intern. Symposium, Nottingham, The Chemical Society (London), (1967), p. 393

/30/ M.A. Shaw, E.W. Leavey: "Friction of Dry Solids in Vacuo. Phil. Mag. Vol. 10, Nr. 66 (Nov. 1930)

/31/ E. Rabinowicz: "The Determination of the Combatibility of Metals through Static Friction Tests". ASLE Trans. 14 (1971) p. 198-205

/32/ J. T. Burwell, C.D. Strang: "On the Empirical Law of Adhesive Wear". Journ. of Applied Physics, Vol. 23, Nr. 1, (1952) p. 18-28

/33/ L.V. Kraghelsky: "Calculation of Wear Rate". Journal of Basic Engineering, Sept. 1965 p. 785-804

/34/ F.P. Bowden and D. Tabor: "Reibung und Schmierung fester Körper". Springer-Verlag, Berlin (1959)

/35/ I.W. Kragelski: "Reibung und Verschleiss". Carl Hansen Verlag, München (1971)

/36/ E. Rabinowicz: "Friction and Wear of Materials". John Wiley and Sons, Inc., New York (1966)

/37/ K.J. Stout, I.R. Thomas (Edt.): Proceedings of Intern. Conference on "Metrology and Properties of Engineering Surfaces". Leicester, U.K. (1979)

/38/ D.F. Elliot, E. Holland, K.A. Tombin: "Some Preliminary Tests on Bearing Materials to Operate under Liquid Sodium". AERE R/R 1891 (Juni 1957)

/39/ W.H. Roberts: "Friction and Wear Behavior of Possible Bearing Materials in Highpurity Liquid Sodium at Temperatures up to 500 ^{o}C". AED-Conf., 1962, 042-5 (1962)

/40/ H.W. Roberts: "The Friction and Wear Behavior of Molybdenum-Tungsten-Chromium Alloys in High-Temperature Sodium Environments". ASLE Paper No. 64 LC-25 (1964)

/41/ W. Dietz, H. Weber, E. Wild: "Friction Behavior of Inconel 718 and Stellite 6 as Fuel Assembly Duct Pad Material". IAEA/SM-173/VII-18 (1974)

/42/ H.U. Borgstedt, K. Mattes, E. Wild: "Selbstverschweiss-, Reib- und Verschleissverhalten spezieller Werkstoffe in Natrium". KfK-Ext. 7/75-1

/43/ H. Schneider: "Composition of Surface Layers of Different Materials in Respect to their Tribological Behaviour in Sodium". Second Intern. Conference on Liquid Metal Technology in Energy Production, Richland, (1980) CONF-800401-P1 p. 3/43

/44/ A. Schallamack: "The Load Dependence of Rubber Friction". The Proceedings of the Physical Society. Vol. 65 B, p. 657 (1952)

/45/ H.G. Feller and K. Mälzer: "Über den Einfluß des Parameters Temperatur auf das Reibungs- und Verschleissverhalten von Metallpaarungen bei Trockenreibung". Z. Metall., 67, 8 (1976)

/46/ L.B. Sibley, C.M. Allen: "Friction and Behavior of Refractory Materials at high sliding velocities and temperatures". ASME Lubrication Symposium Miami, Paper No. 61-LUBS-15 (1961)

/47/ M.F. Amateau, W.A. Glaeser: "Survey of Materials for High Temperature Bearing and Sliding Application". Wear, Nr. 7 (1964) p. 385

/48/ E. Wild, K.J. Mack: "Friction and Wear in Liquid Metal Systems: Comparability Problems of Test Results Obtained from Different Test Facilities". Intern. Conference on Liquid Metal Technology in Energy Production. Champion, PA (1976)

/49/ L.B. Sibley, C.M. Allan: "Friction and Wear Behavior of Refractory Materials at High Sliding Velocities". ASME Lubrication Symposium Miami, FL. (1961)

/50/ D.M. Rowson: "An Analysis of Stick-Slip Motion", Wear 31 (1975) p. 213

/51/ E. Wild, K.J. Mack: "Experimental Parameter Investigations on the Tribological Behavior of Stellite 6 in Sodium". Nuclear Technology Vol. 42 (1979) p. 216

/52/ H. Uetz, J. Foehl: "Erscheinungsformen von Verschleiss-Schäden".VDI-Berichte Nr. 243 (1975)

/53/ K.H. Kloos, E. Broszeit, H.J. Schröder: "Einfluß oszillierender Normalkräfte auf Reibung und Verschleiß". Z. f. Werkstofftechnik Nr. 7 (1976) p. 220

/54/ E. Wild, K.J. Mack: "Influence of Superimposed Oscillating Movement and Load on the Behavior of Tribo-Systems in Liquid Sodium". 2nd Intern. Conference on Liquid Metal Technology in Energy Production, Richland, WA, (1980) CONF-800401-P1 p. 3/12

/55/ T. Sakamoto, T. Tsukizoe: "Metal Transfer in the Frictional Contact of a Rough Hard Surface". Wear, 47 (1978) p. 301

/56/ E. Wild, K.J. Mack: "Lubrication of Nuclear Reactor Components". Conference "Frontiers of Lubrication" Neapel 1978, Tribology International Vol. 11 (1978), p. 321

/57/ E. Rabinowicz: "The Formation of Spherical Wear Particles". Wear, 42 (1977) p. 149

/58/ A.W. Ruff: "Characterization of Debris Particles Recovered From Wearing Systems". Wear, 42 (1977) p. 49-62

/59/ E. Wild, K.J. Mack: "Lubrication Problems in Sodium Cooled Fast Breeder Reactors". Hebda, M.; Kajdas, C.; Hamilton, G.M. /Hrsg./ 3rd Internat. Tribology Congress. EUROTRIB 81. Warszawa, PL, September 21-24, 1981. Vol. 4: Other Tribological Problems.

/60/ E. Wild, K.J. Mack: "Ferritic Steels in Reactor Tribology". Conference on "Ferritic Steels for Fast Reactor Steam Generators". BNES, London (1977)

/61/ R.T. Spurr: "The "ploughing" Contribution to Friction". British Journal of Applied Physics. Vol. 7 (July 1956) p. 260-261

/62/ H.U. Borgstedt, G. Drechsler, G. Frees, H. Schneider: Unpublished Report

/63/ H. Schneider: "Investigations of Changes in the Surface Layer Composition of Materials Exposed to Sodium by Glow Discharge Optical and Auger Electron Spectroscopy". Proc. of Intern. Conf. on Liquid Metal Technology in Energy Production, Champion, PA., (1976) p. 716-722

/64/ H.U. Borgstedt, G. Drechsler, G. Frees, H. Schneider: "Chemische Veränderungen an Oberflächen von Nickellegierungen infolge Natriumkorrosion". Materials Chemistry 1 (1976) p. 217

/65/ G.A. Whitlow, R.L. Miller, W.L. Wilson, T.A. Galioto: "Observations on the In-Sodium Corrosion and Tribology of Aluminide Coatings on Inconel 718". Reprinted from Microstructural Science, Vol. 3, (1975) p. 774-787

/66/ H.U. Borgstedt: "Natriumkorrosion von verschleissresistenten Kobaltlegierungen (Stellite)". Werkstoffe und Korrosion 29, (1978) p. 81-91

/67/ H. Schneider, E. Nold: Private Communication

/68/ Du Pont Bulletin No. 1 "Tribaloy" (1973)

/69/ Union Carbide, Physikalische und mechanische Eigenschaften einiger UCAR-Schichten Coatings Service Schichtkennwerte

/70/ W. Teller: "Explosionsplattieren - Möglichkeiten und Grenzen". Sonderdruck aus Maschinenmarkt, Vogel-Verlag 75. Jahrg. Heft 100, Dez. 1969

/71/ H. Schneider et. al.: Private Communication (1977)

Movement	Oscillating, intermittent
Pressure (MPa)	< 60
Velocity ($mm \times min^{-1}$)	0·1000
Sodium temperature (K)	< 900
Viscosity	$\approx \eta(H_2O)$
O_2 content (ppm)	< 10

Tab. I TRIBOLOGICAL OPERATING CONDITIONS IN A SODIUM COOLED FAST BREEDER REACTOR

Fuel cladding/spacer
Fuel element load pads
Control rod guides
Flowmeter
Heat exchanger tube supports
Centering knobs
Valve rods, valve seats

Tab. II IMPORTANT LOCATIONS OF RUBBING CONTACT

Steels	1.4961, 1.4981 (austenitic) DTO_2, 1.6770 (ferritic)
Superalloys	Inconel 718, annealed Inconel 718, heat treated Inconel 750, Hastelloy C, Nimonic 90 Tribaloy 700
Coatings	Stellite 6 H Stellite 6 B Stellite 1 Colmonoy 5 Colmonoy 6 Colmonoy 56 Akrit Co 50 FeCr 50 Tribaloy 700
Coated carbides	WC-Ni (85-15) Ferro TiC U Ferro TiC T Cr_3C_2 (LC-1C, LC-1H)
Special task	Armco Iron TZM (Mo 99.4) Tantal

Tab. III MATERIALS UNDER INVESTIGATION

1.	Specimen preparation	Machining of substrates, application of coatings, surface finish
2.	Control	Metallurgical qualification, dimensions, geometry, surface roughness, hardness, weight
3.	Documentation	
4.	Test run	Friction force measurement, parameter variation
5.	Demounting of specimens	
6.	Cleaning	Methanol, H_2O
7.	Evaluation (wear)	Weight control, change of length control, planimetry, photography, metallography
8.	Documentation	
9.	Storing	

Tab. IV TEST SPECIMENS HANDLING PROGRAM

Test No.	MATERIALS			
	PIN (3)	Process	DISK	Process
1	Steel 1.4981	annealed	FeCr 50	Plasma spr.
2	"	"	Stellite 6 H	weld-depos.
3	"	"	TZM	wrought
4	"	"	Inconel 718	annealed
5	Stellite 6 H	weld-depos.	Ferro TiC U	sintered
6	"	"	Steel 1.4981	annealed
7	"	"	Inconel 718	"
8	Ferro TiC U	sintered	"	"
9	"	"	Stellite 6 H	weld-depos.
10	"	"	Hastelloy C	"
11	"	"	Hastelloy C	"
12	"	"	Steel 1.4981	annealed
13	"	"	"	"
14	"	"	FeCr 50	plasma-spr.
15	Ferro TiC U	sintered	Ferro TiC U	sintered
16	"	"	"	"
17	"	"	"	"
18	"	"	"	"
19	Ferro TiC T	"	Steel 1.4981	annealed
20	"	"	Hastelloy C	weld-depos.

Tab. V — TEST MATRIX 1 HYBRID PAIRINGS

Test No.	MATERIALS			
	PIN (3)	Process	DISK	Process
21	Ferro TiC T	sintered	Steel 1.4981	annealed
22	"	"	"	"
23	"	"	"	"
24	"	"	Inconel 718	annealed
25	FeCr 50	plasma-spray	Ferro TiC U	sintered
26	"	"	"	"
27	Inconel 718	annealed	Inconel 718	annealed
28	"	"	Steel 1.4981	"
29	"	"	TZM	wrought
30	"	"	Ferro TiC U	sintered
31	TZM	wrought	Steel 1.4981	annealed
32	"	"	TZM	wrought
33	"	"	Inconel 718	annealed
34		"	Steel 1.4981	"
35	"	"	Ferro TiC U	sintered
36	"	"	"	"
37	Colmonoy 5	fuse-welded	Steel 1.4981	wrought
38	"	"	"	"
39	Colmonoy 6	"	Inconel 718	annealed
40	"	"	Steel 1.4981	"

Tab. VI — TEST MATRIX 2 HYBRID PAIRINGS

Test No.	MATERIALS			
	PIN (3)	Process	DISK	Process
41	Colmonoy 56	fuse-welded	Steel 1.4981	wrought
42	"	"	"	"
43	Tantal	wrought	Inconel 718	annealed
44	Comonoy 56	fuse-welded	"	"
45	Stellite 6 H	weld.-depos.	Steel 1.4981	wrought
46	Colmonoy 6	fuse-welded	"	"
47	"	"	Inconel 718	annealed
48	FeCr 50	"	"	"
49	"	"	"	"
50	Steel 1.4981	wrought	Comonoy 6	fuse-welded
51	"	"	"	"
52	Inconel 718	annealed	"	"
53	Steel 1.4981	"	"	"
54	Colmonoy 6	fuse-welded	Steel 1.4981	wrought
55	"	"	"	"
56	Steel 1.4981	wrought	Colmonoy 6	fuse-welded
57	Stellite 1	weld-depos.	WC (Ni)	sintered
58	"	"	Steel 1.4961	wrought
59	Steel 1.4961	annealed	"	"
60	Colmonoy 6	fuse-weld.	WC (Ni)	sintered

Tab. VII TEST MATRIX 3 HYBRID PAIRINGS

Test No.	MATERIALS			
	PIN (3)	Process	DISK	Process
61	Colmonoy 6	fuse-welded	WC (Ni)	sintered
62	Stellite 1	weld-depos.	Steel 1.4961	annealed
63	"	"	"	"
64	Steel 1.4981	wrought	Steel 1.4981	"
65	Stellite 1	weld-depos.	Steel 1.4961	wrought
66	"	"	"	"
67	Stellite 6 H	"	Inconel 718	annealed
68	"	"	"	"
69	"	"	"	"
70	Inconel 718	annealed	Stellite 6 H	weld-depos.
71	"	"	"	"
72	"	"	"	"
73	"	"	"	"
74	"	"	"	"
75	Stellite 6 H	weld-depos.	Inconel 718	annealed
76	"	"	"	"
77	Armco Fe	wrought	Akrit-Co 50	fuse-weld.
78	Akrit Co 50	fuse-weld.	"	"
79	Colmonoy 6	"	Inconel 718	annealed

Tab. VIII TEST MATRIX 4 HYBRID PAIRINGS

Test No.	MATERIALS			
	PIN (3)	Process	DISK	Process
80	Stellite 6 H	weld-depos.	Inconel 718	annealed
81	Armco Fe	wrought	Akrit Co 50	fuse-weld.
82	Akrit Co 50	fuse-weld.	"	"
83	Colmonoy 6	"	Inconel 718	annealed
84	Stellite 6 H	weld-depos.	"	"
85	"	"	Steel 1.4961	wrought
86	"	"	"	"
87	Stellite 1	"	"	"
88	Colmonoy 6	"	"	"
89	Inconel 718	annealed	"	"
90	"	"	"	"
91	Stellite 6 H	weld-depos.	Inconel 718	annealed
92	Colmonoy 6	fuse-weld.	"	"
93	Stellite 6 H	weld-depos.	TZM	wrought
94	Colmonoy 6	fuse-weld.	"	"
95	Nimonic 80 a	wrought	Colmonoy 6	fuse-weld.
96	Inconel 750	"	Steel 1.4981	wrought
97	Inconel 750	annealed	Steel 1.4961	wrought
98	"	"	"	"
99	"	"	"	"

Tab. IX — TEST MATRIX 5
HYBRID PAIRINGS

Test No.	MATERIALS			
	PIN (3)	Process	DISK	Process
100	Stellite 6 H	weld.-depos.	Stellite 6 H	weld-depos.
101	"	"	"	"
102	Steel 1.4961	annealed	Steel 1.4961	annealed
103	TZM	wrought	TZM	wrought
104	"	"	"	"
105	Nimonic 80	"	Nimonic 80	"
106	"	"	"	"
107	Inconel 718	annealed	Inconel 718	annealed
108	"	"	"	"
109	"	"	"	"
110	Hastelloy C	wrought	Hastelloy C	wrought
111	"	"	"	"
112	Nimonic 80	"	Nimonic 80	"
113	Inconel 750	"	Inconel 750	"
114	"	"	"	"
115	Inconel 718	annealed	Inconel 718	annealed

Tab. X — TEST MATRIX 6
LIKE MATERIALS

Test No.	MATERIALS			
	PIN (3)	Process	DISK	Process
118	Inconel 718	annealed	Steel 1.4961	wrought
119	"	"	"	"
120	"	"	"	"
121	"	"	"	"
122	"	"	"	"
123	"	"	"	"
124	Stellite 6 H	weld-depos.	"	"
125	"	"	"	"
126	"	"	"	"
127	"	"	"	"
128	"	"	"	"
129	"	"	"	"
130	Steel 1.4961	wrought	Steel 1.4961	wrought
131	"	"	"	"
132	"	"	"	"

Tab. XI — TEST MATRIX 7
INSTRUMENT PANEL MATERIALS

Test No.	MATERIALS			
	PIN (3)	Process	DISK	Process
170	Inconel 718	annealed	Inconel 718	annealed
171	"	"	"	"
173	"	heat-treated	"	heat-treated
174	"	"	"	"
175	Inconel 750	annealed	Inconel 750	annealed
180	"	"	"	"
223	"	"	"	"
225	Stellite 6 H	weld-depos.	Stellite 6 H	weld-depos.
227	"	"	"	"
228	"	"	"	"
229	TZM	wrought	TZM	wrought
230	"	"	"	"
231	"	"	"	"
239	Hastelloy C	annealed	Hastelloy C	annealed
240	"	"	"	"
242	"	"	"	"
247	Inconel 718	"	Inconel 718	"
248	"	"	"	"
249	"	heat-treated	"	heat-treated
250	"	"	"	"

Tab. XII — TEST MATRIX 8
LIKE MATERIALS

Test No.	MATERIALS			
	PIN (3)	Process	DISK	Process
403	Steel 6770	wrought	Steel 6770	wrought
404	"	"	"	"
405	"	"	"	"
406	Steel 90 Mn V8	"	Steel 90 Mn V8	"
407	"	"	"	"
408	"	"	"	"
409	Steel 6770	"	Colmonoy 5	fuse welded
410	"	"	"	"
411	"	"	"	"
412	Steel 90 Mn V8	"	"	"
413	"	"	"	"
414	"	"	"	"

Tab.XIII TEST MATRIX 9
FERRITIC HTX MATERIALS

Test No.	MATERIALS			
	PIN (3)	Process	DISK	Process
440	Steel DTO_2	sintered	Steel DTO_2	sintered
⌇	"	"	"	"
451	"	"	"	"
452	Steel B3	annealed	Steel B3	annealed
⌇	"	"	"	
455	"	"	"	
456	Steel B3	annealed	LC-1H	D-Gun
⌇	"	"	"	"
459	"	"	"	"
460	Steel B3	annealed	Colmonoy 56	fuse welded
⌇	"	"	"	"
463	"	"	"	"

Na-temperature 653/723/873 K
Movement continuously rotating
1300 mm/min
Cumulat. rubbing dist. $S_{CR} = 10^5$ cm
load = 3,2 MPa

Tab.XIV TEST MATRIX 10
FERRITIC CLADDING MATERIALS

Test No.	MATERIALS			
	PIN (3)Disk 2	Process	DISK Plate	Process
292	LC - 1 H	D - Gun	LC - 1 H	D - Gun
⎫	"	"	"	"
295	"	"	"	"
304	"	"	"	"
311	Tribaloy 700	D - Gun	Tribaloy 700	D - Gun
⎫	"	"	"	"
314	"	"	"	"
319	"	"	"	"
323	Inconel 718 A	Diffusion	Inconel 718 A	Diffusion
⎫	"	"	"	"
329	"	"	"	"
434	Inconel 718 A	Diffusion	Tribaloy 700	D - Gun
⎫	"	"	"	"
439	"	"	"	"

Tab. XV — TEST MATRIX 11 (Co-free)PAD MATERIALS

Specimen geometry		Pin-Disk Plate-Plate
Relative movement		oscillating (rotating)
Stroke length	± mm	5
Velocity	cm/s	∿ 11 (7)
Rubbing distance	$cm \cdot 10^5$	∿ 6.3 (11)
Contact pressure	MPa	0.6/1.2
Na-temperature	K	523-873
O_2-Content in Na	ppm	⩽ 10

Tab. XVI — STANDARD TEST PROGRAM OPERATING CONDITIONS (KfK-IA)

TEST No.	MATERIALS		PARAMETER UNDER INVESTIGATION	TEST CONDITIONS
	PIN (3)	DISK		
189	Stellite 6H	Steel 1.4961	0	TEST SECTION I "PIN-DISK"
190	"	"	4	
193	"	"	15	Sodium temperature 823 K
210	"	"	24	
212	"	"	30	
213	Inconel 750	Steel 1.4981	0	
218	"	"	4	
219	"	"	15	$S_{CR} = 10^6$ cm
220	"	"	24	TIME OF SODIUM PRE-EXPOSURE h
221	"	"	35	
222	"	"	45	
282	Stellite 6H	Stellite 6H	1800	823
283	"	"	"	773 Sodium temperature
284	"	"	"	823 K
285	"	"	"	823
	RIDER	PLATE		
320	Stellite 6H	Stellite 6H	6500	TEST SECTION III (tilting)
321	"	"	"	
322	"	"	0	

Tab. XVII — TEST MATRIX 12

TEST No.	MATERIALS		PARAMETER UNDER INVESTIGATION	TEST CONDITIONS
	DISK (2)	PLATE		
			ENVIRONMENT	
393	LC-1H	LC-1H	Sodium	TEST SECTION II "DISK-PLATE"
394	"	"		
395	"	"		
396	"	"		Sodium temperature
397	"	"	Argon	873 K
398	"	"		
399	"	"		
400	"	"	Argon + Sodium	
401	"	"		

Tab. XVIII — TEST MATRIX 13

TEST No.	MATERIALS		PARAMETER UNDER INVESTIGATION	TEST CONDITIONS
	PIN (3)	DISK		
274	Stellite 6 H	Stellite 6 H		
}	"	"		
277	"	"		
			O_2 - Content in Sodium	TEST SECTION I
278	Inconel 718	Inconel 718		Standard
}	"	"	10 ppm/1 ppm	Conditions
279	"	"		
330	"	"		
251	Steel 1.4961	Steel 1.4961		TEST SECTION I
252	Inconel 718	Inconel 718	NORMAL LOAD Kgf	Na temperature
253	Stellite 6H	Stellite 6H	50/100/150	673 K
254	Colmonov 4	Colmonov 4	PRESSURE MPa	
255	WC-Ni	WC-Ni	25/50/75	Velocity 0,2 m/min

Tab. XIX — TEST MATRIX 14

TEST No.	MATERIALS		PARAMETER UNDER INVESTIGATION	TEST CONDITIONS
	PIN (3)	DISK		
256	Inconel 718	Inconel 718		TEST SECTION II
257	"	"		LOAD 8 MPa
258	"	"		
259	"	"		(Test Nr. 260 = 20 MPa
260	Stellite 6 H	Stellite 6 H		" " 261 = 50 ")
261	"	"		
262	"	"		
264	Inconel 718 an.	Inconel 718 an.	SODIUM	
266	"	"	TEMPERATURE	
267	"	"		
			473 - 873 K	
265	Stellite 6 H	Stellite 6 H		
268	"	"		TEST SECTION I
269	"	"		
				"PIN-DISK"
270	Inconel 718	Inconel 718		
271	"	"		STANDARD TEST PROGRAM
272	"	"		
273	"	"		
281	"	"		

Tab. XX — TEST MATRIX 15

TEST No.	MATERIALS		PARAMETER UNDER INVESTIGATION	TEST CONDITIONS
	DISK (2)	PLATE		
286	Inconel 718 ht.	Inconel 718 ht.	Sodium temperature K 673/873 673/523/873	TEST SECTION II
287	"	"		
288	"	"		
289	Inconel 718 ht.	Stellite 6 B		
290	"	"		
291	"	"		
	PIN (3)	DISK		TEST SECTION I
296	Stellite 6 H	Stellite 6 B		
{	"	"		
300	"	"		
	DISK (2)	PLATE		TEST SECTION II
301	Stellite 6 B	Stellite 6 B		
302	"	"		
303	"	"		
305	"	"		
306	"	Inconel 718		
307	"	"		
308	"	"		
309	"	"		
310	"	Stellite 6 B		

Tab. XXI — TEST MATRIX 16

TEST No.	MATERIALS		PARAMETER UNDER INVESTIGATION	TEST CONDITIONS
	DISK (2)	PLATE		
315	Stellite 6 H	Stellite 6 H	ELASTICITY OF TEST SECTION	TEST SECTION I/II NA-TEMPERATURE 873 K
316	"	"		
317	Inconel 718	Inconel 718		
318	"	"		

Tab. XXII — TEST MATRIX 17

TEST No.	MATERIALS		PARAMETER UNDER INVESTIGATION	TEST CONDITIONS
	DISK (2)	PLATE		
330	LC-1H	LC-1H		TEST SECTION II "DISK-PLATE"
⎨	"	"		
335	"	"		
336	Tribaloy 700	Tribaloy 700	Superimposition of vibration on slow oscillation.	
⎨	"	"		
341	"	"		
342	LC-1H	LC-1H	Superimposition of cycling load on constant static load	SODIUM TEMPERATURE 773 K
⎨				
348	"	"		
349	"	"		
⎨	"	"		
355	"	"		

Tab. XXIII TEST MATRIX 18

TEST No.	MATERIALS		PARAMETER UNDER INVESTIGATION	TEST CONDITIONS
	DISK (2)	PLATE		
356	LC-1C	LC-1C	DIFFERENT TEST SECTION CRITERIA	USARD PROGRAM
⎨	"	"		
363	"	"		
364	LC-1C	LC-1C		IA-KfK PROGRAM — TEST SECTION II "DISK-PLATE"
⎨	"	"		
369	"	"		
370	Stellite 6H	Stellite 6H		
371	"	"		
372	"	"		USARD PROGRAM
373	Inconel 718	Inconel 718		
374	"	"		
375	"	"		

Tab. XXIV TEST MATRIX 19

TEST No.	MATERIALS		PARAMETER UNDER INVESTIGATION	TEST CONDITIONS
	DISK (2)	PLATE		
376	LC-1H	LC-1H		
≀	"	"	SURFACE ROUGHNESS	
≀	"	"		
381	"	"	brushed Rt < 30 µm	TEST SECTION II
382	"	"		Specimens dismantled for wear measurement
383	"	"	ground Rt < 5 µm	
384	"	"	lapped Rt < 0,5 µm	
				Na/Ar-TEMPERAT. 873 K
385	"	"		
≀	"	"		
389	"	"		
390	"	"	ENVIRONMENT ARGON	
391	"	"		
392	"	"		

Tab. XXV — TEST MATRIX 20

TEST No.	MATERIALS		PARAMETER UNDER INVESTIGATION	TEST CONDITIONS
	CENTER.KNUBS	TANK WALL		
			SODIUM TEMPERAT.	
415	Steel 6770	Steel 6770	573 K	300 CYCLES ± 2 mm
415 a	"	"	823 K	
				2 CYCLES AT A TIME
416	"	"	TIME OF DWELL	FOLLOWING A DEFINED
416 a	"	"	0 - 13 h	PERIODE OF DWELL
	CENTERKNUBS	TUBE WALL		SODIUM TEMPERATURE 823 K
417	Steel 6770	Colmonoy 5	GEOMETRY	1500 CYCLES ± 0,5 mm
417a	"	"		
418	"	"		
	HTX TUBE	TUBE PLATE		SODIUM TEMPERATURE
419	Steel 6770	Colmonoy 5	SMOOTH	523/823 K
419 a	"	"	TUBE SURFACE	REL. MOVEMENT
420	"	"	FINNED	± 5 mm axial
420 a	"	"	TUBE SURFACE	

Tab. XXVI — TEST MATRIX 21

TEST No.	MATERIALS		PARAMETER UNDER INVESTIGATION	TEST CONDITIONS
	CLADDING	GRID SPACER	TEMP. K	
422	Steel 1.4970	Steel 1.4981	633	TEST SECTION II
423	"	"	753 F_N = 8 N.	
424	"	"	873	
	CLADDING	WIRE SPACER		MOVEMENT
425	Steel 1.4970	Steel 1.4981	633	TEST oscillating
426	"	"	753	SECTION I ± 1 mm
427	"	"	873 F_N = 15 N.	
428	"	"	633	v = 2,5 mm/min
429	"	"	753	
430	"	"	873	TEST
431	"	"	633 F_N = 30 N.	SECTION II
432	"	"	753	
433	"	"	873	

Tab. XXVII TEST MATRIX 22

TEST No.	MATERIALS		PARAMETER UNDER INVESTIGATION	TEST CONDITIONS
	CLADDING	WIRE SPACER		
464	Steel DTO_2	Steel DTO_2		
465	"	"	F_N = 8 N	Na-TEMPERATURE
466	"	"	TEST	873 K
467	"	"	SECTION	RELAT. MOVEMENT
468	"	"	I	oscillating ± 1 mm
469	"	"		
470	"	"	F_N = 22,5 N	VELOCITY = 50 mm/min
471	"	"		
472	"	"		CUMULAT. RUBBING
473	"	"	TEST	DISTANCE = 5 x 10^3 cm
474	"	"	SECTION	
475	"	"	II	
476	"	"	F_N = 100 N	
477	"	"		

Tab. XXVIII TEST MATRIX 23

TESTSECTION	C OF TORQUE AND FORCE LINKS (µm/kgf)	C OF COMPONENTS OF STRUCTURE (µm/kgf)	C OF TOTAL SYSTEM (µm/kgf)
I a	814	20	834
I b	380	12	392
I c	434	8	442
I d	0.015	72.985	73
II a	0.015	68.785	68.8
II b	0.015	28.485	28.5

Tab. XXIX ELASTICITY C OF TESTSECTION I AND II

NORMAL LOAD [N]	200	400	600	800	1000
WEAR RATE [cm^3/cm-Kgf]	$0.8 \cdot 10^{-11}$	$1.6 \cdot 10^{-11}$	$3.2 \cdot 10^{-11}$	$5.6 \cdot 10^{-11}$	$8 \cdot 10^{-11}$

Tab. XXX SURFACE WEAR OF LC-1H (FUNCTION OF CYCLING LOAD)

Relative movement		oscillating
Stroke length	± mm	2
Velocity	mm/min	50
Rubbing distance	m	50
Normal load	N	8/22.5/100
Na-temperature	K	653/723/873

Tab. XXXI DTO_2-PROGRAM TEST CONDITIONS

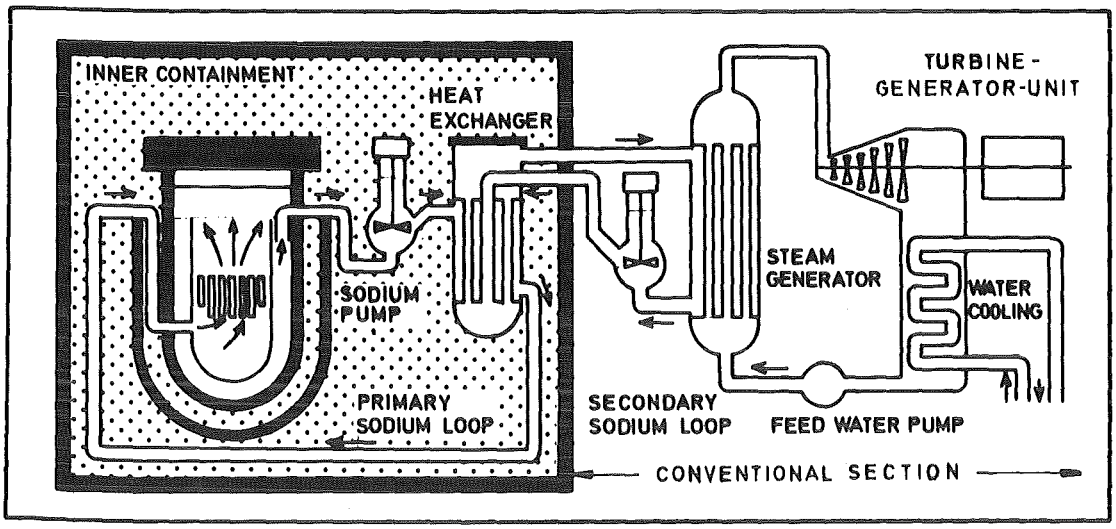

Fig. 1 Schematic Diagram of a Sodium Cooled Fast Reactor

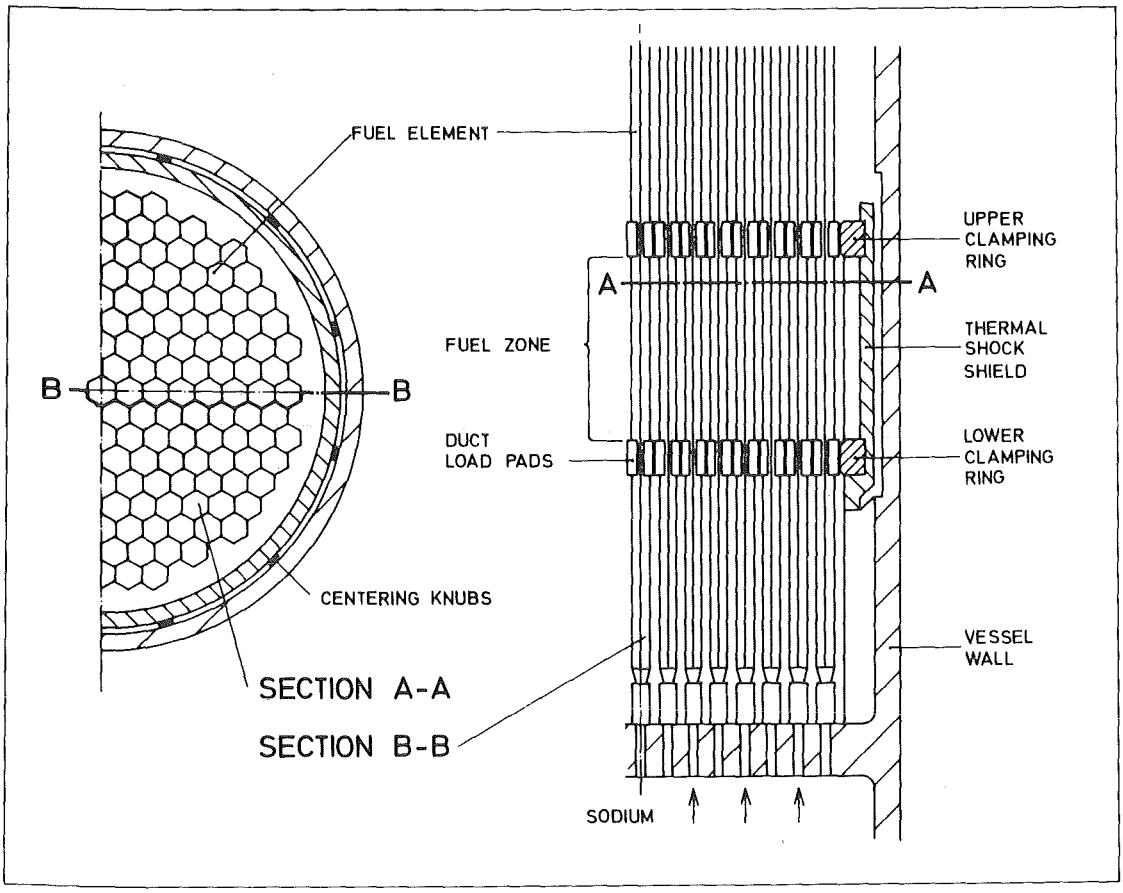

Fig. 2 Schematic Diagram of a Core Restraint System

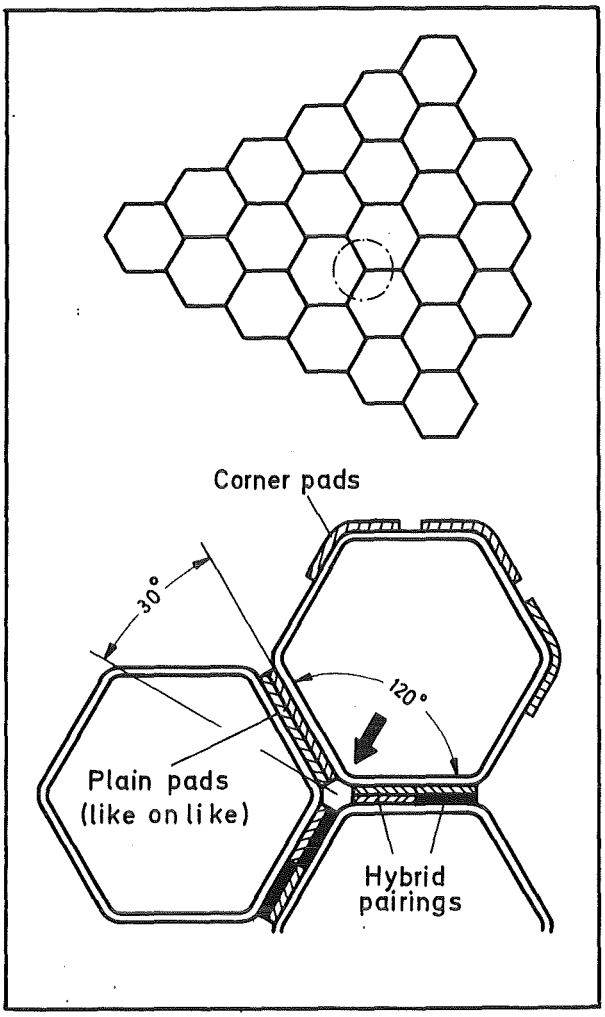

Fig. 3 Arrangement of Fuel Element Duct Load Pads

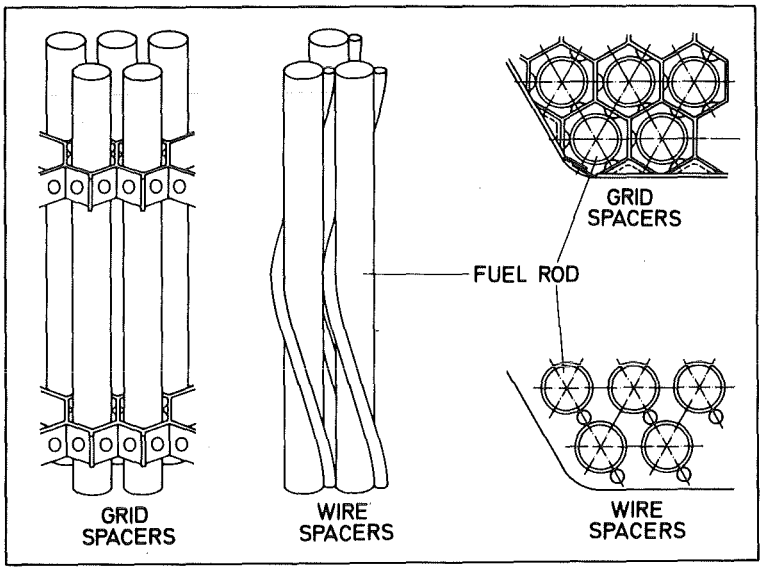

Fig. 4 Inner Fuel Rod Arrangement

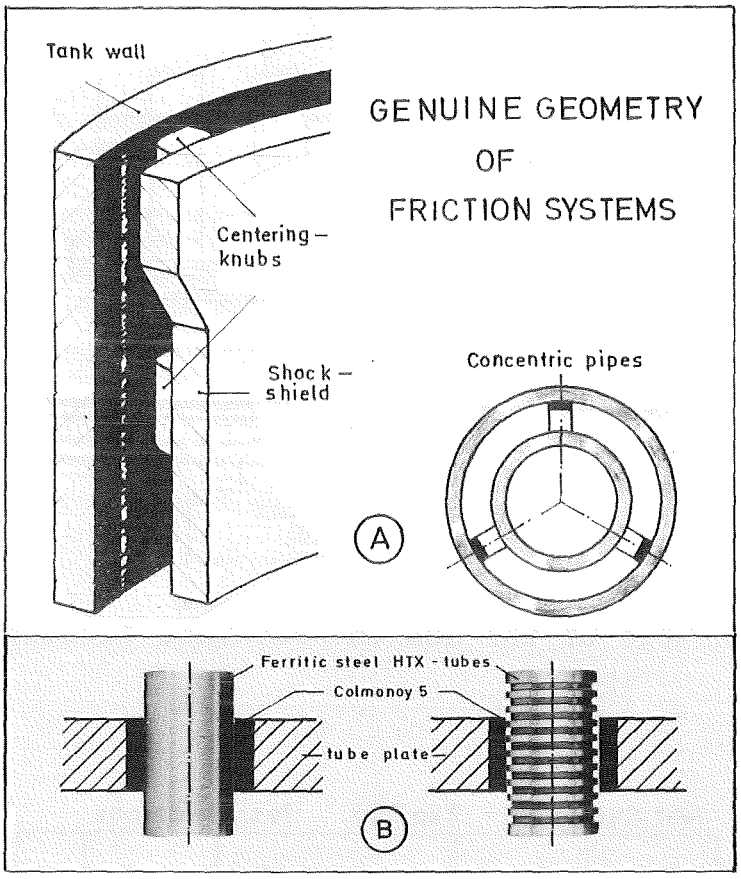

Fig. 5 Different Contact Geometries

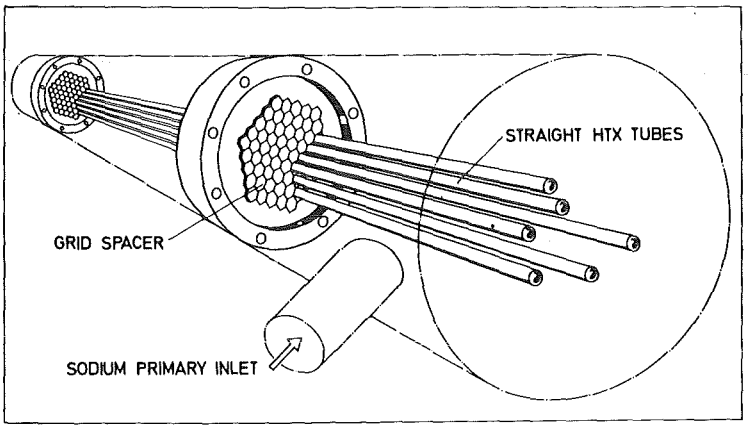

Fig. 6 Schematic of a Straight Tube Heat Exchanger

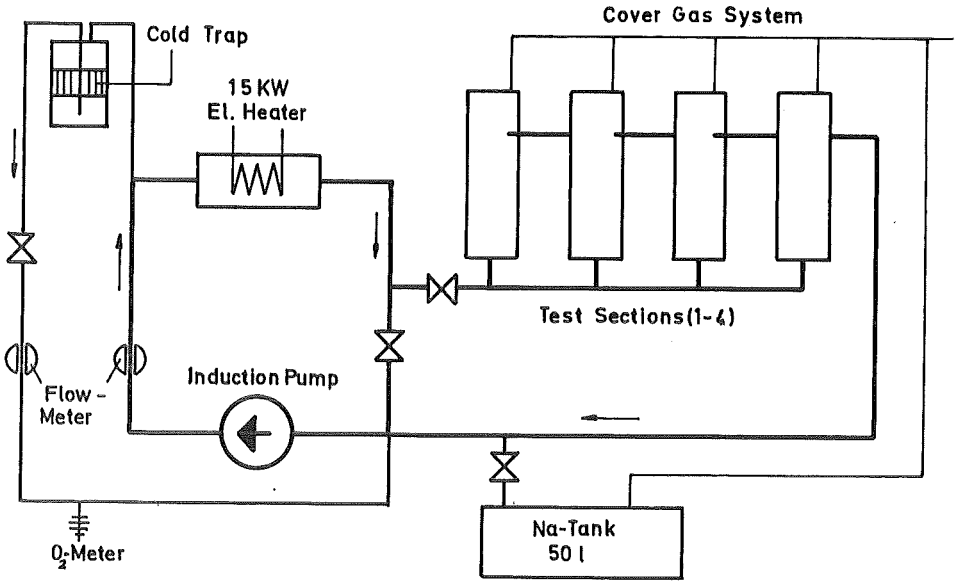

Fig. 7 Schematic of the Sodium Wear Test Facility NVP I

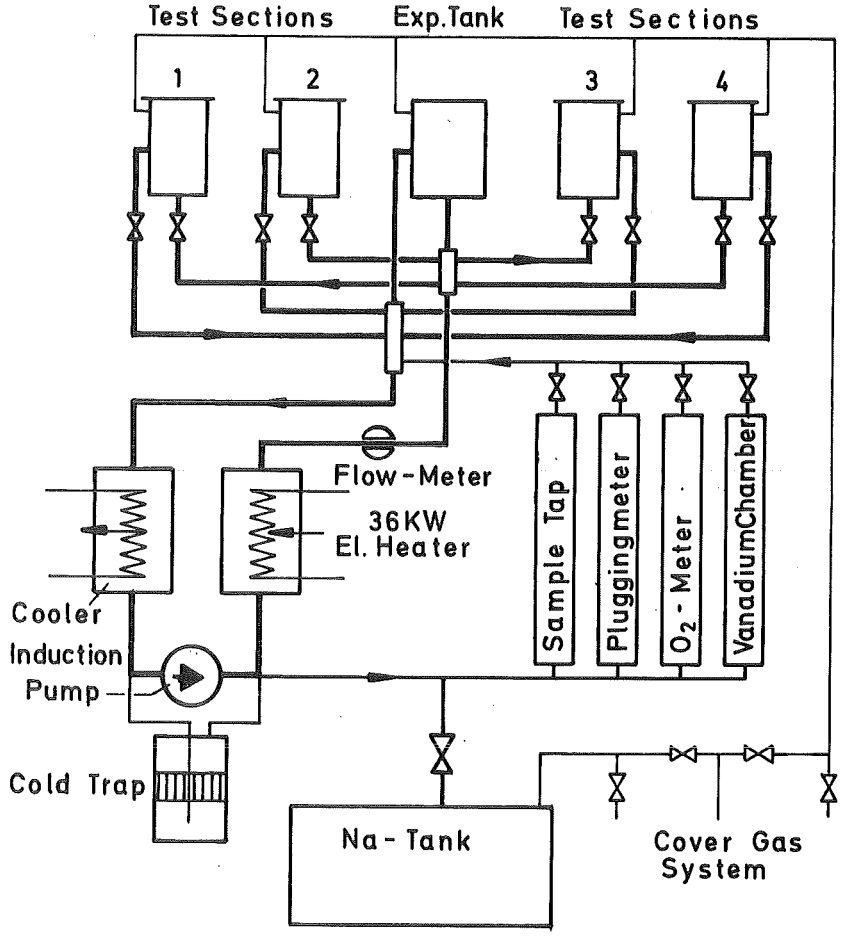

Fig. 8 Schematic of the Sodium Wear Test Facility NVP II

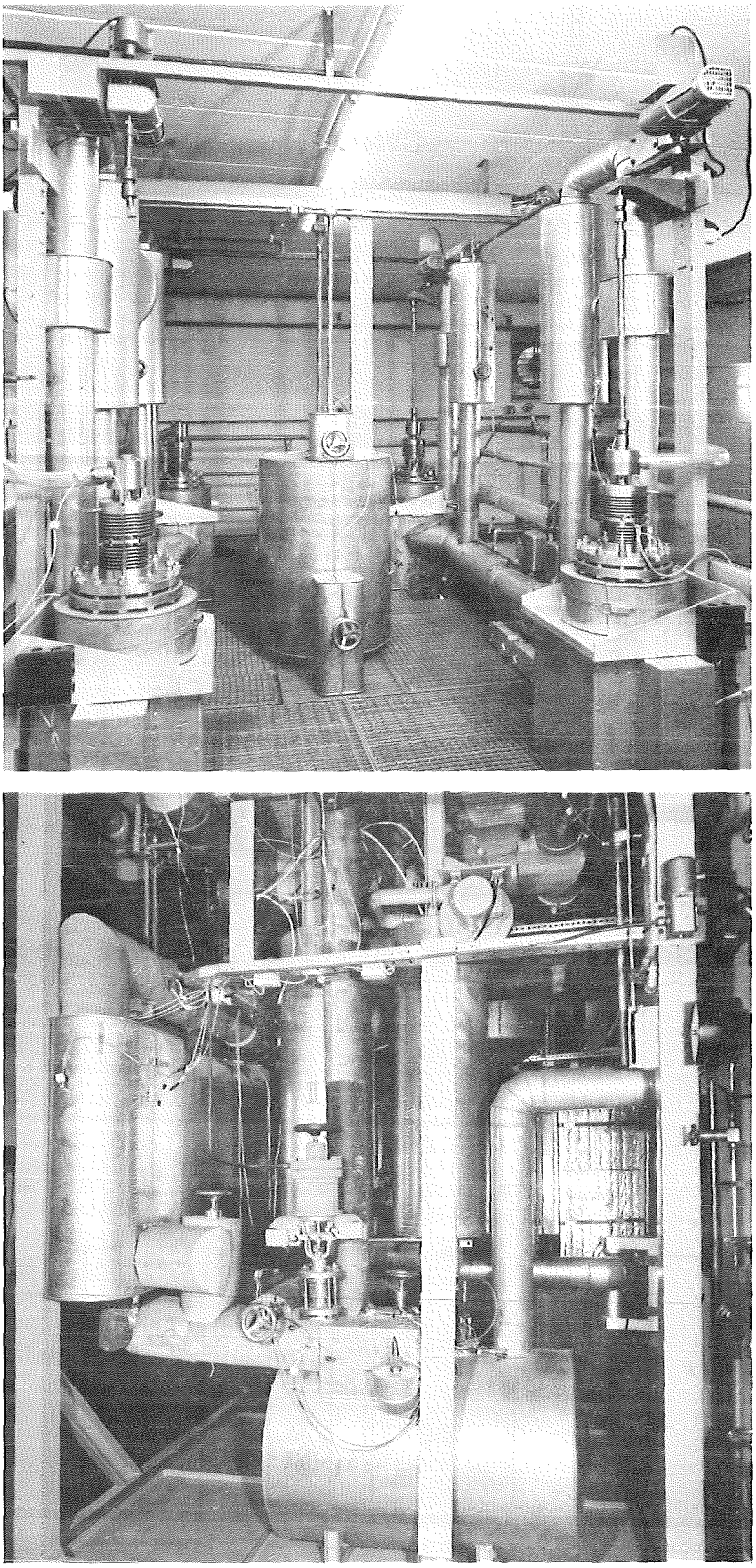

Fig. 9 SODIUM WEAR TEST FACILITY NVP II
(a) operating platform; test sections
(b) purification- and supply loop

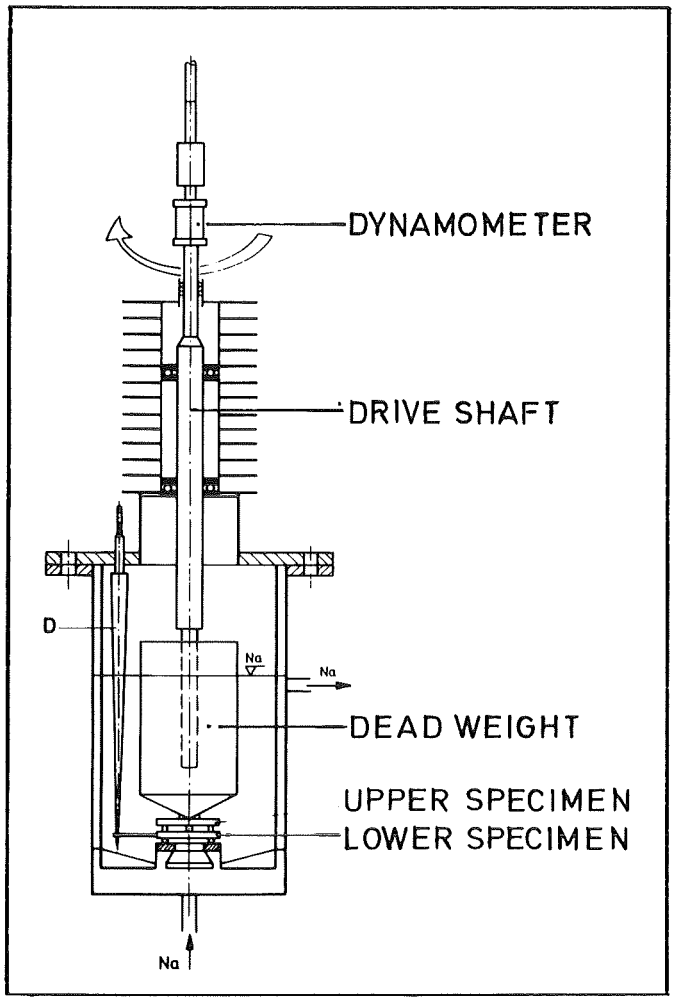

Fig. 10 Test Section I (for rotating relative movement)

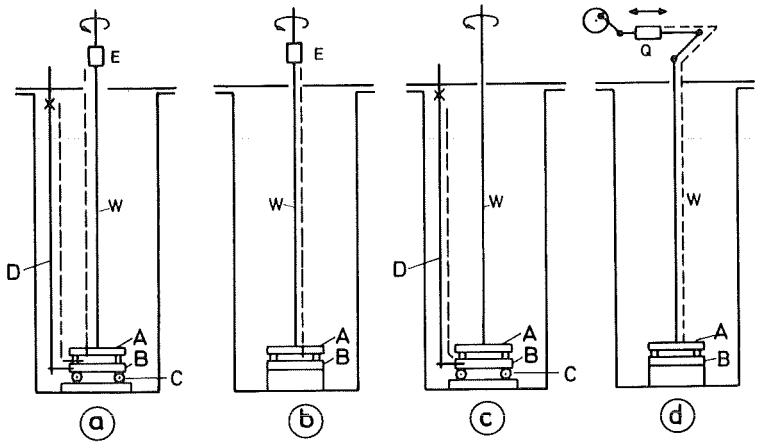

A = Upper Specimen
B = Lower Specimen
--- Elastic Length
E = Dynamometer
C = Axial Ball Bearing
D = Bending Lever
Q = Quartz Force Link
W = Drive Shaft

Fig. 11 Test Section I (schematic of different elasticity)

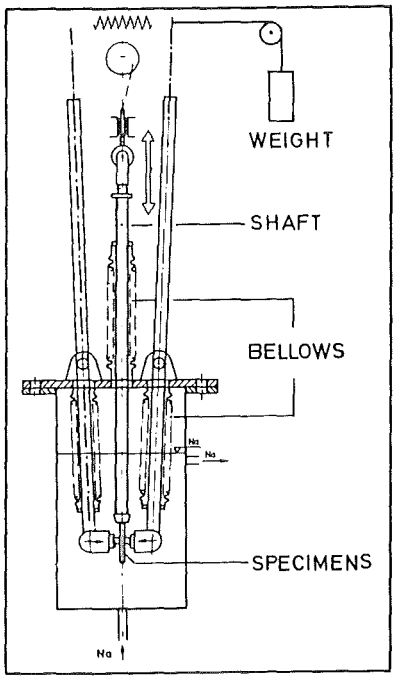

Fig. 12 Test Section II (for translatory oscillating movement)

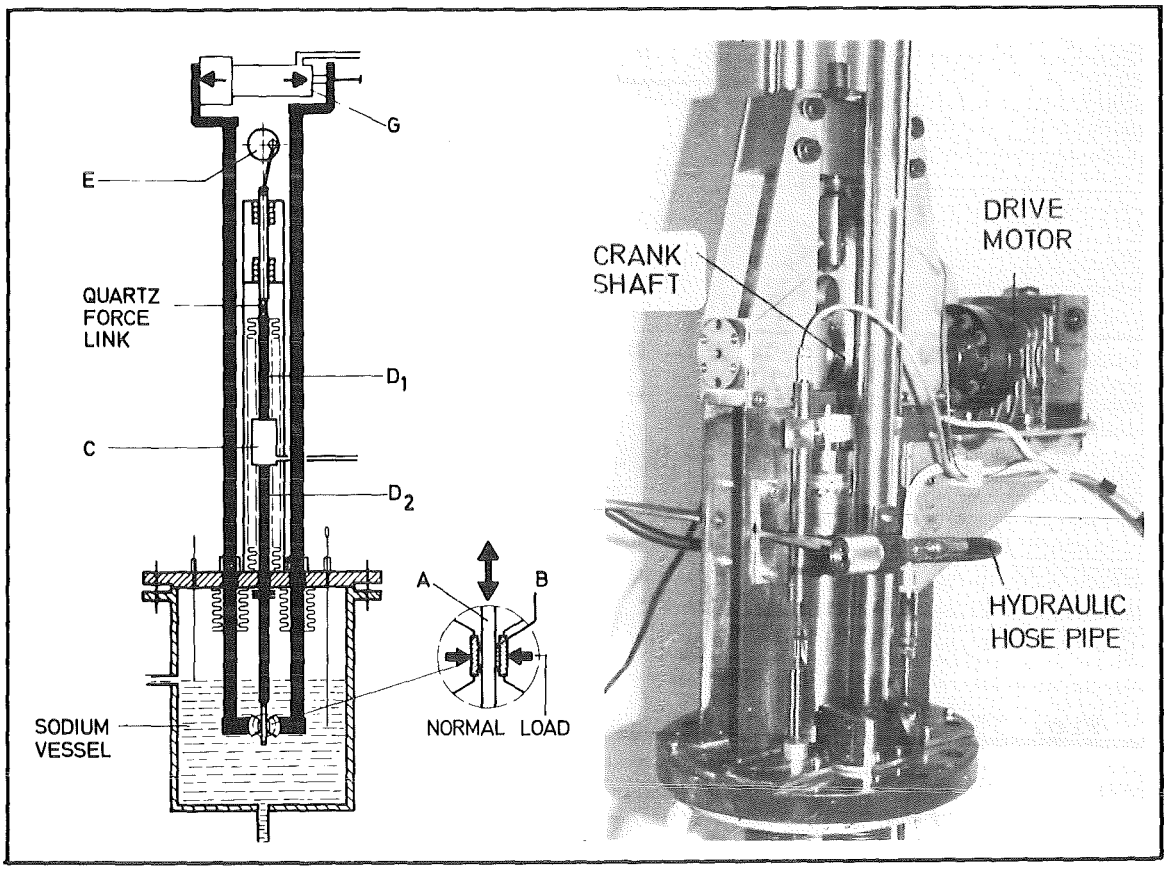

Fig. 13 Test Section II (for hydraulic transmission of superimposed vibratory movement)

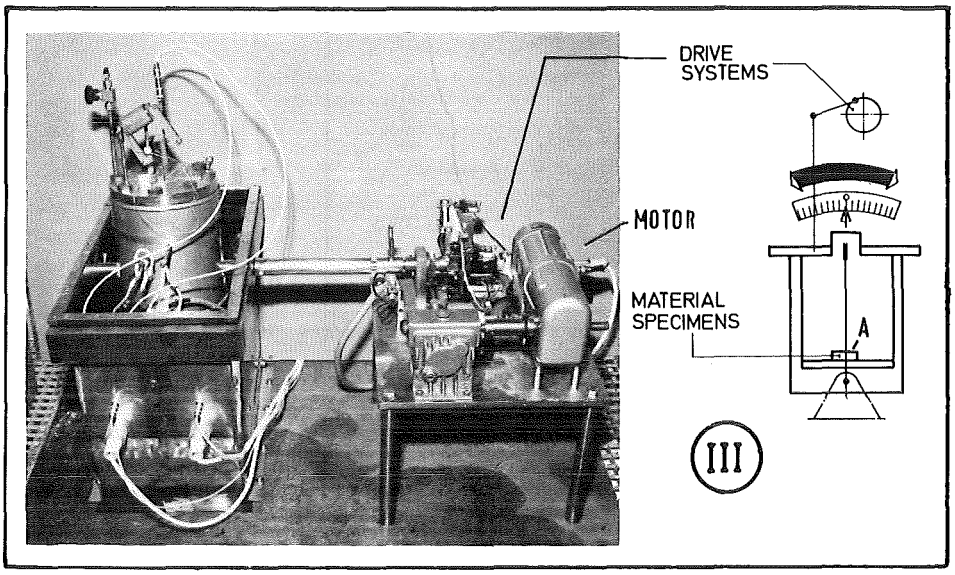

Fig. 14 Test Section III (tilting plane)

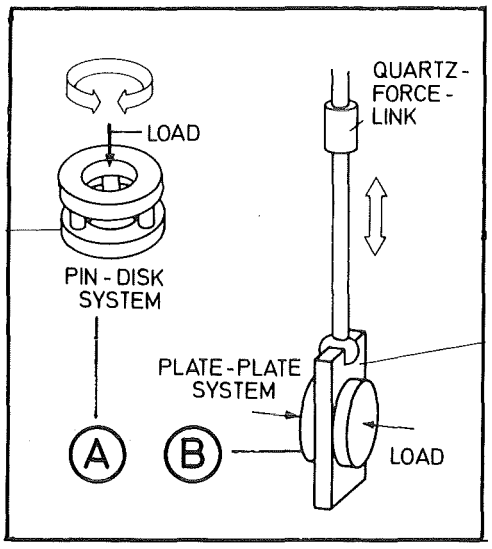

Fig. 15 Standard Specimen Configuration
for Test Section I and II
A = for Test Section I
B = for Test Section II

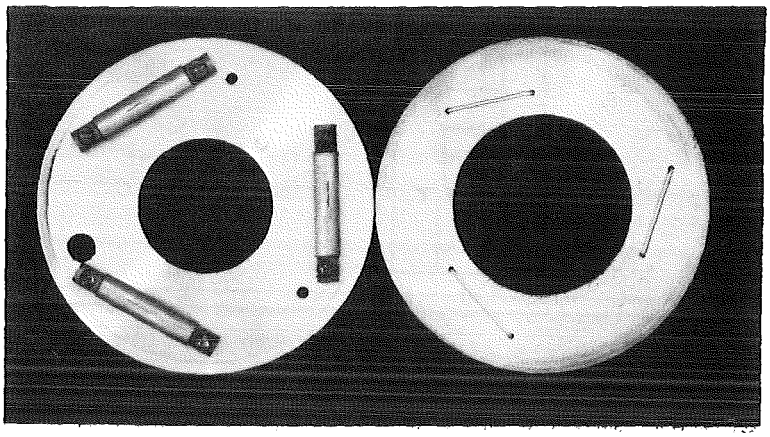

Fig. 16 Fuel Pin Wire Spacer System (test section I)

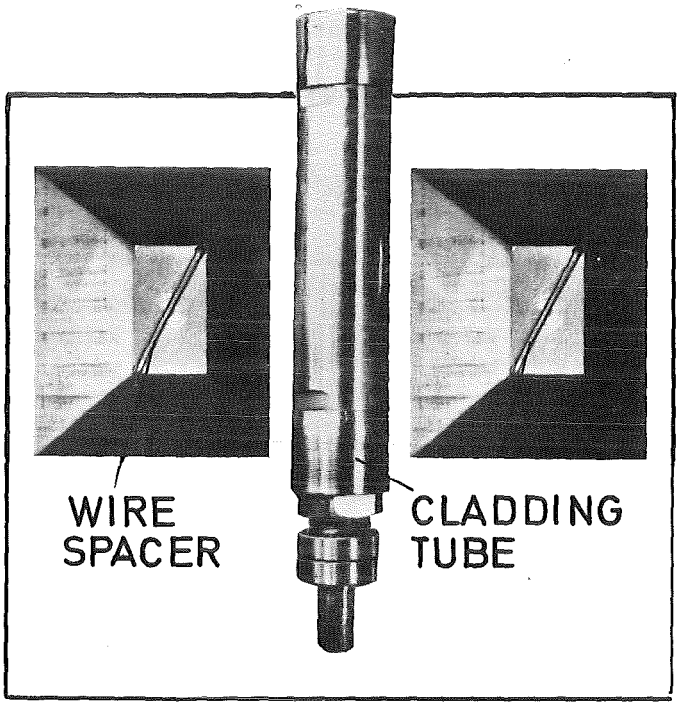

Fig. 17 Fuel Pin Wire Spacer System (test section II)

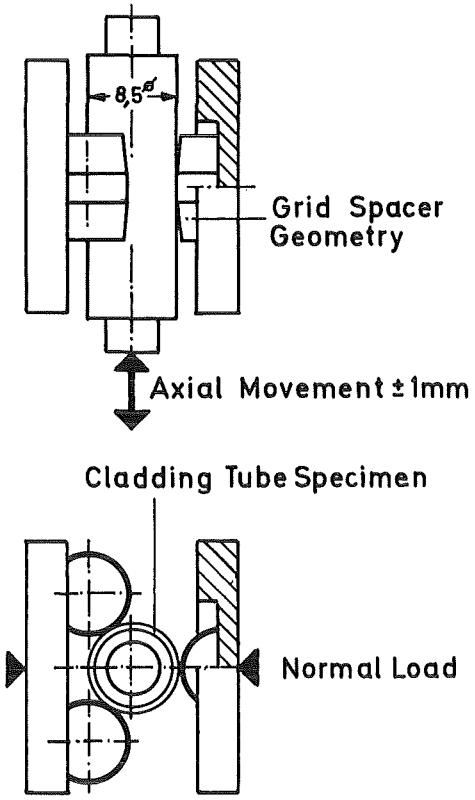

Fig. 18 Fuel Pin Grid Spacer System (test section II)

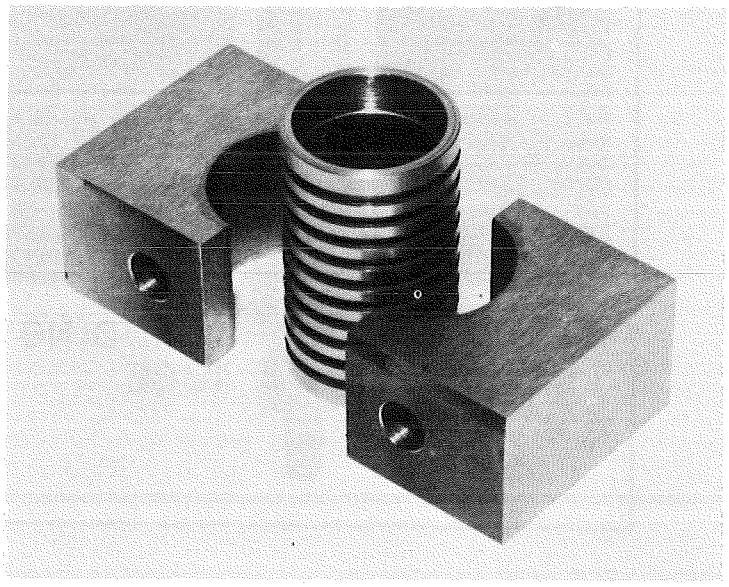

Fig. 19 HTX-Tube/Tube Support Specimens

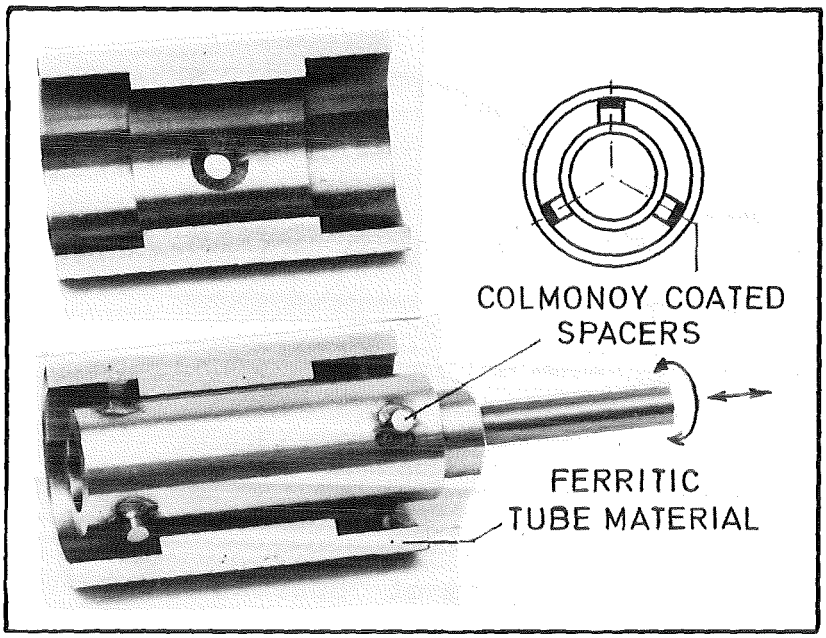

Fig. 20 Concentric Pipe Spacer Specimens

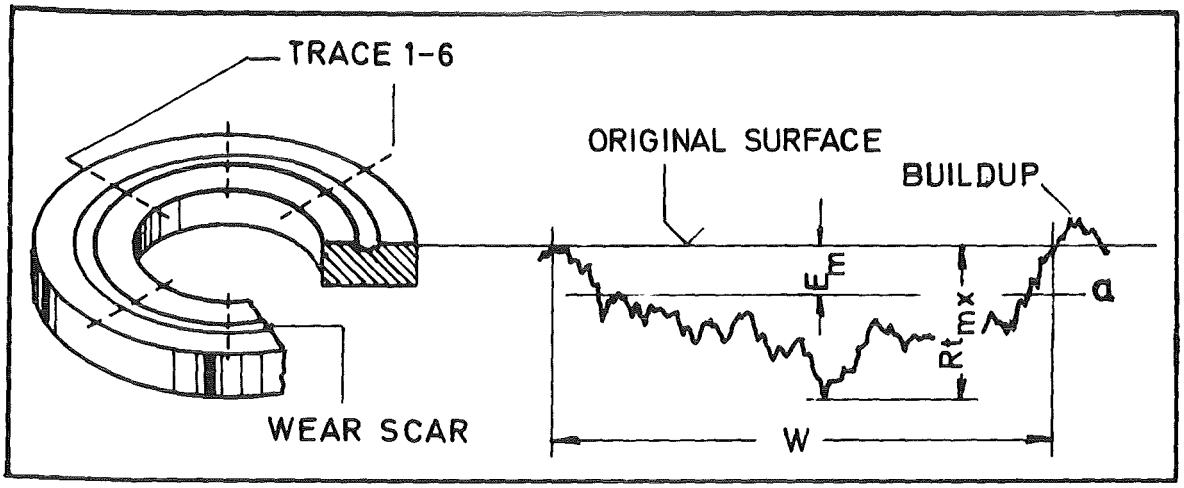

Fig. 21 Schematic of Wear Profile Measurement

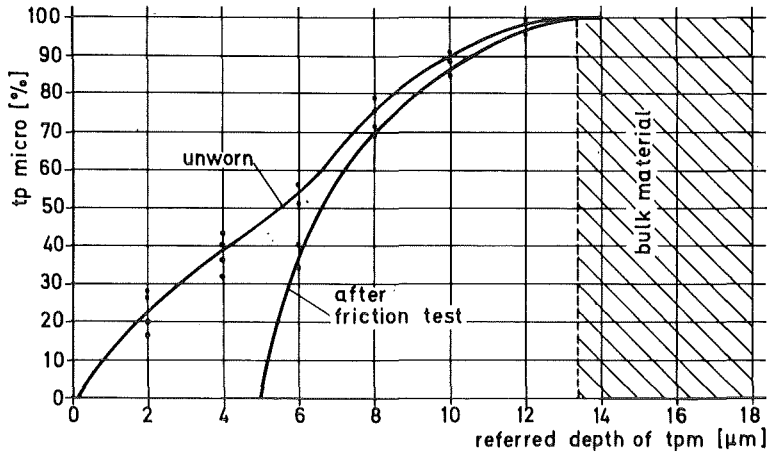

Fig. 22 Typical Diagram of "Bearing Area"

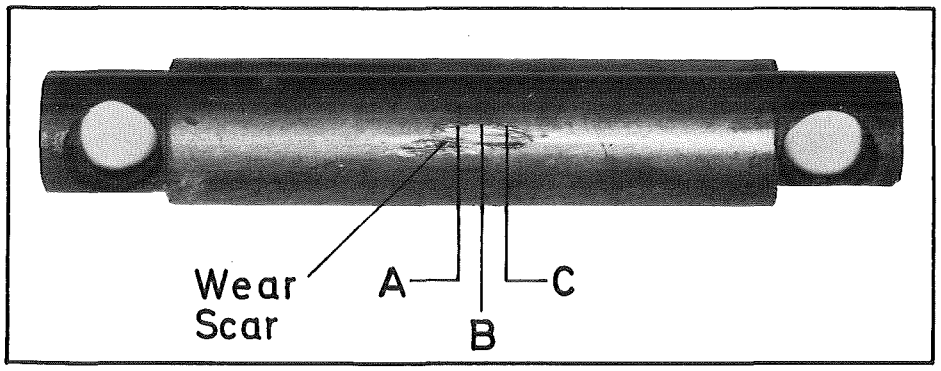

Fig. 23 Traces of Wear Measurement (on cladding tubes)

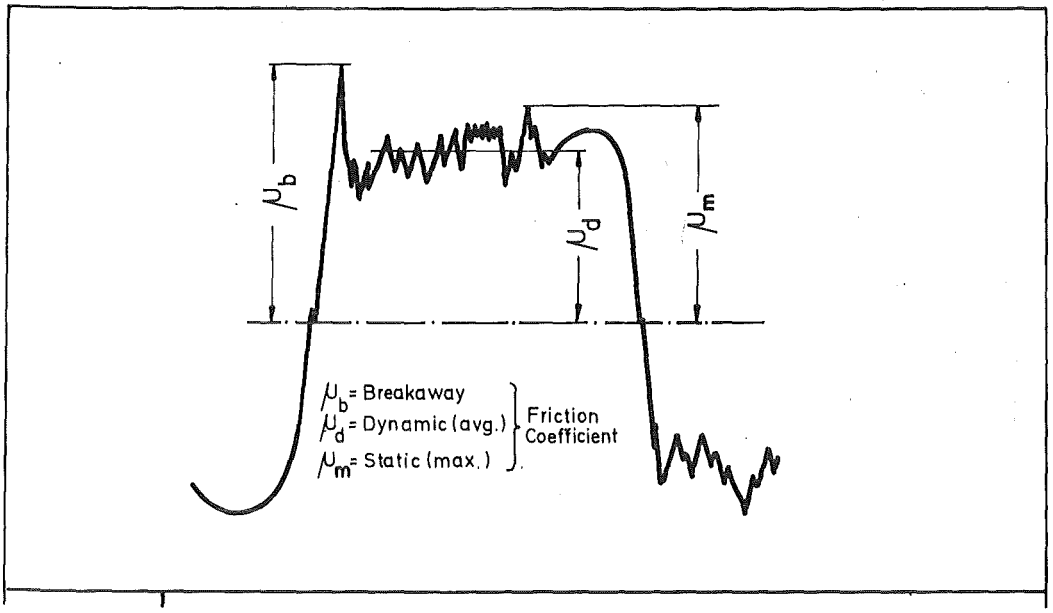

Fig. 24 Typical Recorder Trace (oscillating friction force)

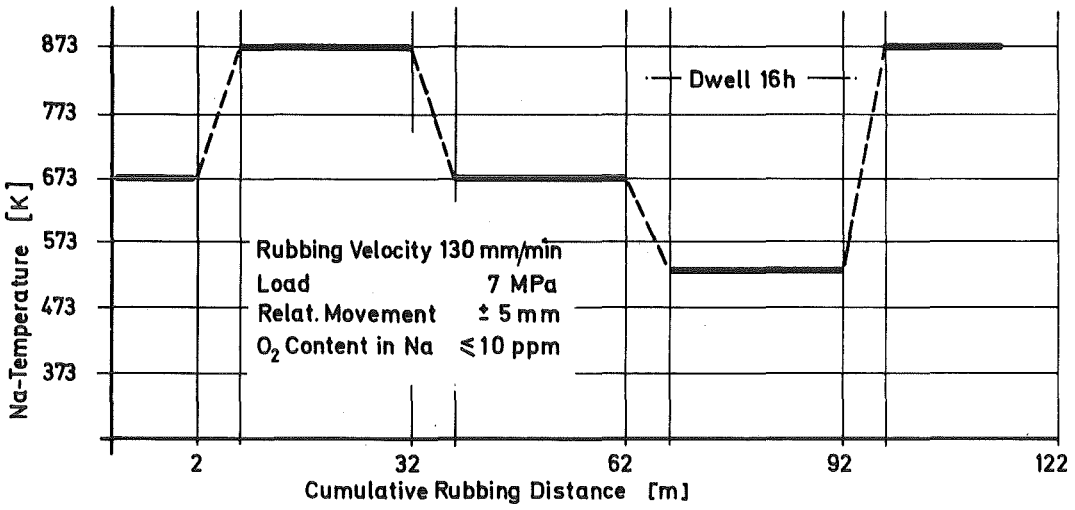

Fig. 25 KfK-INTERATOM Standard Test Pattern

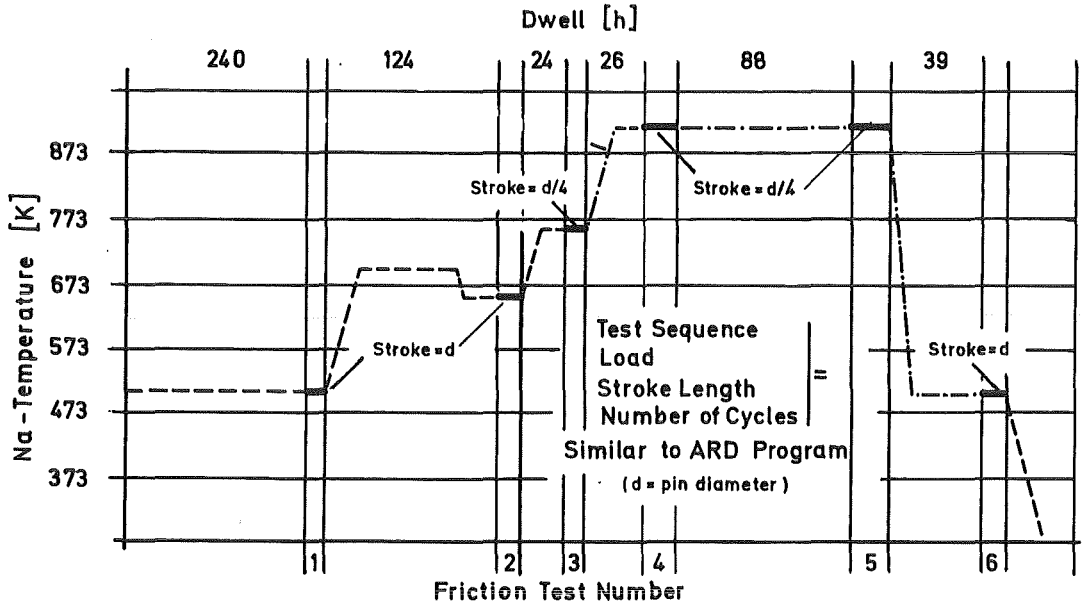

Fig. 26 KfK-USARD Test Pattern

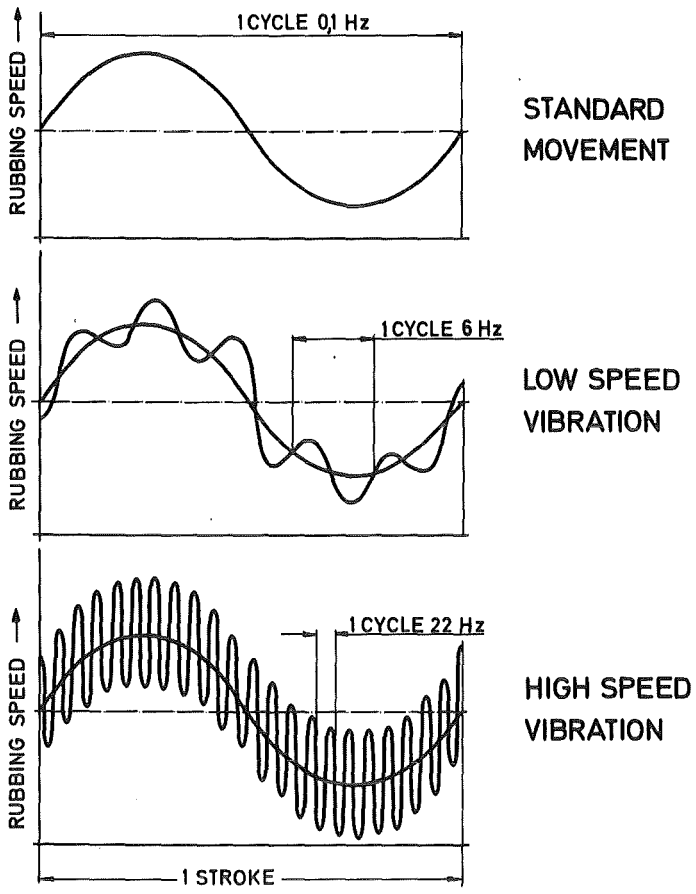

Fig. 27 Cycling Relative Movement

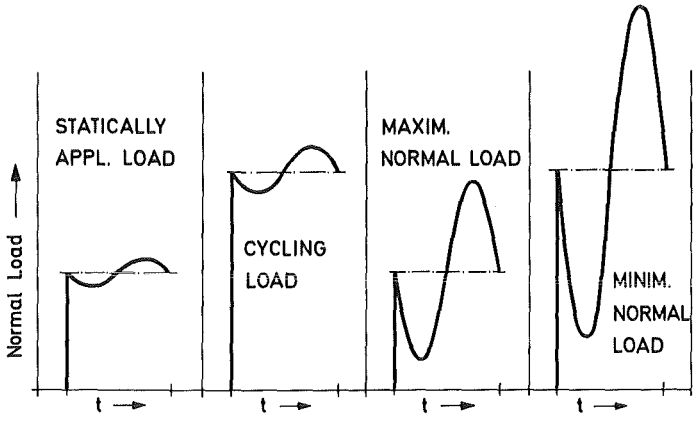

Fig. 28 Cycling Normal Load

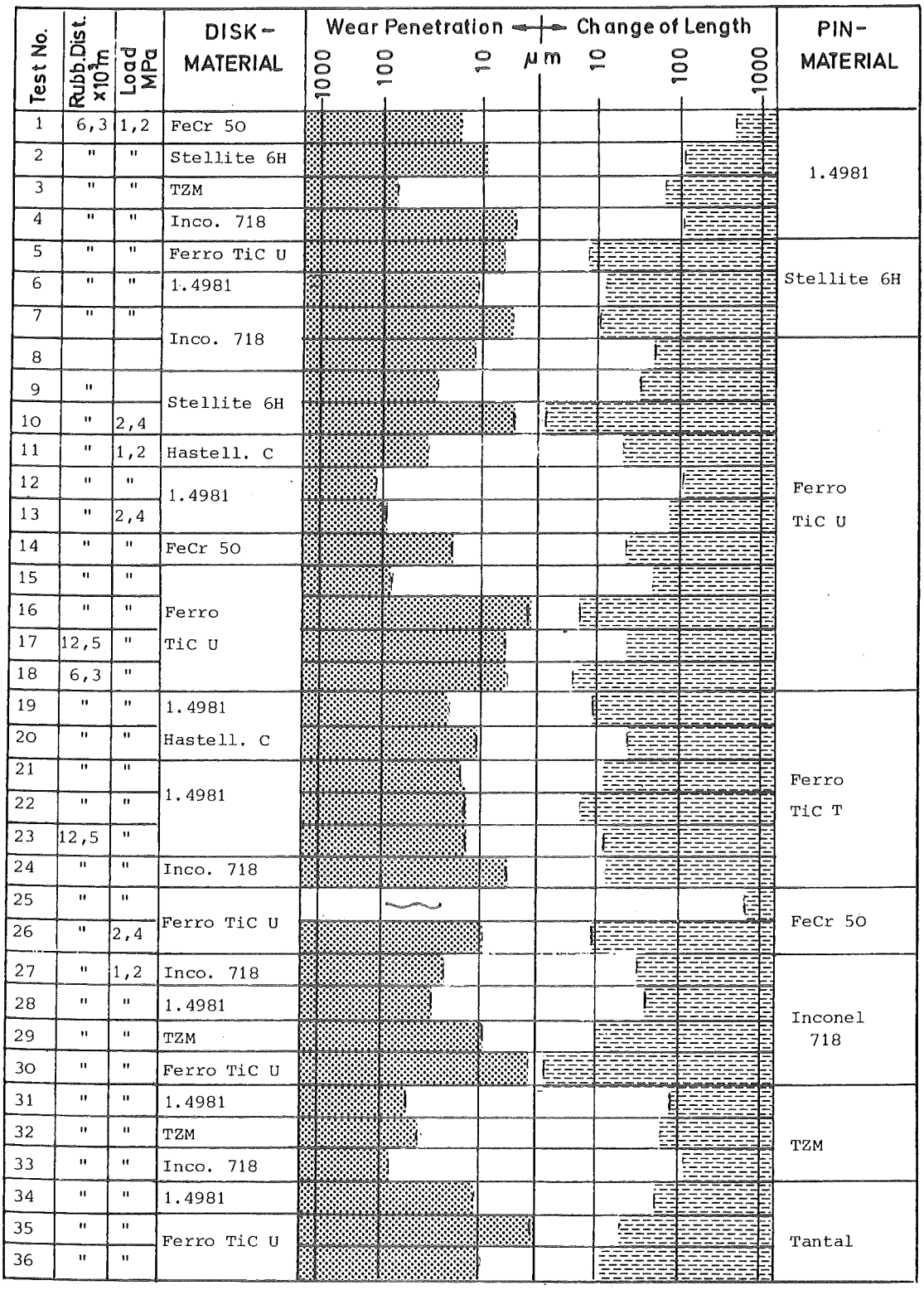

Fig. 29a Material Wear of Hybrid Pairings

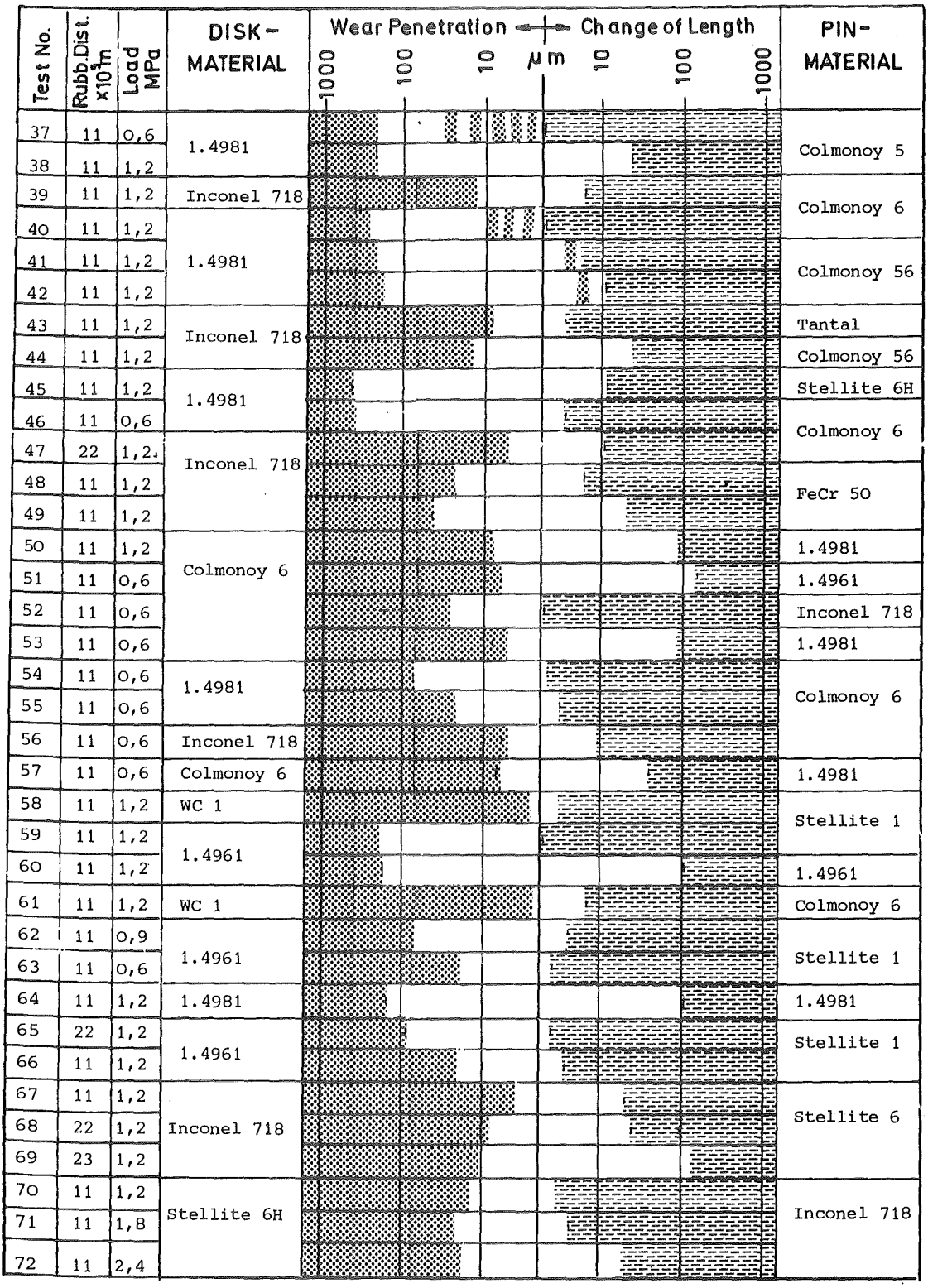

Fig. 29b Material Wear of Hybrid Pairings

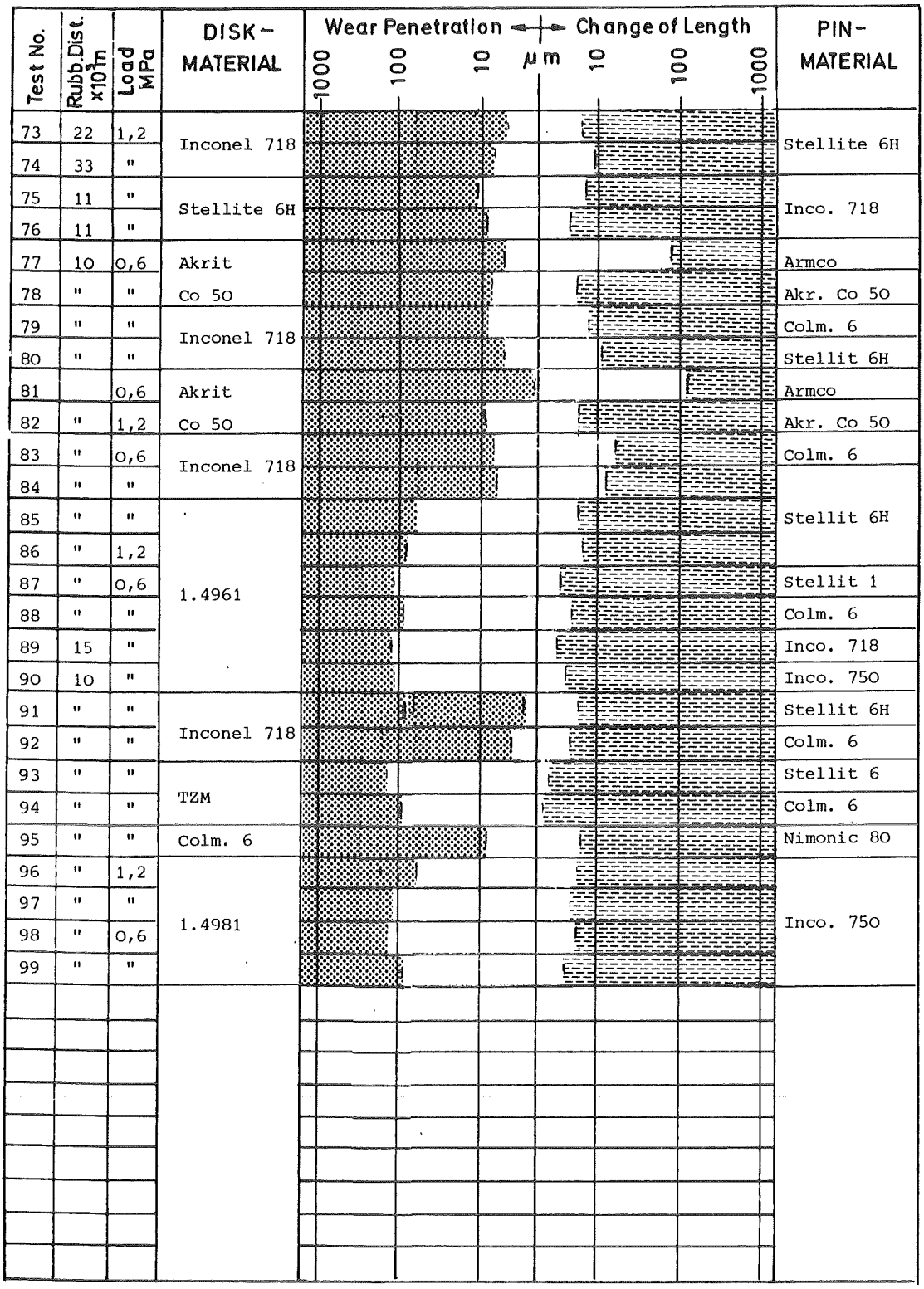

Fig. 29c Material Wear of Hybrid Pairings

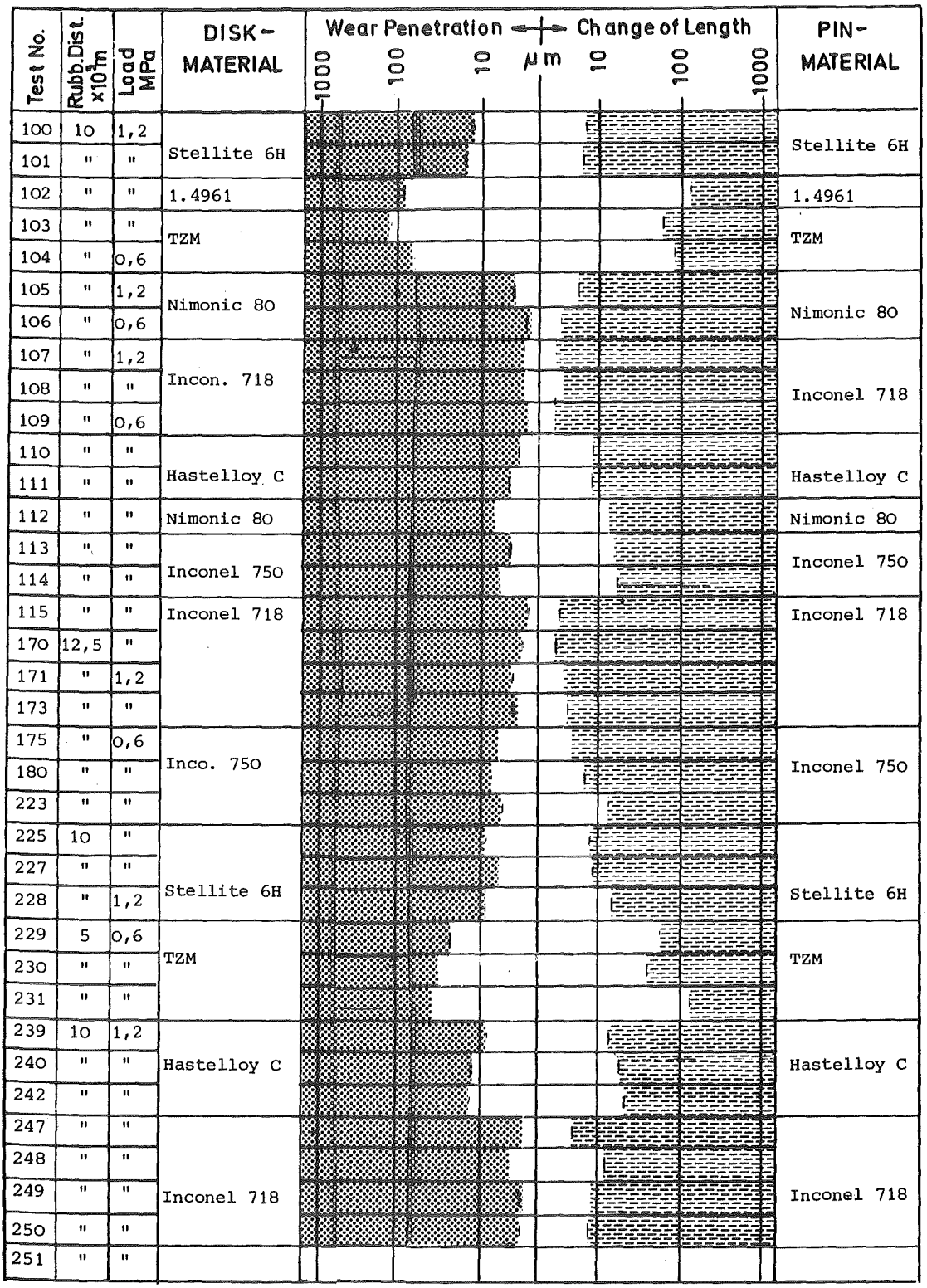

Fig. 29d Material Wear of Like on Like Couples

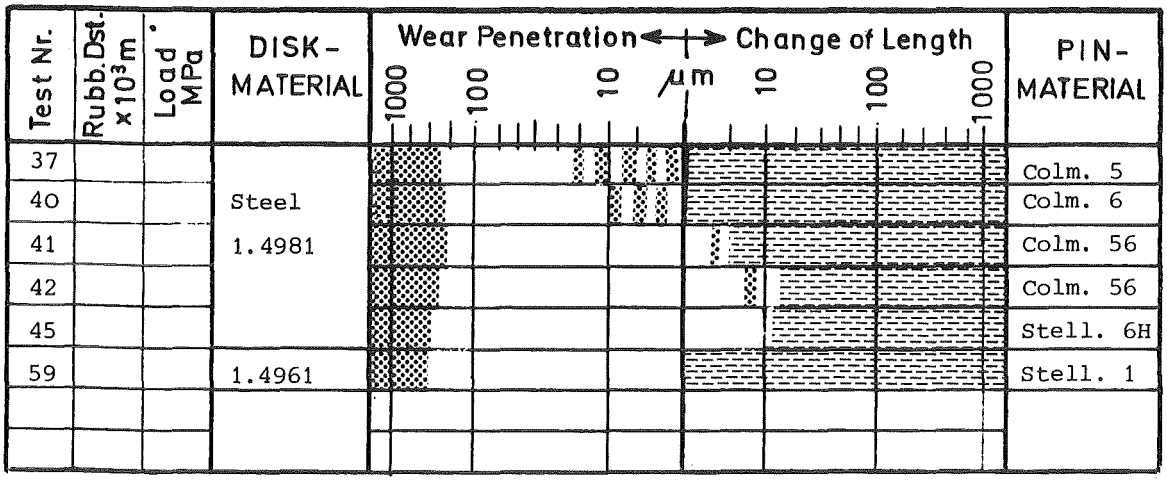

Fig. 30 Wear of "One Side Steel" Pairings

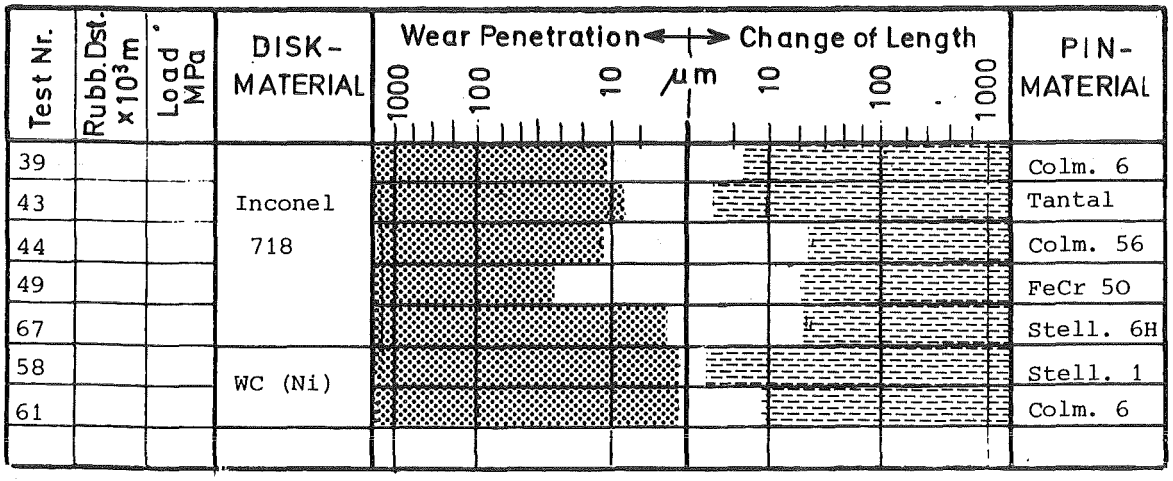

Fig. 31 Wear of Hybrid Pairings

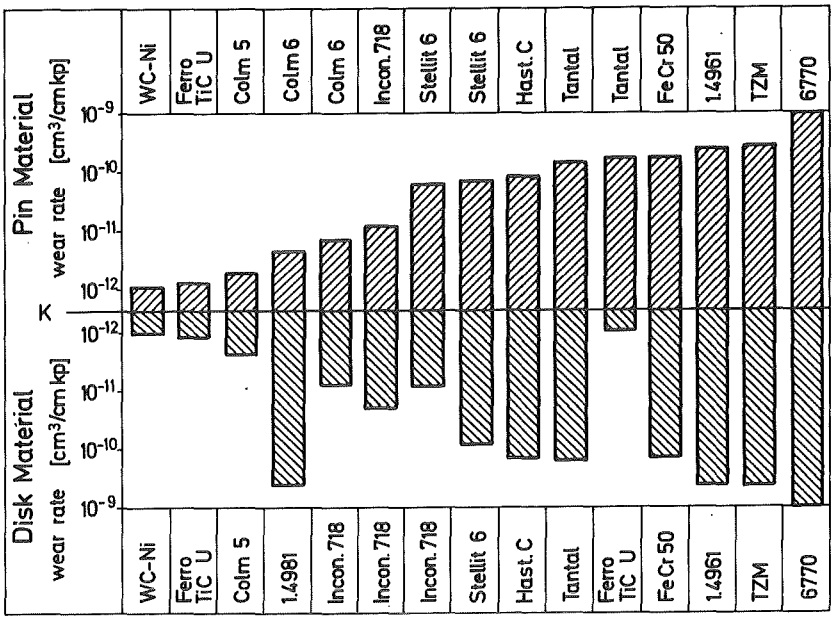

Fig. 32 Wear Rates of Material Couples

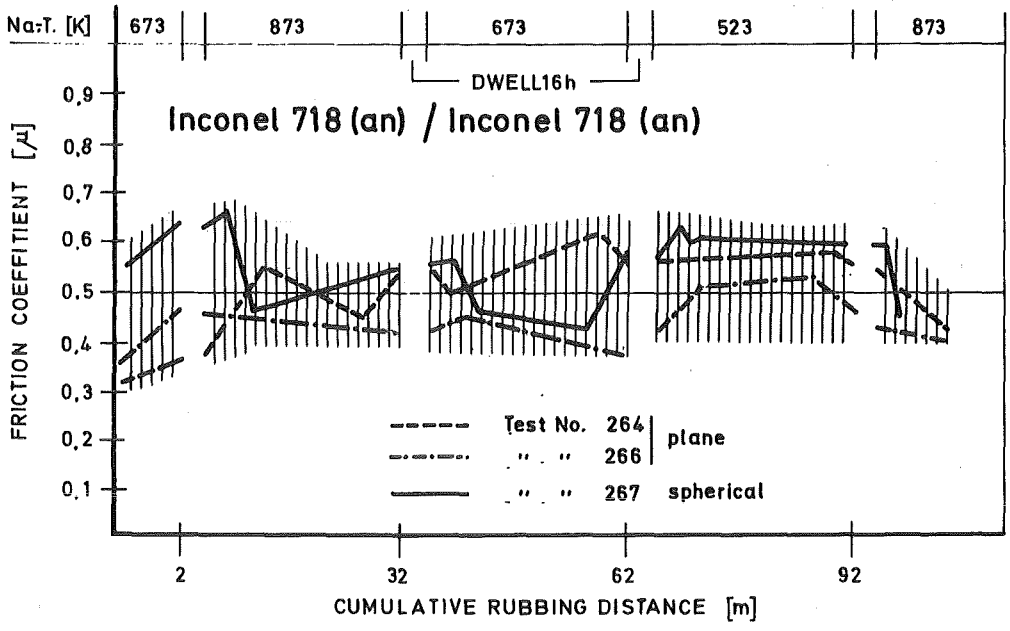

Fig. 33 Average Dynamic Friction Coefficient of Inconel 718 (an)

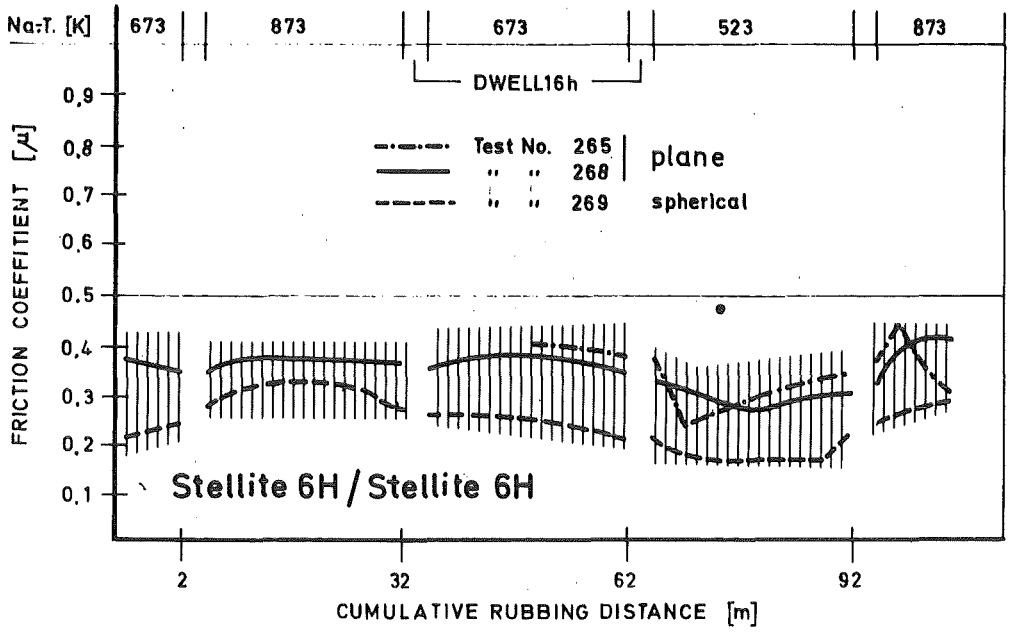

Fig. 34 Average Dynamic Friction Coefficient of Stellite 6 H

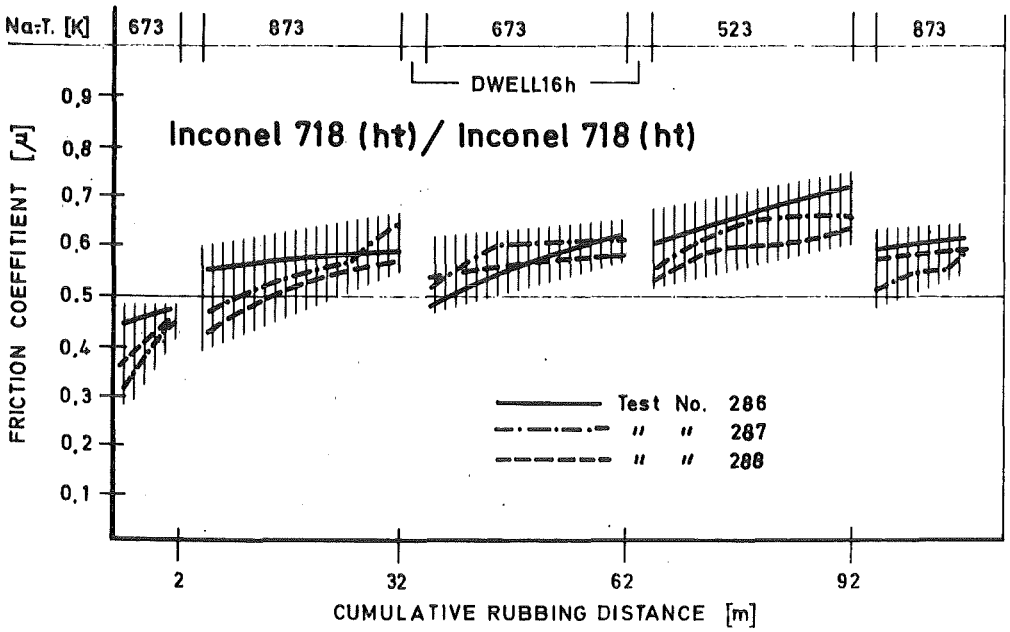

Fig. 35 Average Dynamic Friction Coefficient of Inconel 718 (ht)

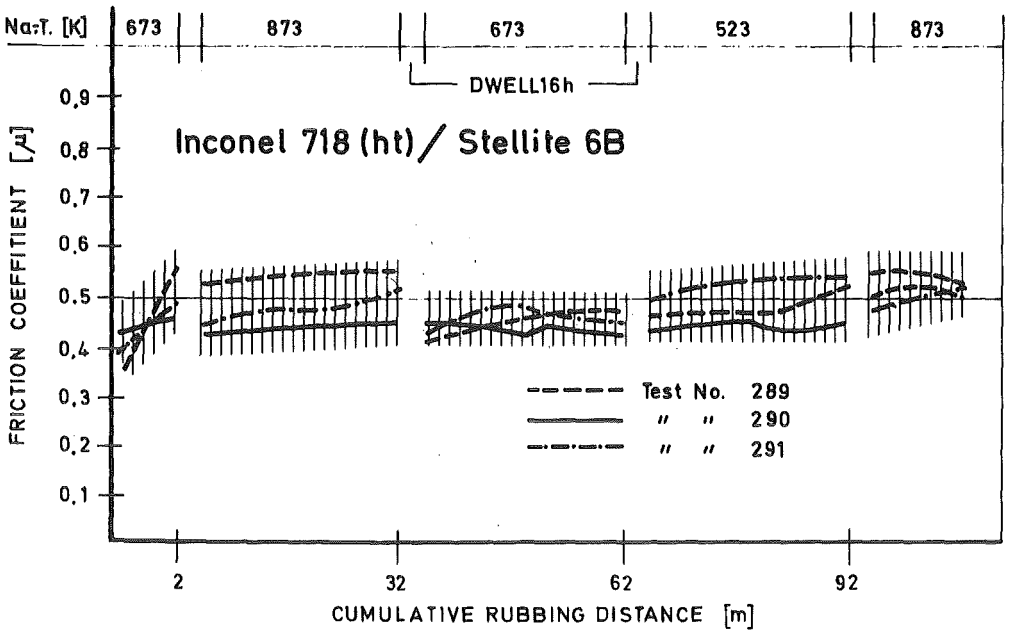

Fig. 36 Average Dynamic Friction Coefficient of Hybrid Pairings

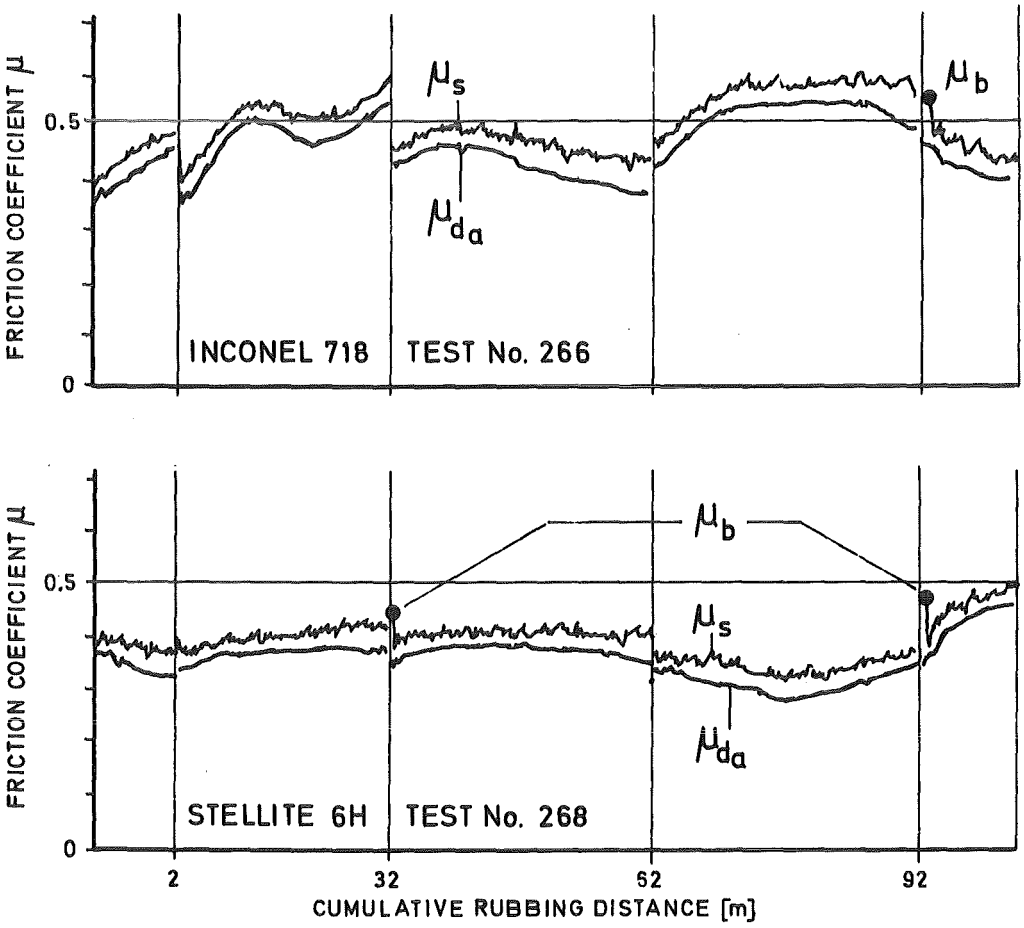

Fig. 37 Recorder Traces of Friction Forces

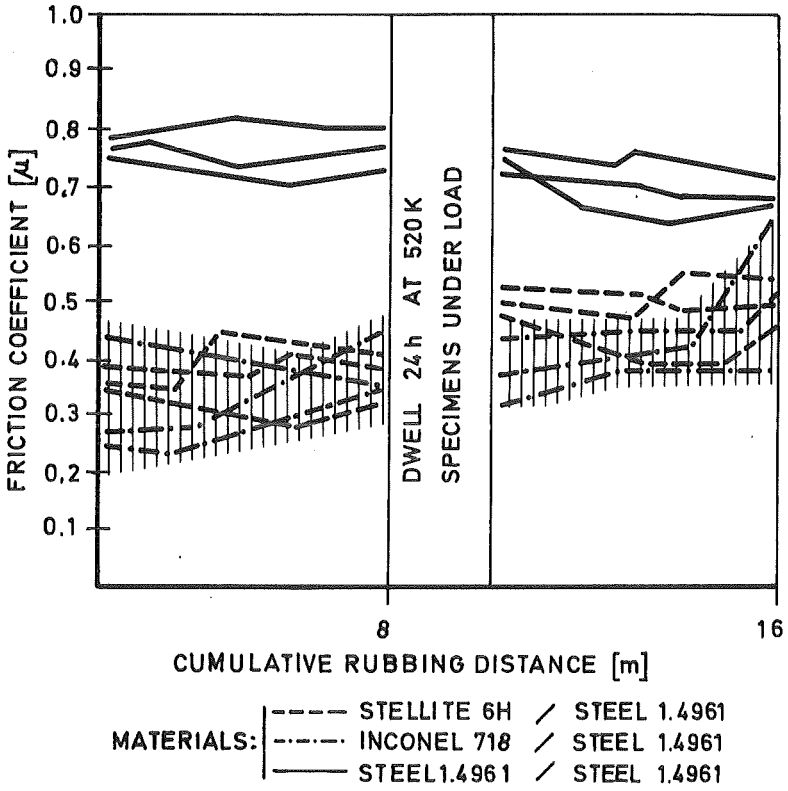

Fig. 38 Dynamic Friction Coefficients of Materials

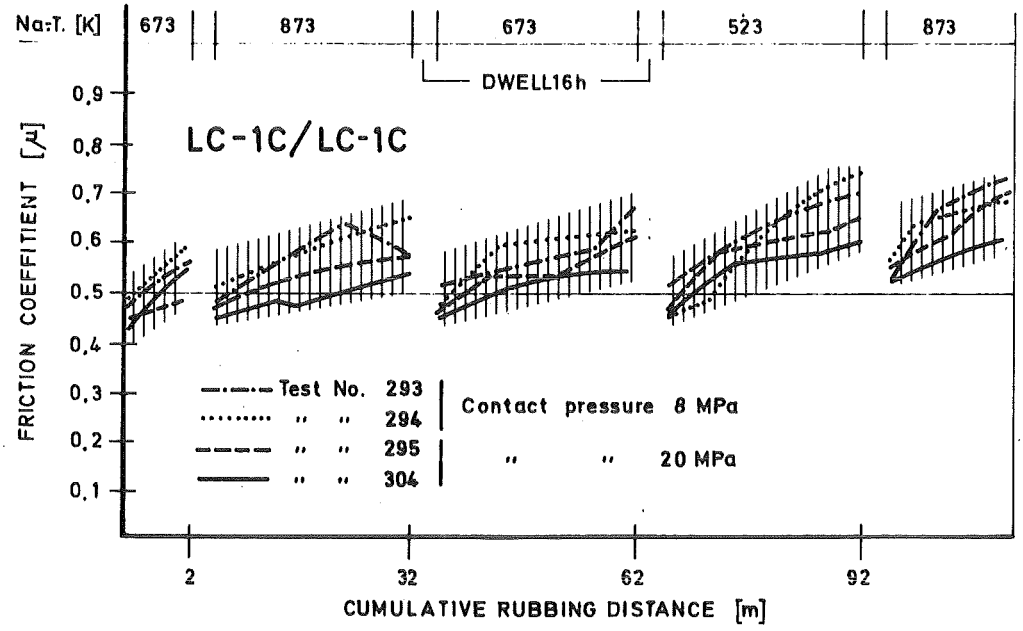

Fig. 39 Dynamic Friction Coefficients of LC-1C

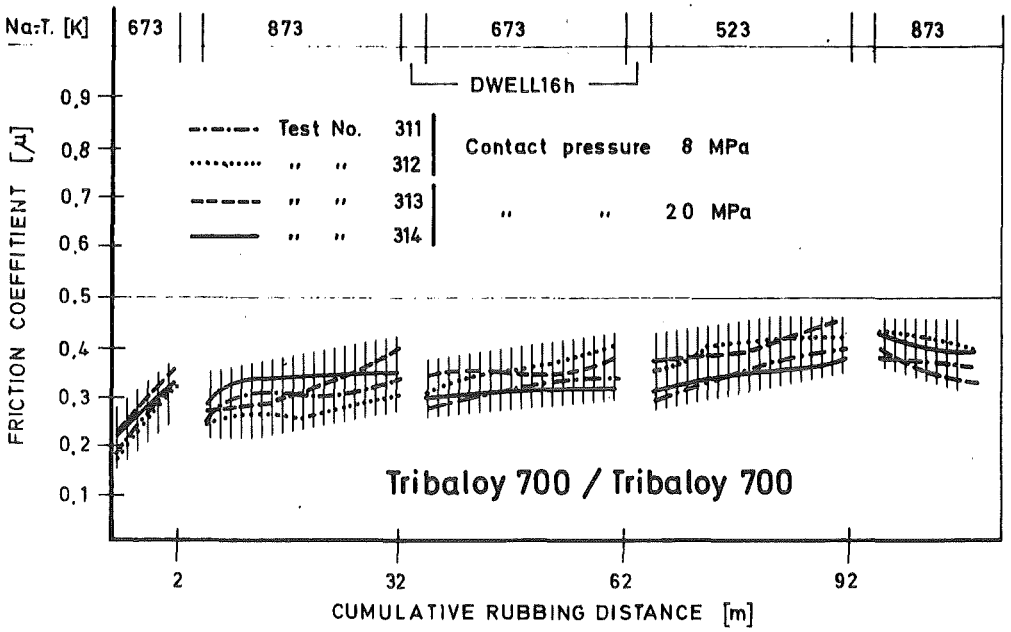

Fig. 40 Dynamic Friction Coefficients of Tribaloy 700

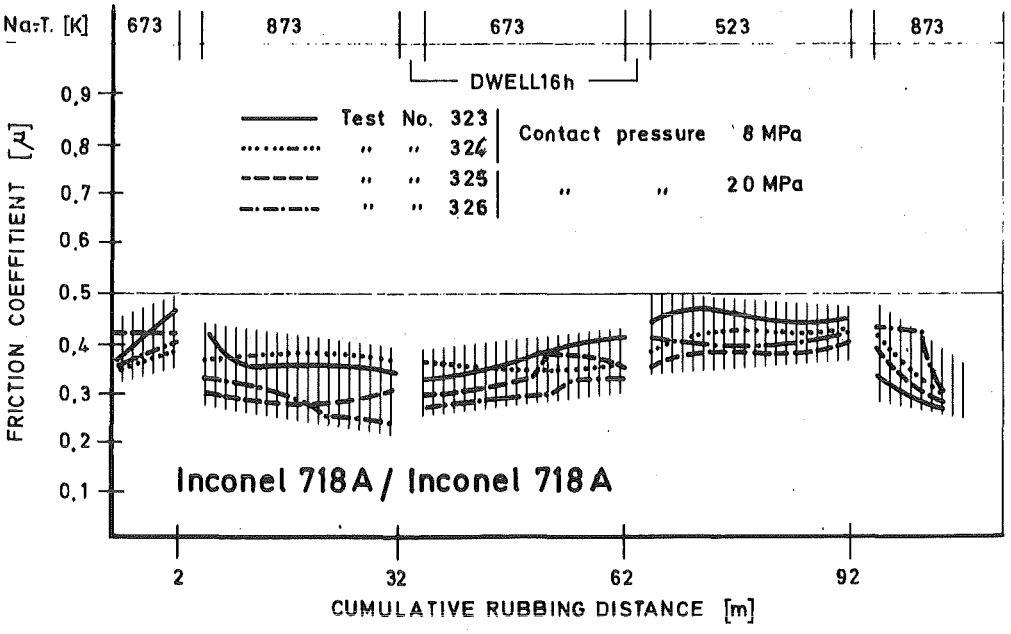

Fig. 41 Dynamic Friction Coefficients of Inconel 718 A

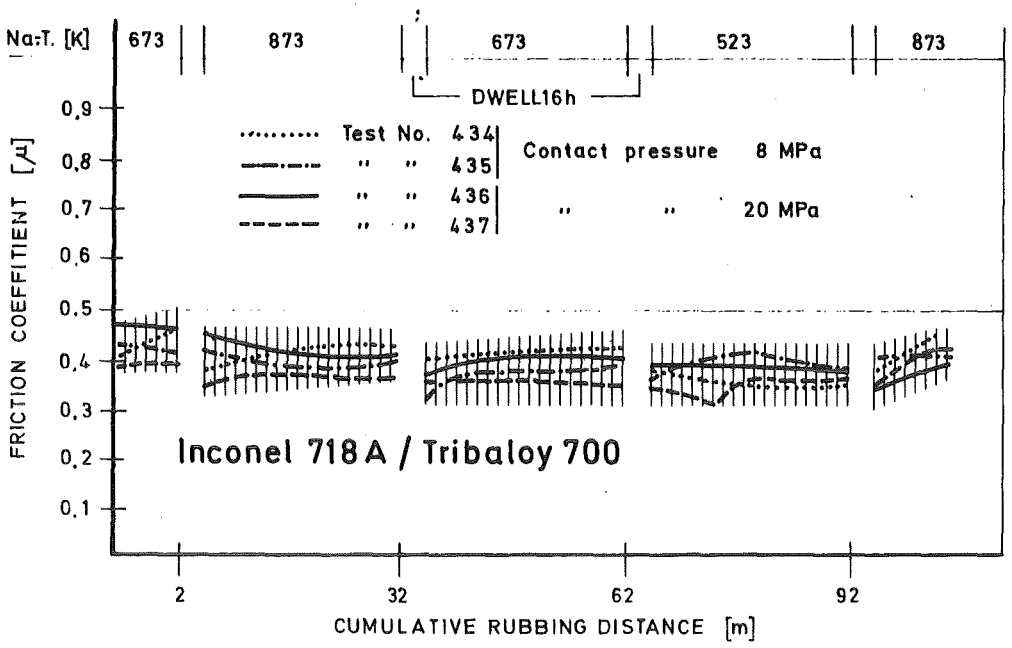

Fig. 42 Dynamic Friction Coefficients of Material Pairings

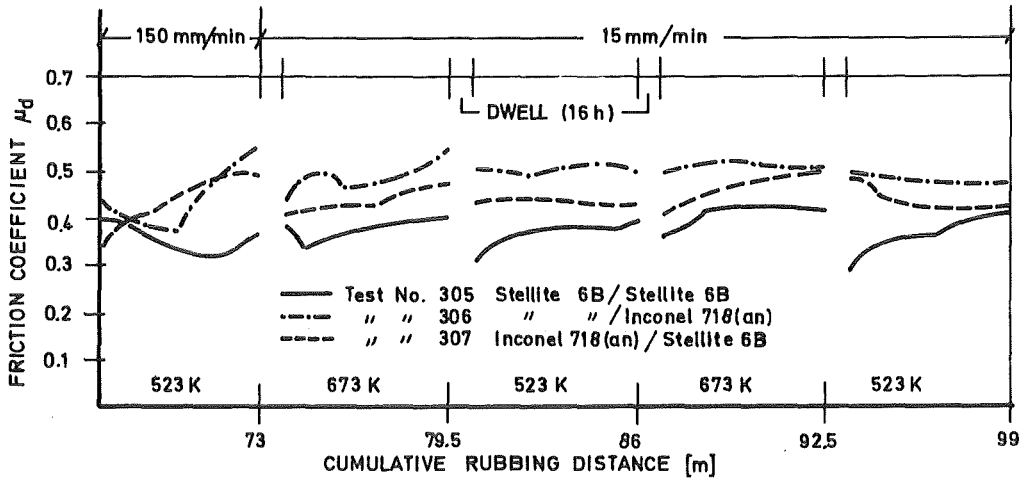

Fig. 43 Dynamic Friction Coefficients of Material Pairings

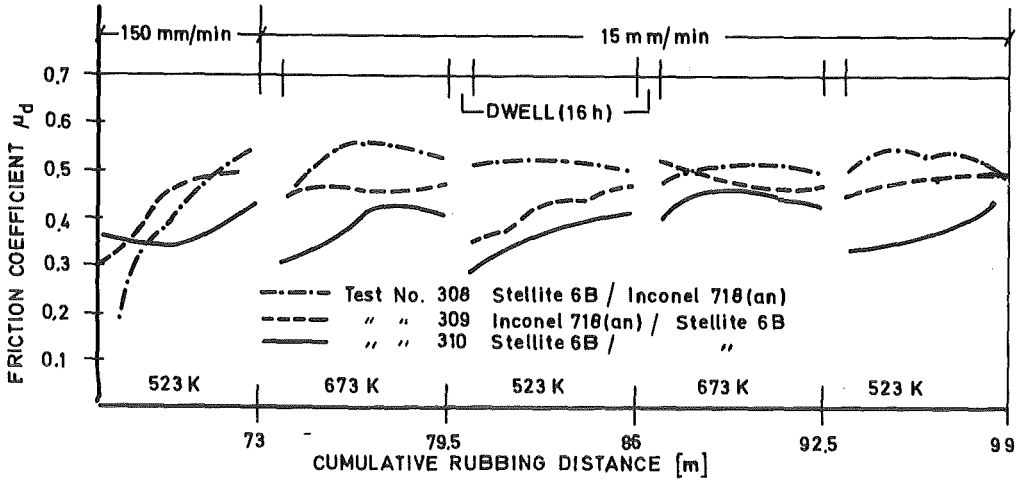

Fig. 44 Dynamic Friction Coefficients of Material Pairings

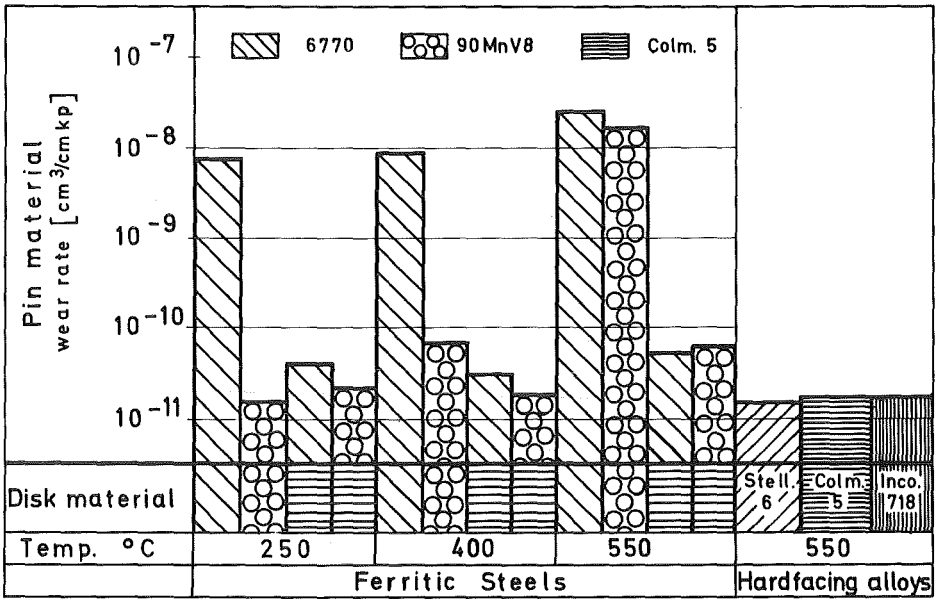

Fig. 45 Wear Rates of Materials (function of Na-temperature)

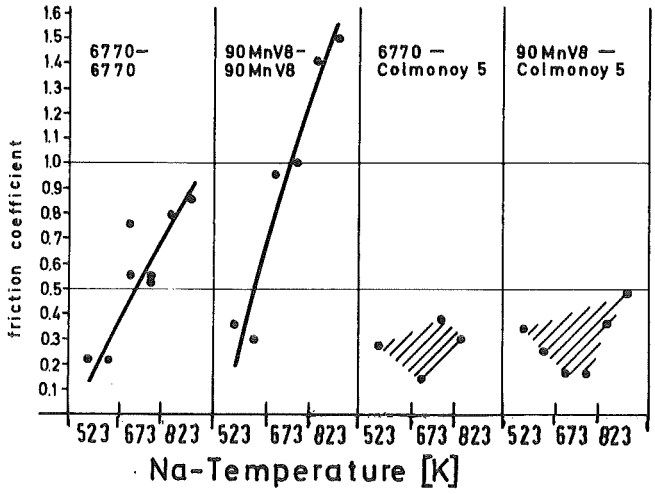

Fig. 46 Friction Coefficient of Materials (function of Na-temperature)

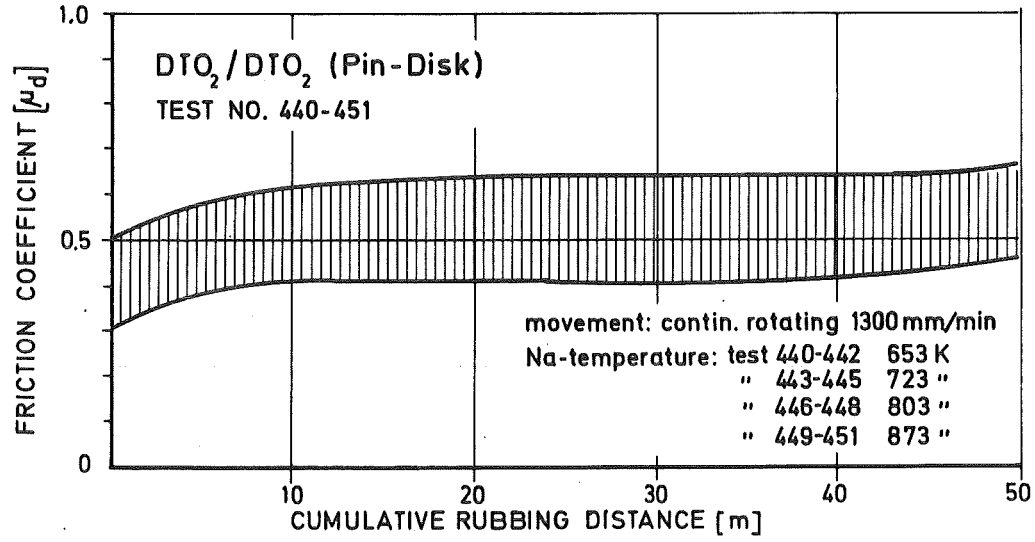

Fig. 47 Dynamic Friction Coefficient of Ferritic Steel (DTO_2) Standard Pairing

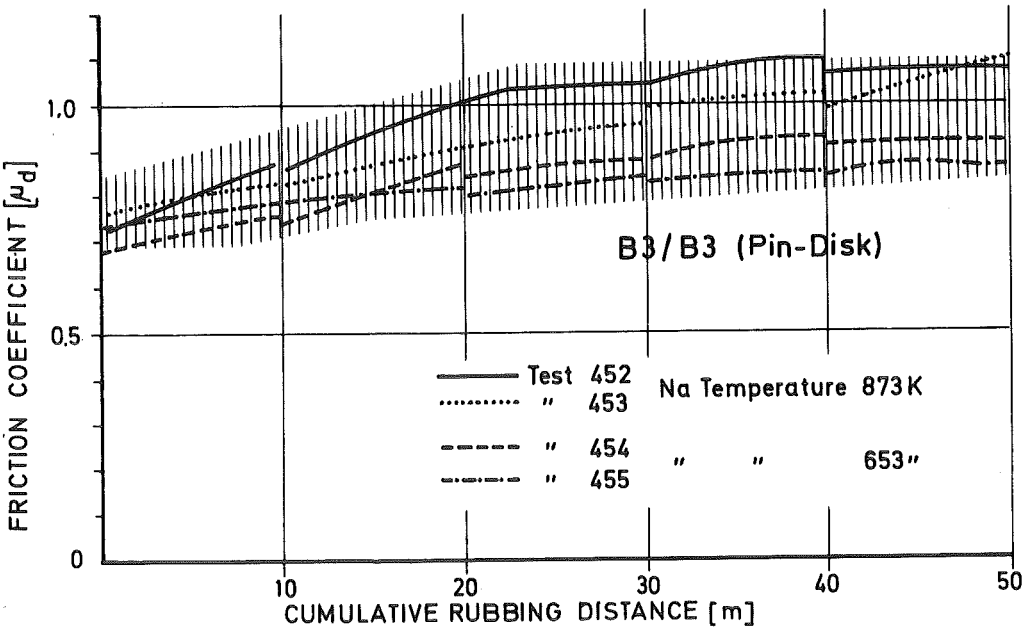

Fig. 48 Dynamic Friction Coefficient of Ferritic Steel (B3) Standard Pairings

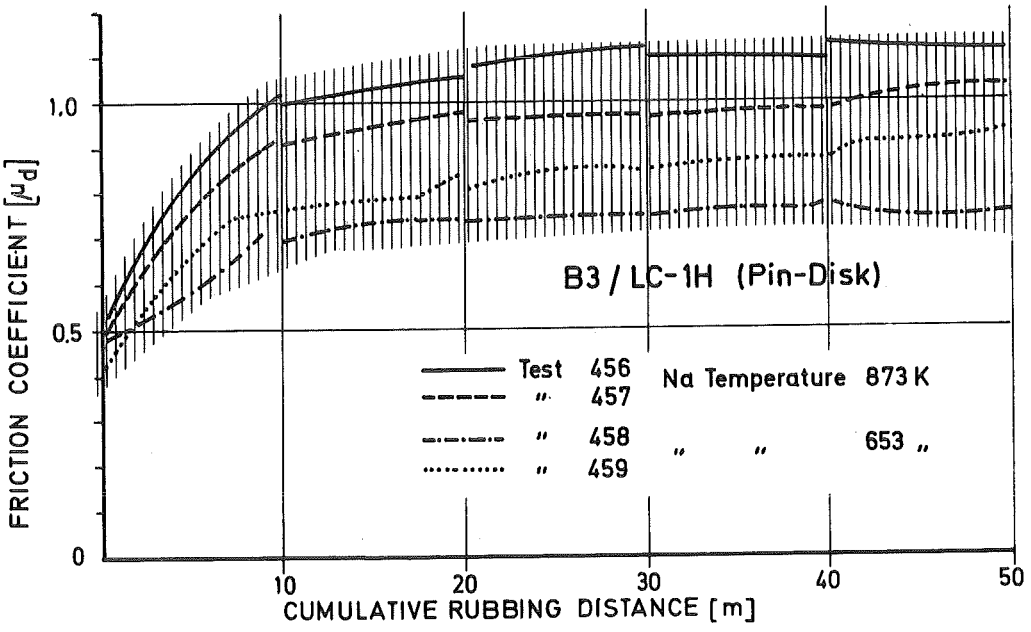

Fig. 49 Dynamic Friction Coefficient of Materials

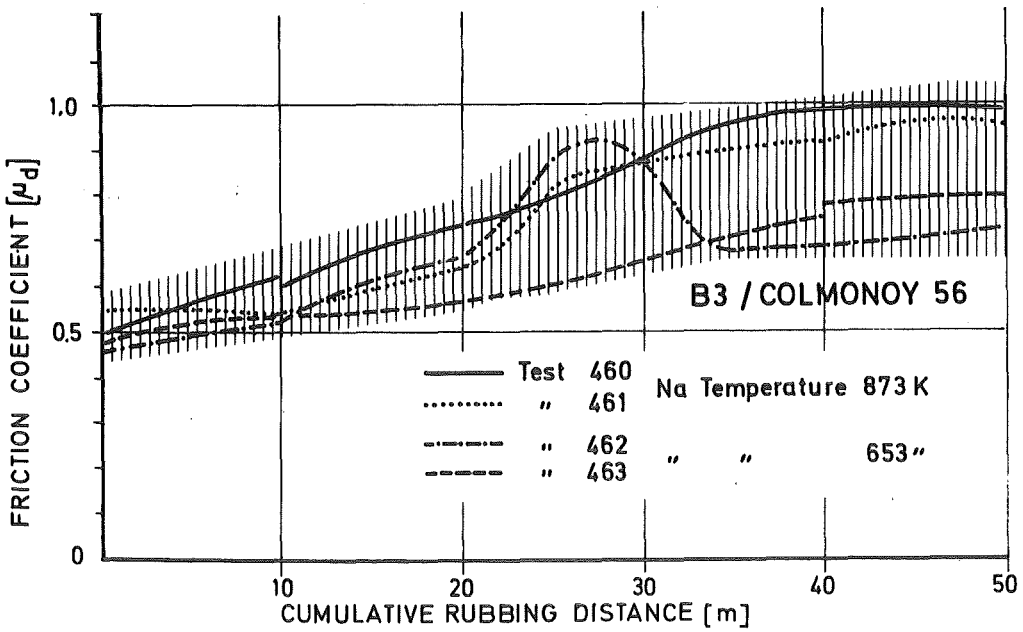

Fig. 50 Dynamic Friction Coefficient of Materials Standard Pairings

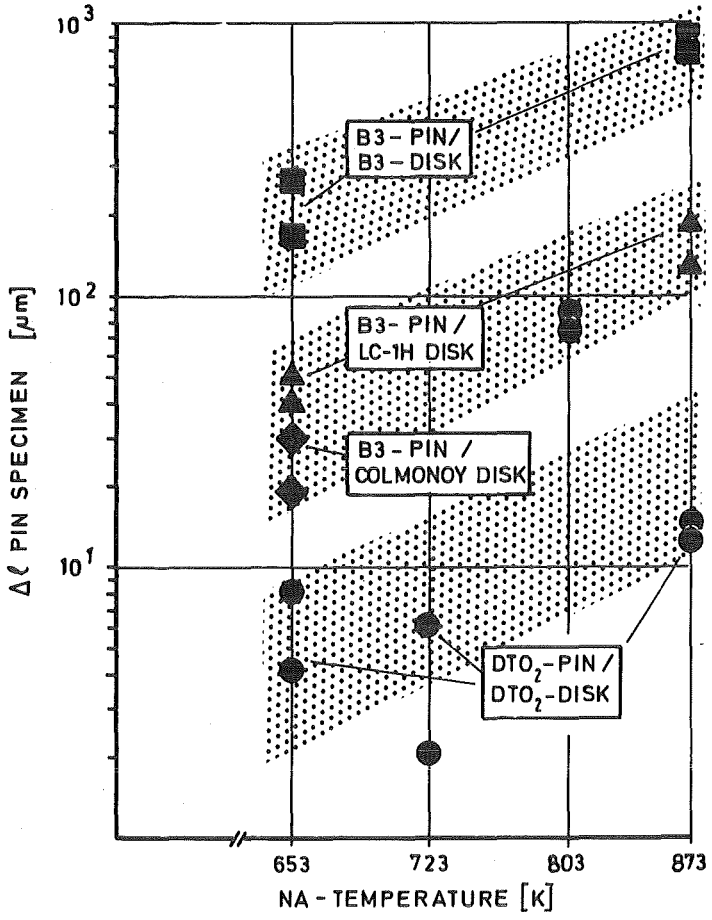

Fig. 51 Relative Wear of Material Couples

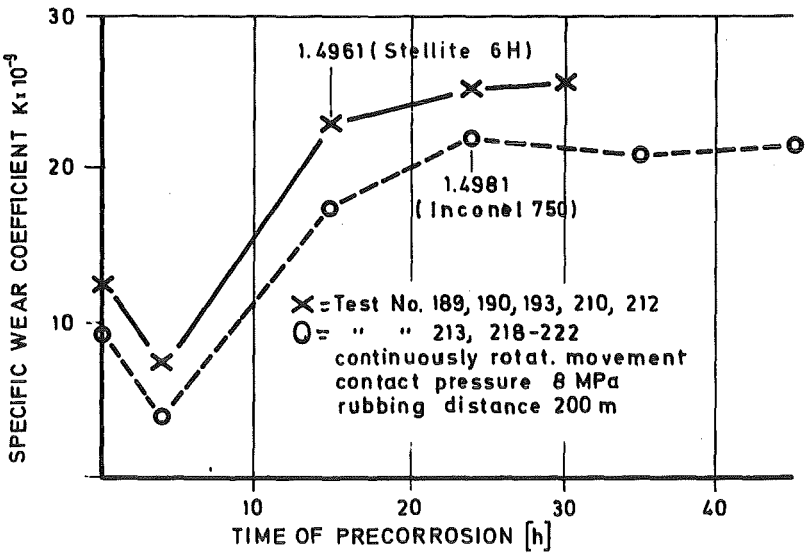

Fig. 52 Material Wear (function of precorrosion)

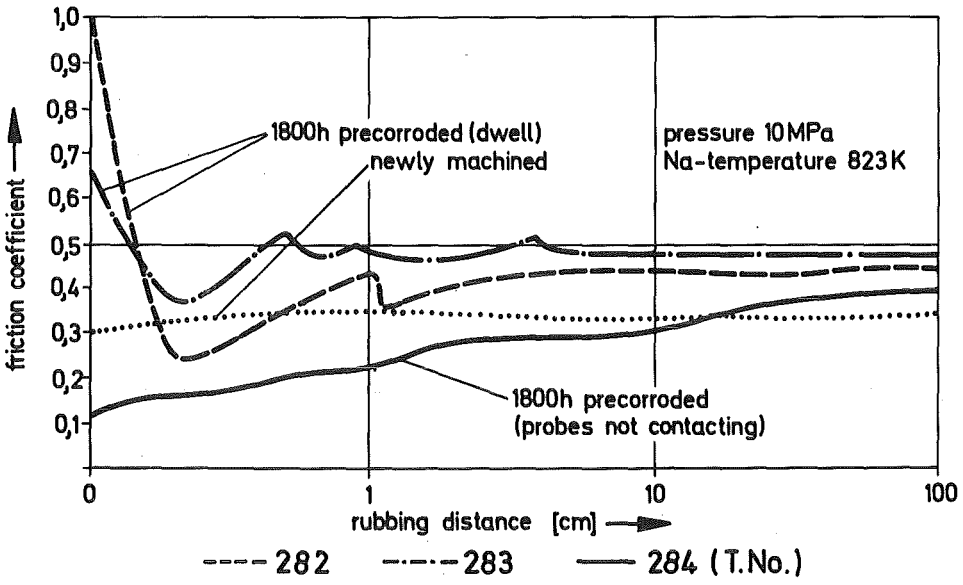

Fig. 53 Dynamic Friction Coefficient of Stellite 6 H (function of precorrosion)

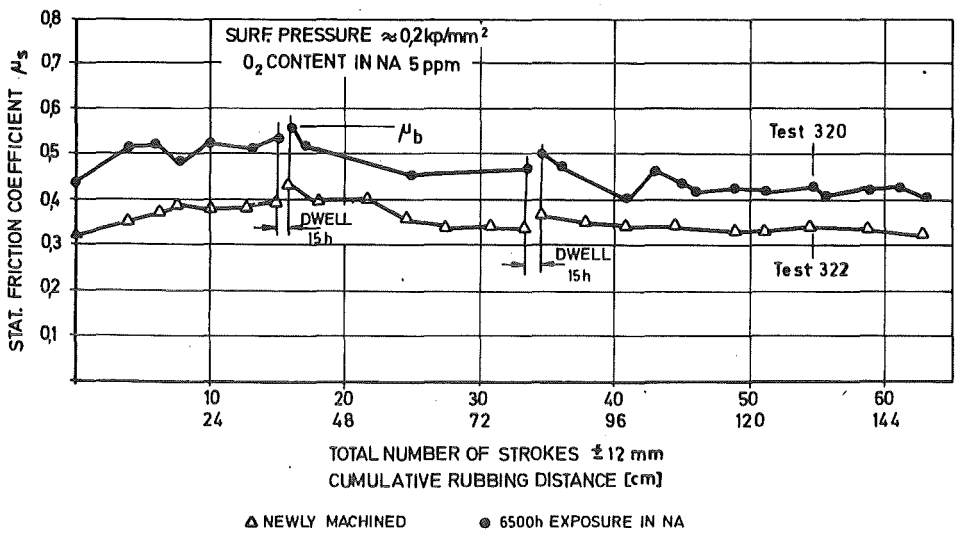

Fig. 54 Dynamic Friction Coefficient of Stellite 6 H (function of precorrosion)

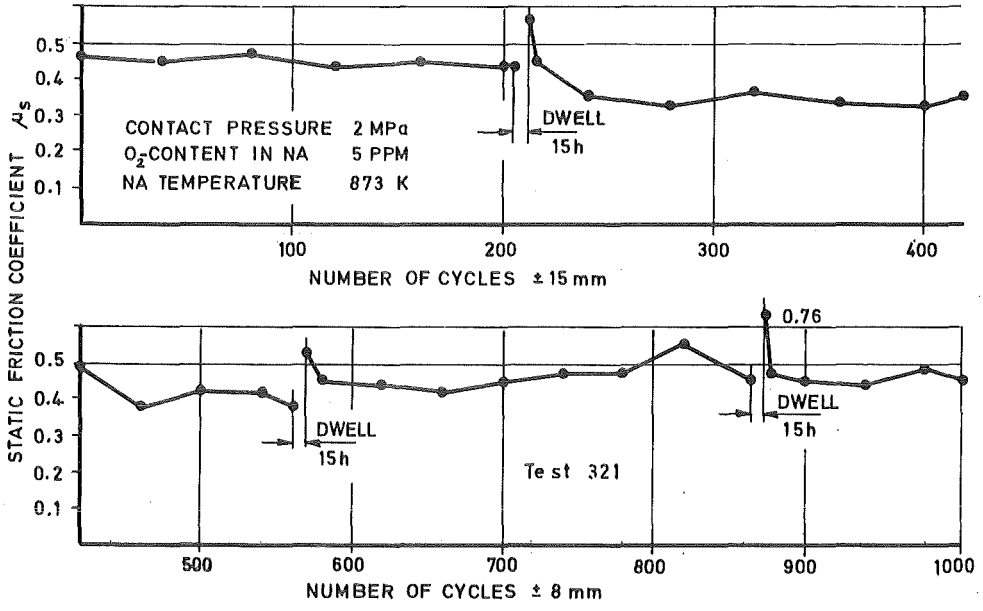

Fig. 55 Dynamic Friction Coefficient of Stellite 6 H (function of precorrosion)

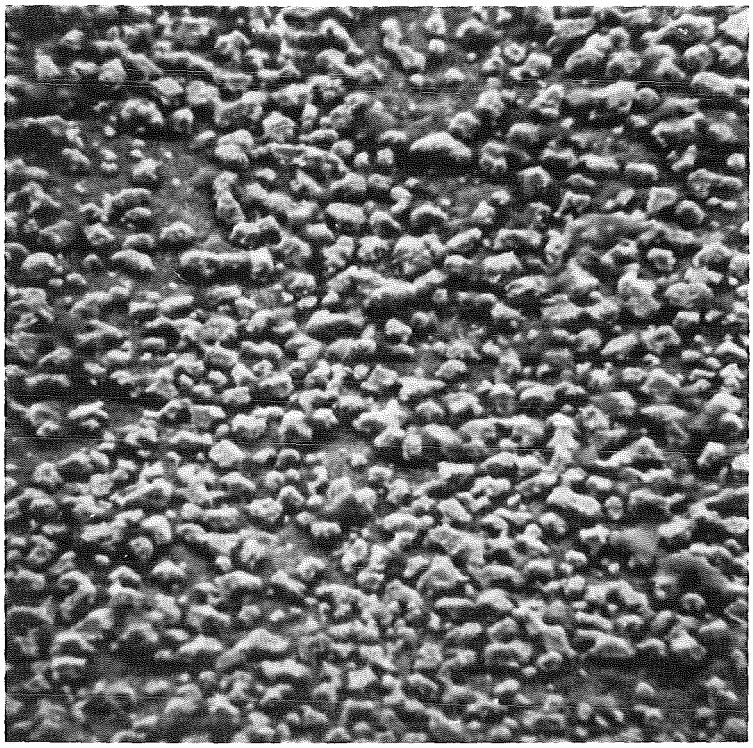

Fig. 56 Stellite 6 H Surface after 6500 h of precorrosion

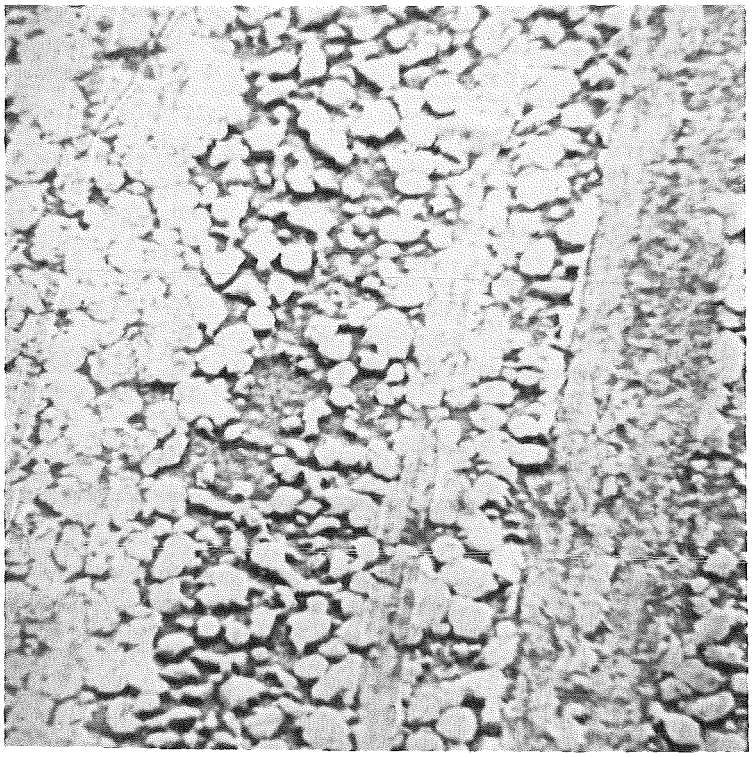

Fig. 57 Deformation of Fe-Co Grains by Friction Load

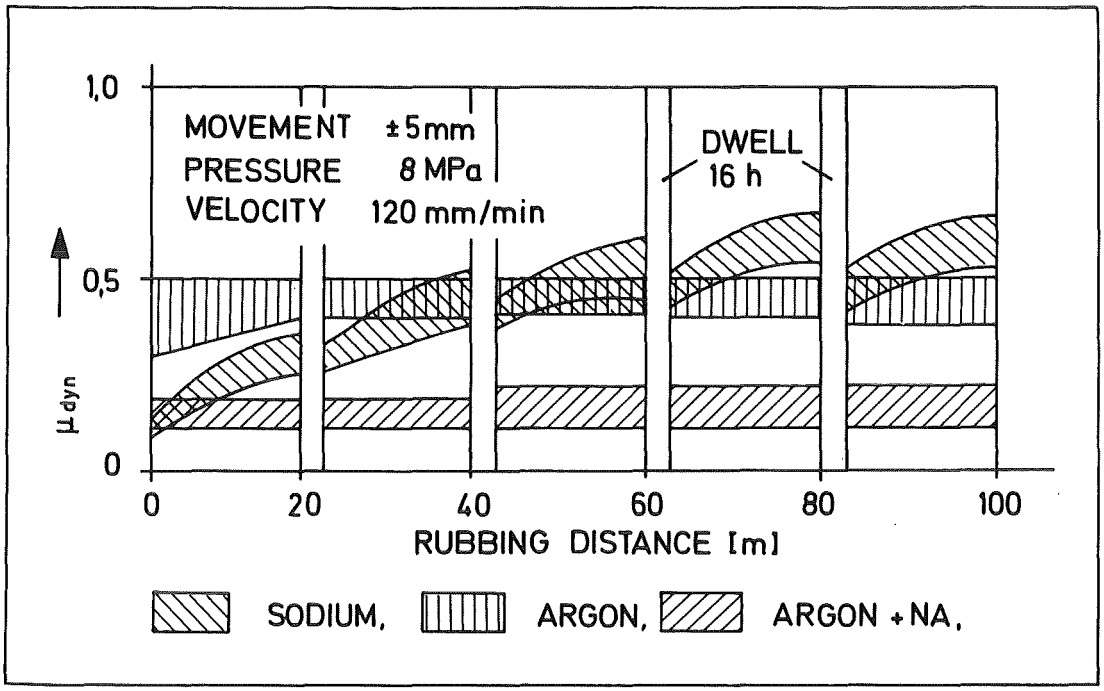

Fig. 58 Dynamic Friction Coefficients of LC-1H (function of environment)

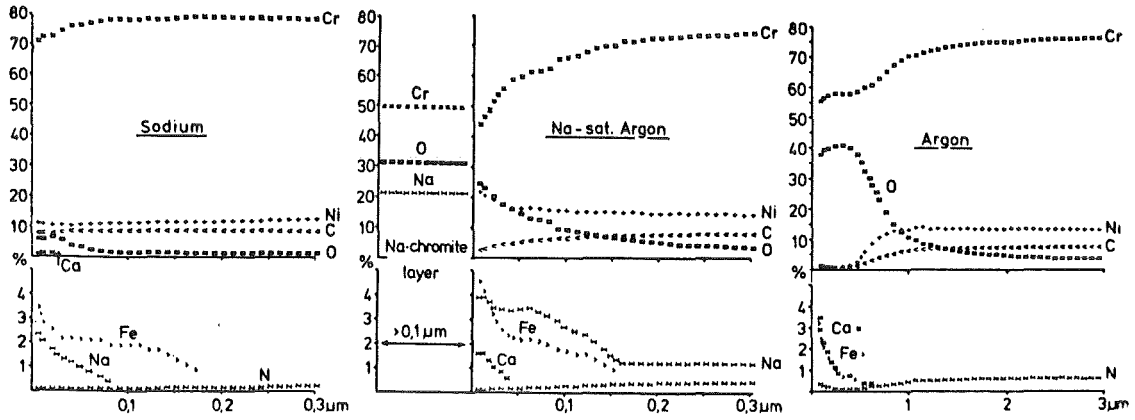

Fig. 59 Surface Composition of Chromium Carbide Coatings LC-1H after Exposure to different Environments

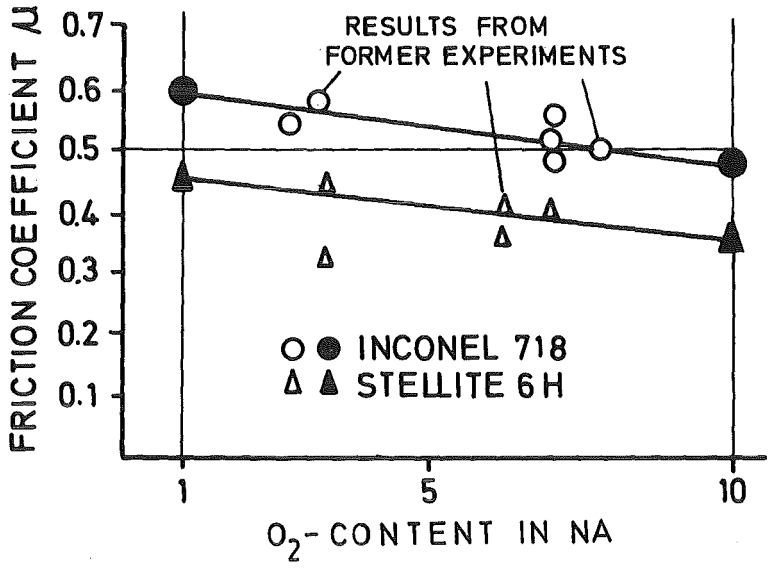

Fig. 60 Dynamic Friction Coefficients of Materials (function of O_2-Content in Na)

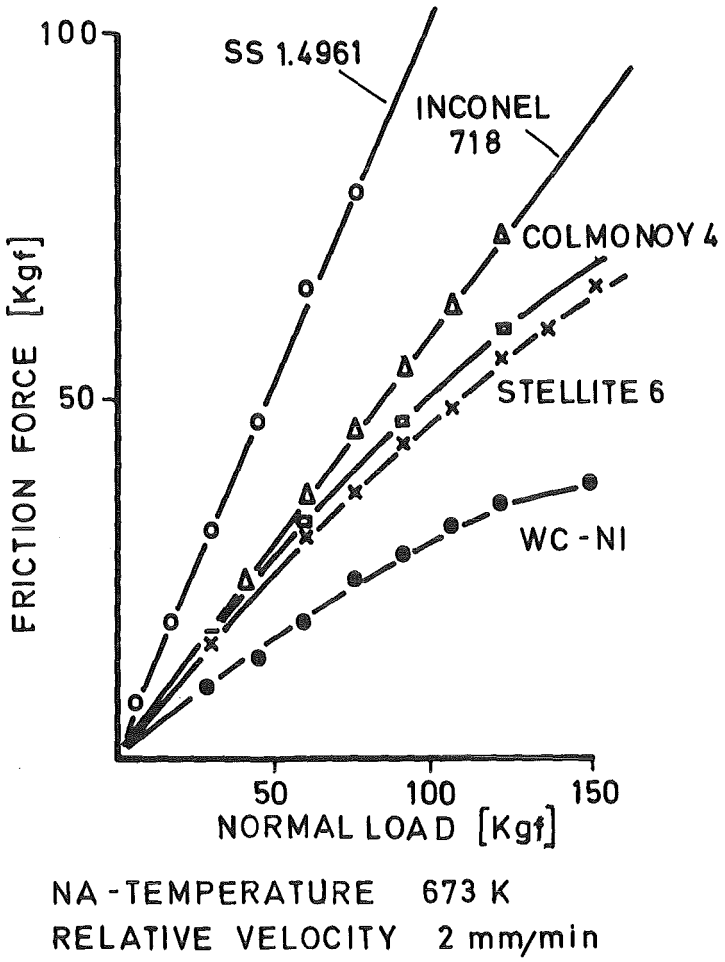

Fig. 61 Friction Forces Measured as Function of Normal Load

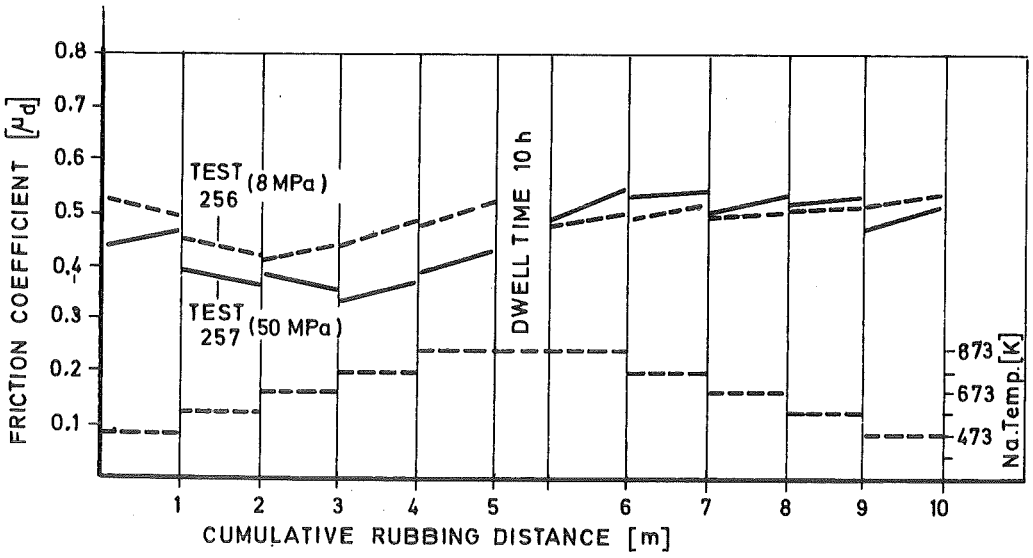

Fig. 62 Dynamic Friction Coefficients of Inconel 718 (function of Na-temperature)

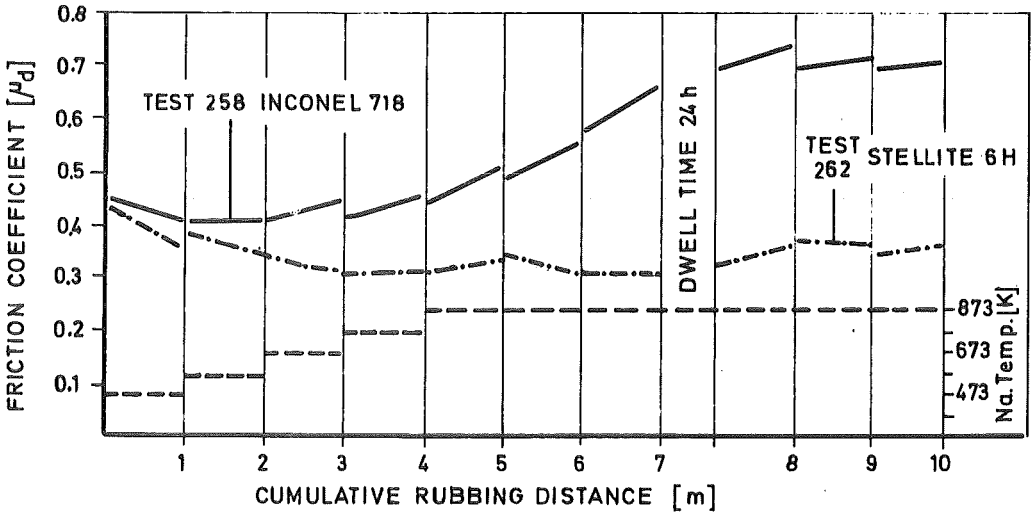

Fig. 63 Dynamic Friction Coefficients of Materials (function of Na-temperature)

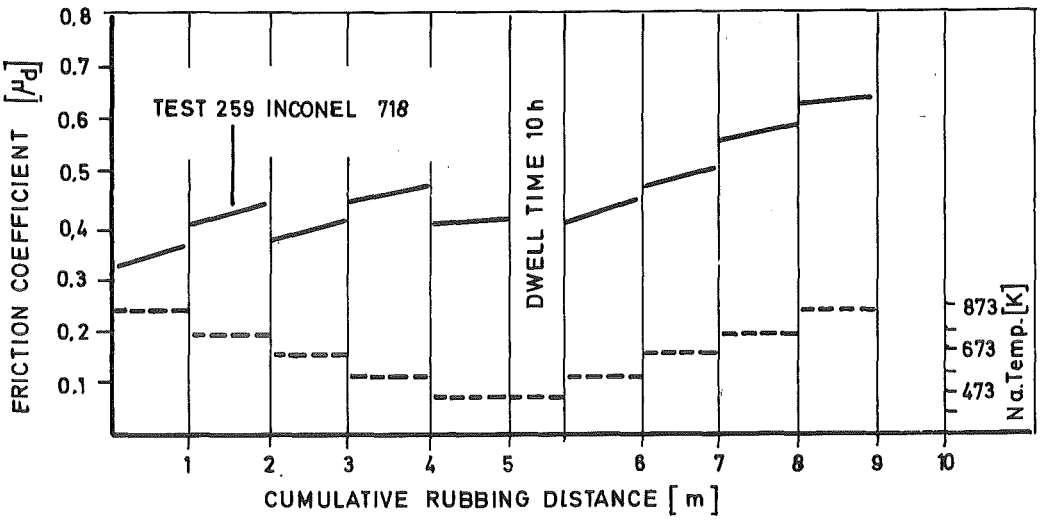

Fig. 64 Dynamic Friction Coefficient of Inconel 718 (function of Na-temperature)

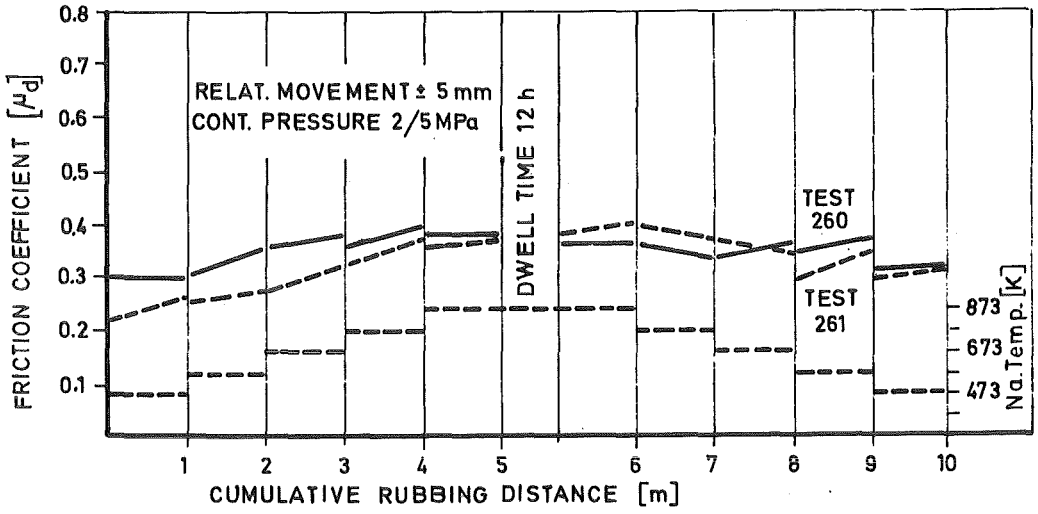

Fig. 65 Dynamic Friction Coefficient of Stellite 6 H (function of Na-temperature)

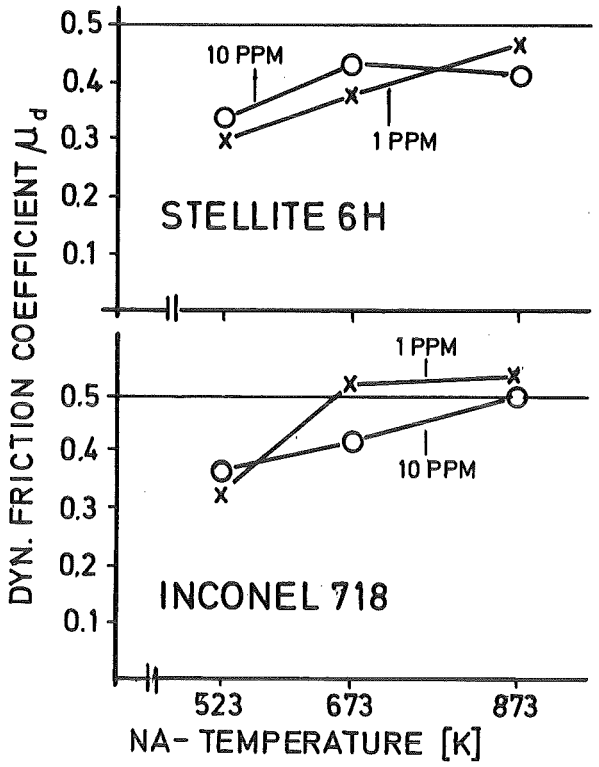

Fig. 66 Dynamic Friction Coefficients of Materials (function of Na-temperature)

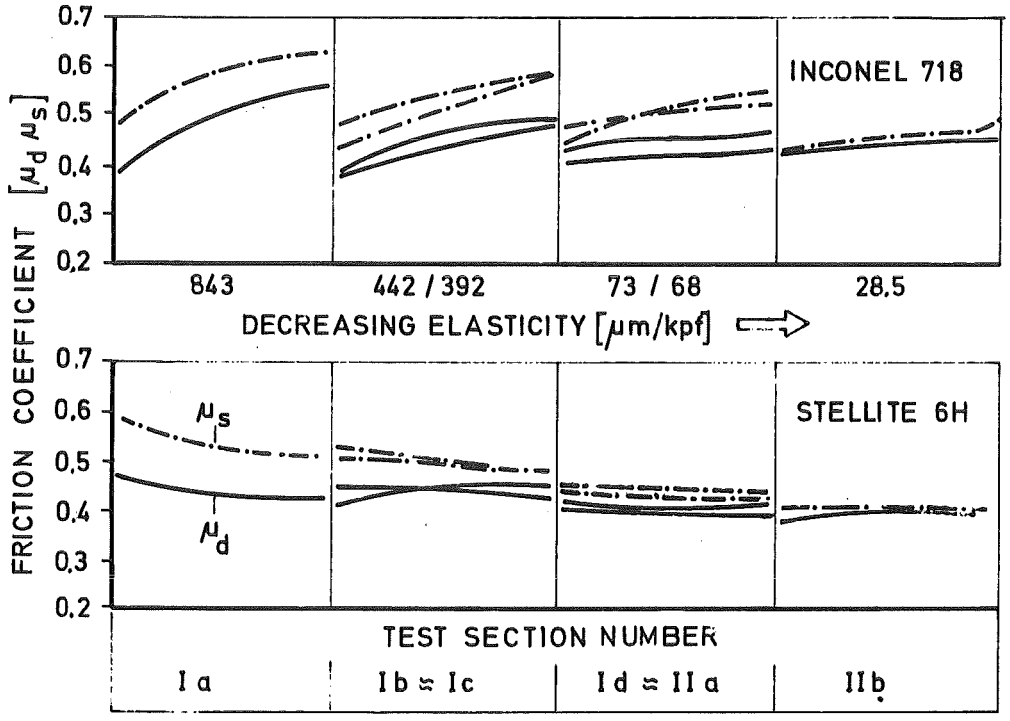

Fig. 67 Friction Coefficients of Materials (function of test section elasticity)

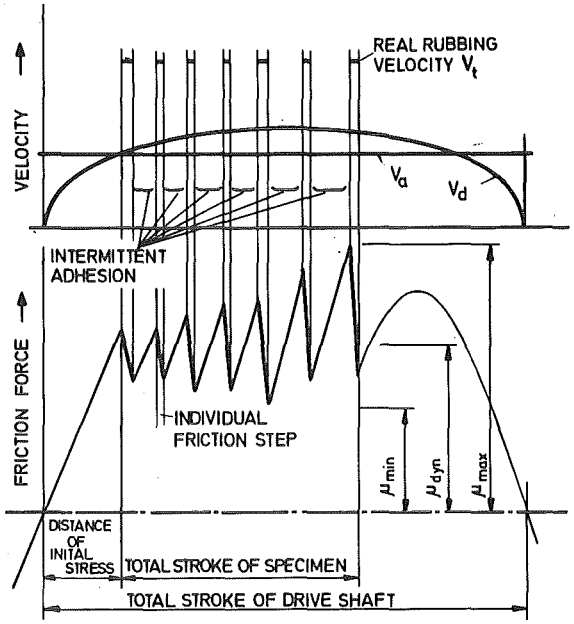

Fig. 68 Friction Force and According Real Rubbing Velocity

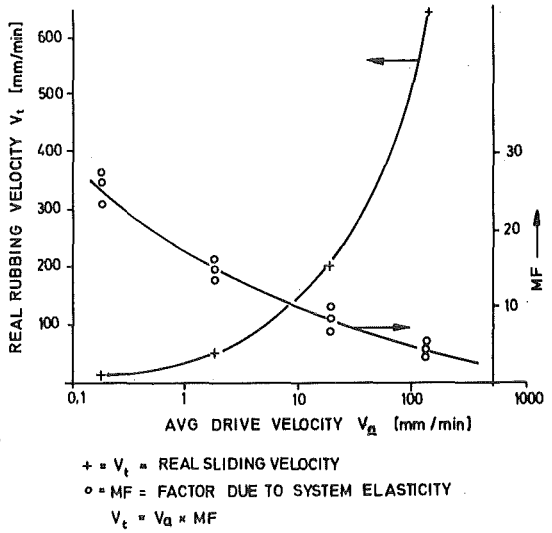

Fig. 69 Ratio of Average Drive Velocity and Real Rubbing Velocity (test section Ia)

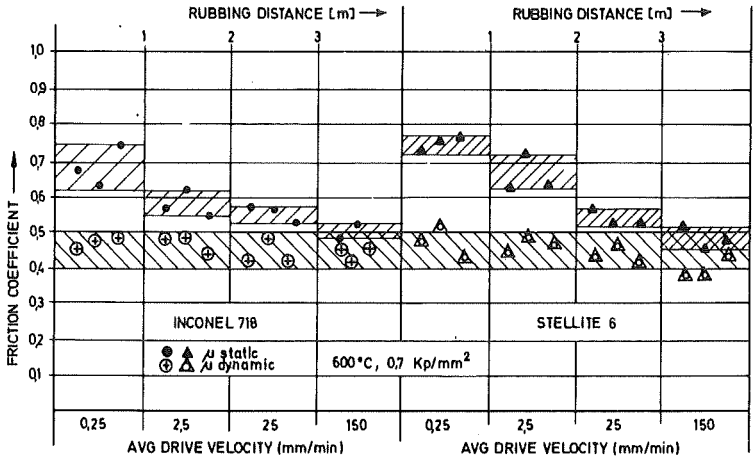

Fig. 70 Friction Coefficient As Function of Average Drive Velocity

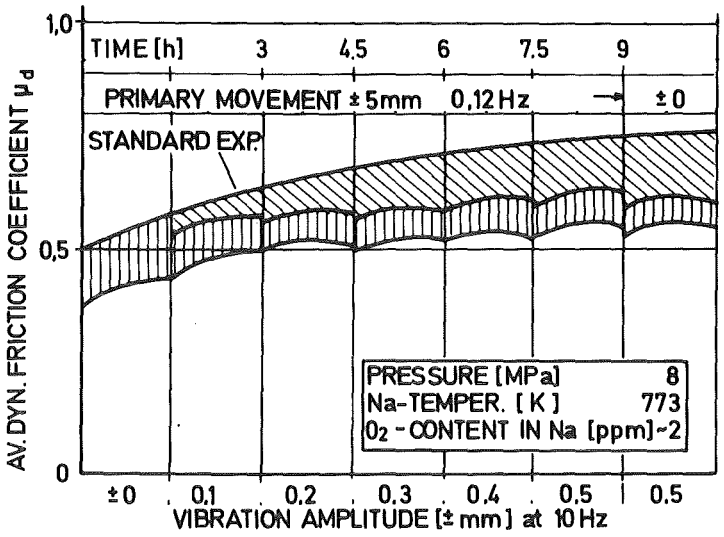

Fig. 71 Dynamic Friction Coefficient of LC-1H (function of superimposed oscillating movement)

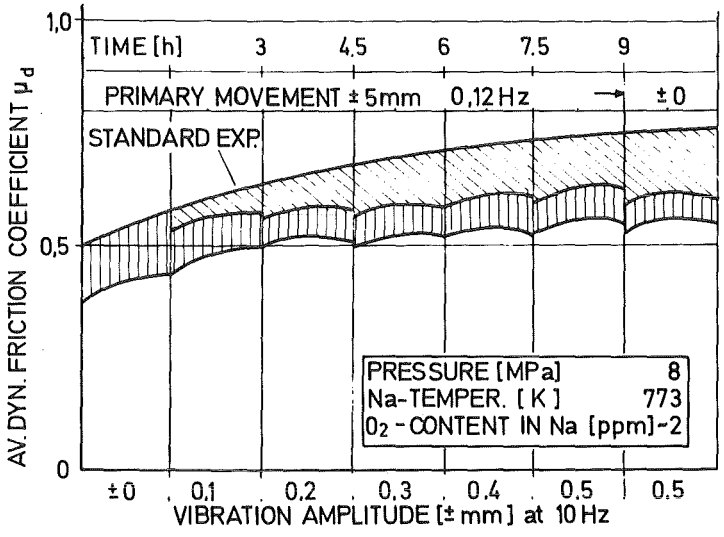

Fig. 72 Dynamic Friction Coefficient of LC-1H (function of superimposed oscillating movement)

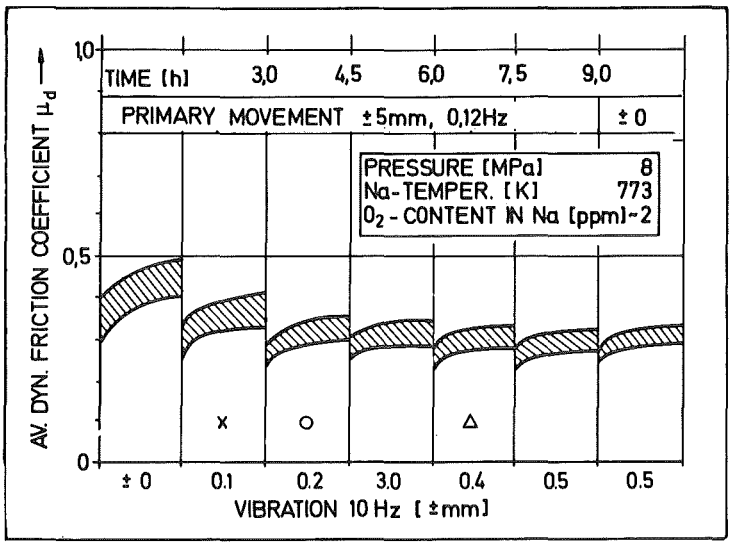

Fig. 73 Dynamic Friction Coefficient of Tribaloy 700 (function of superimposed oscillating movement)

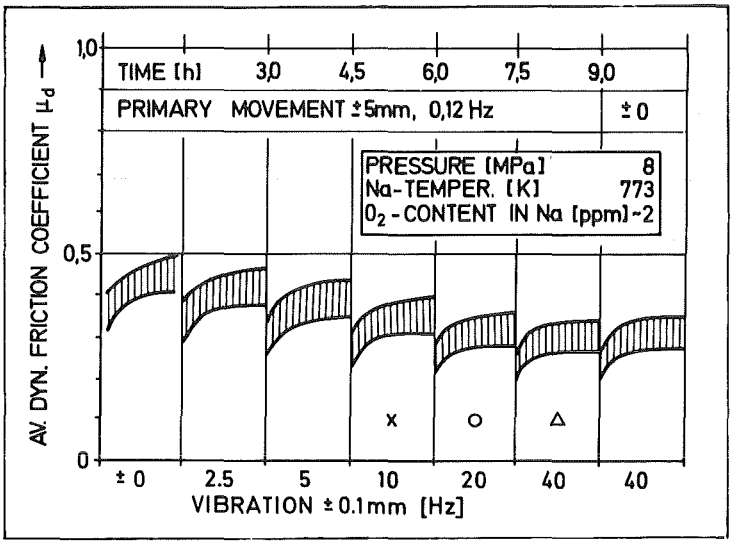

Fig. 74 Dynamic Friction Coefficient of Tribaloy 700 (function of superimposed oscillating movement)

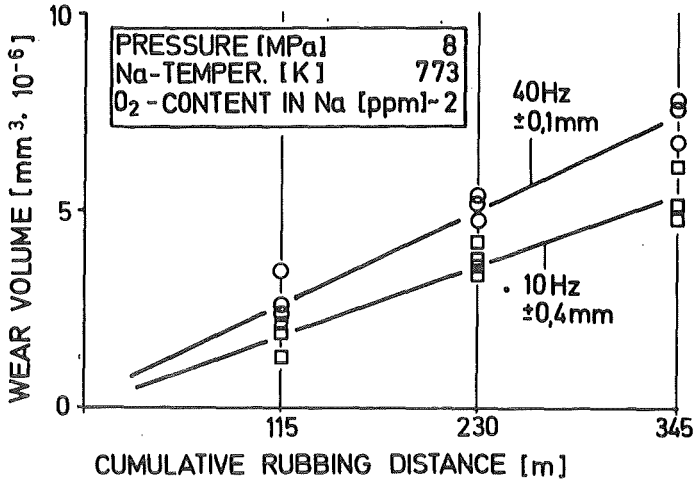

Fig. 75 Material Wear of LC-1H (function of superimposed movement)

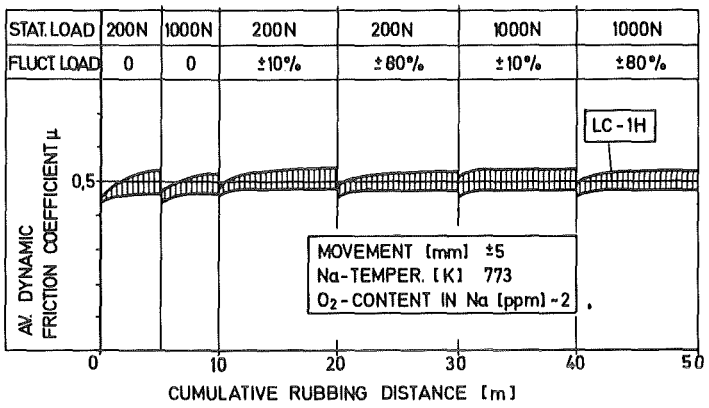

Fig. 76 Dynamic Friction Coefficient of LC-1H (function of cycling normal load)

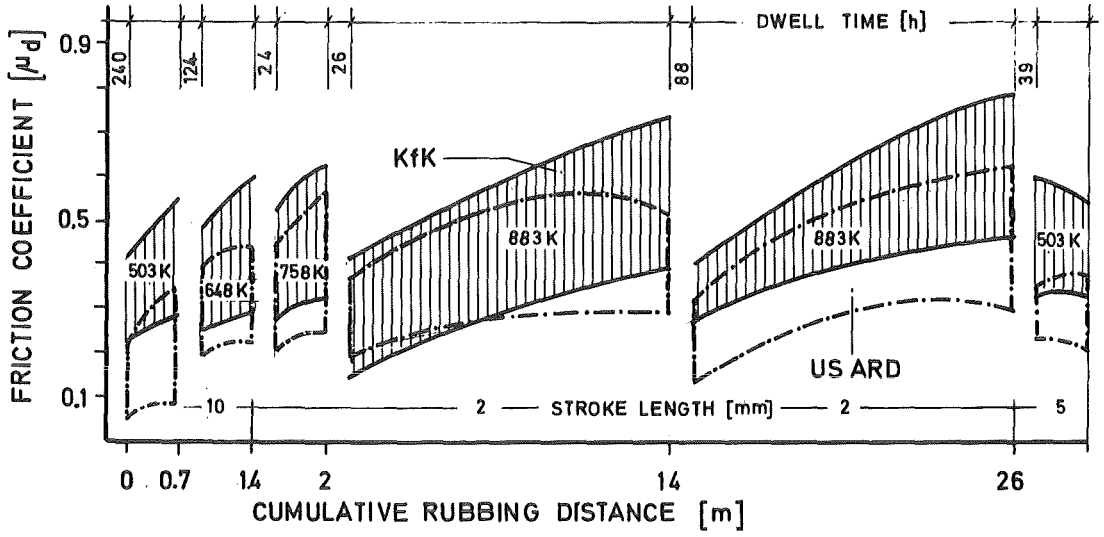

Fig. 77 Dynamic Friction Coefficient of LC-1H (comparison of KfK- and USARD test section criteria)

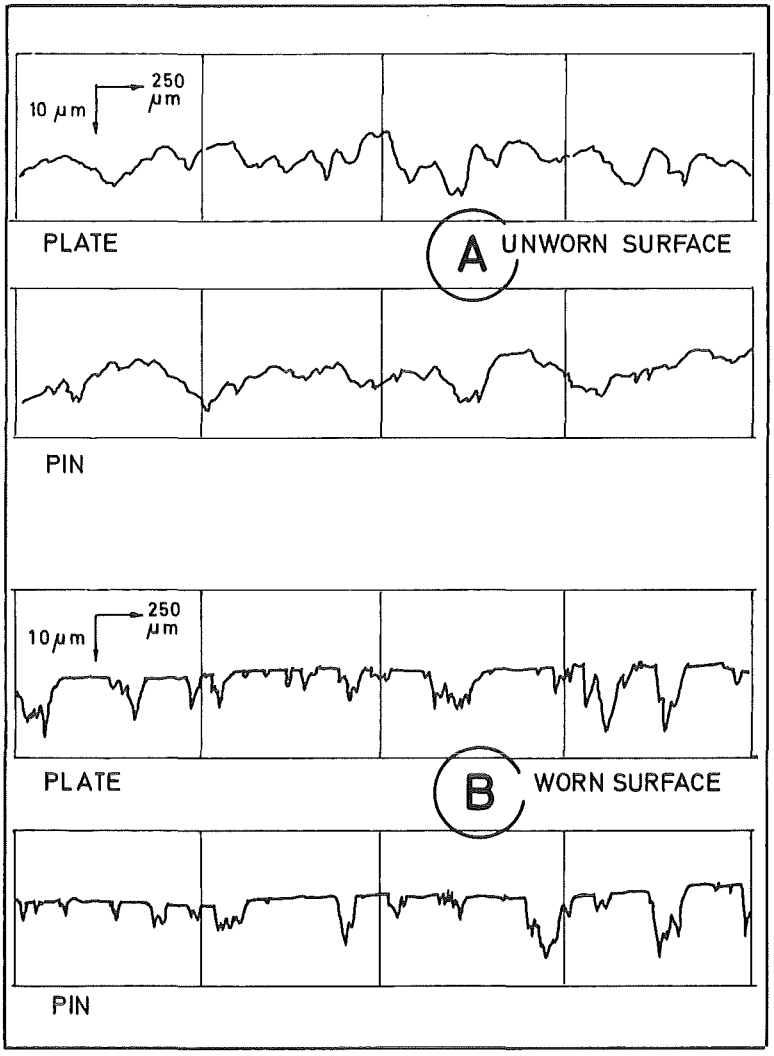

Fig. 78 Surface Profiles of D-gun coated LC-1H

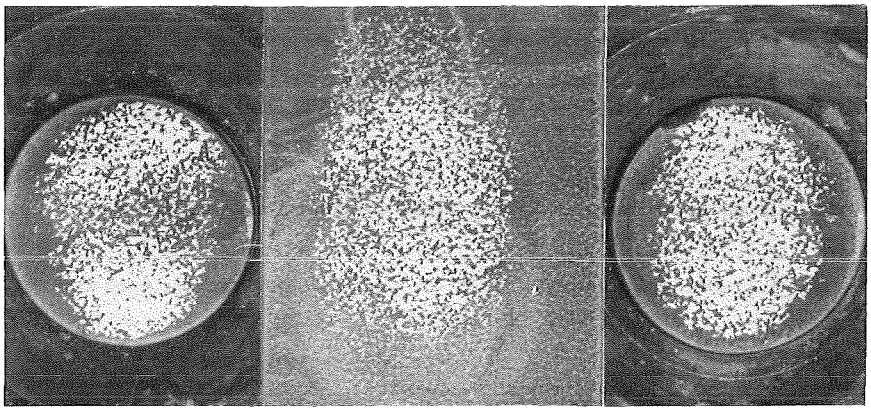

Fig. 79 Worn Surfaces of LC-1H Specimens

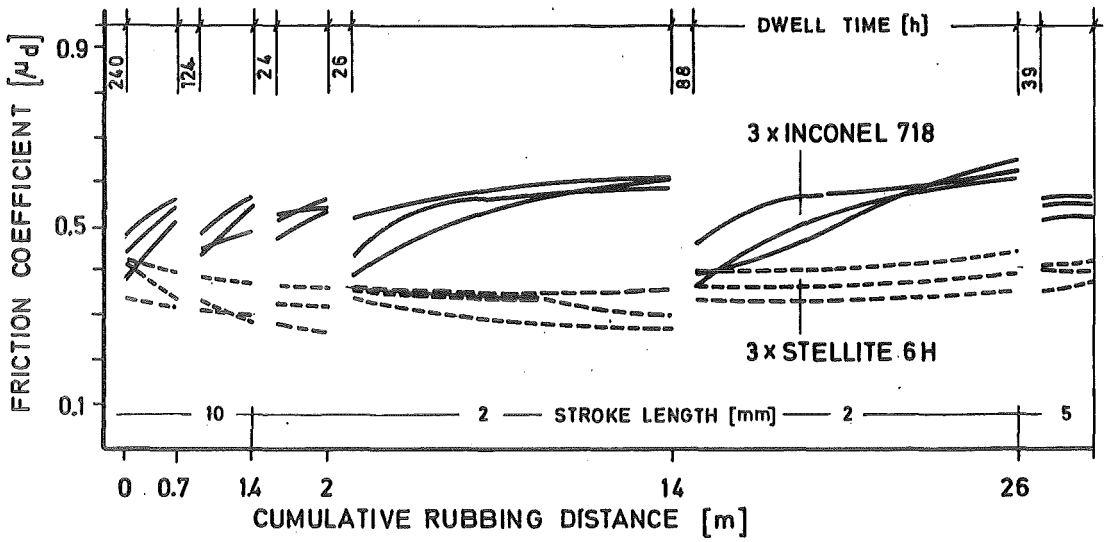

Fig. 80 Dynamic Friction Coefficients of Materials (USARD-KfK, test program)

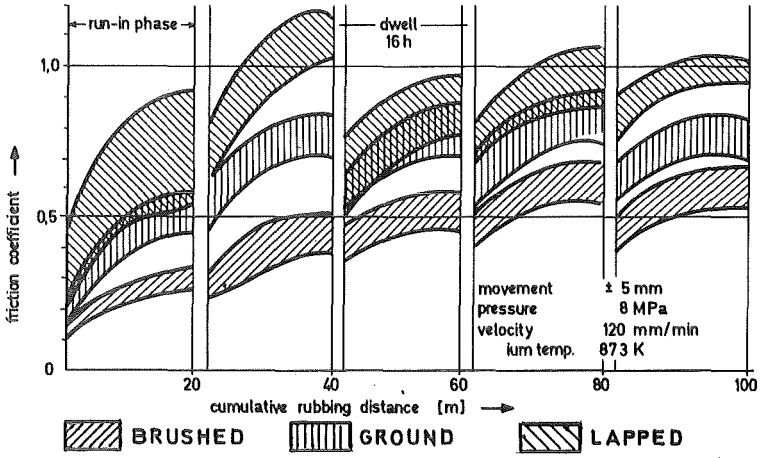

Fig. 81 Dynamic Friction Coefficients of LC-1H (function of surface macro roughness)

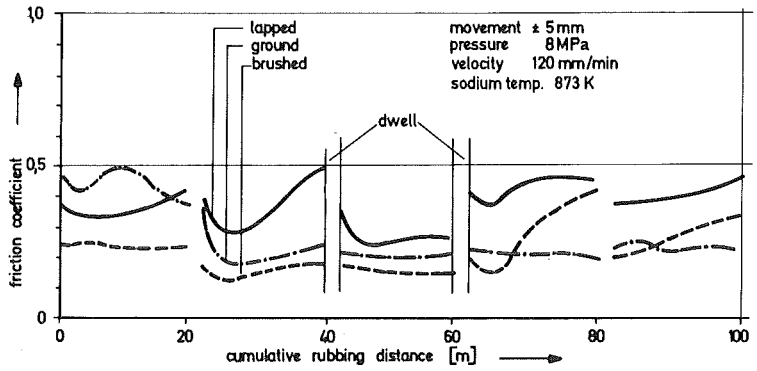

Fig. 82 Dynamic Friction Coefficient of LC-1H (specimens dismantled for wear measurement)

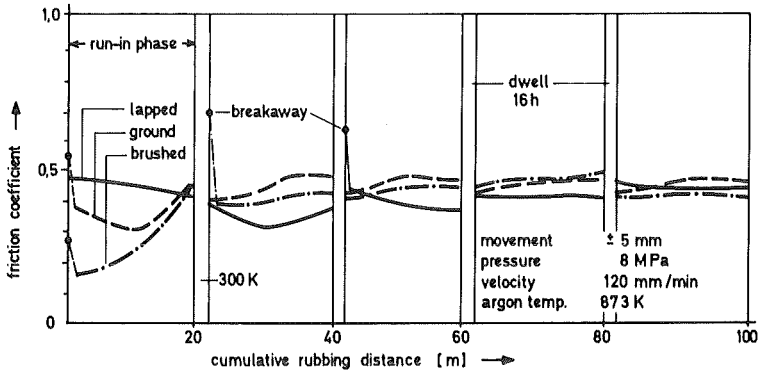

Fig. 83 Dynamic Friction Coefficient of LC-1H in Argon

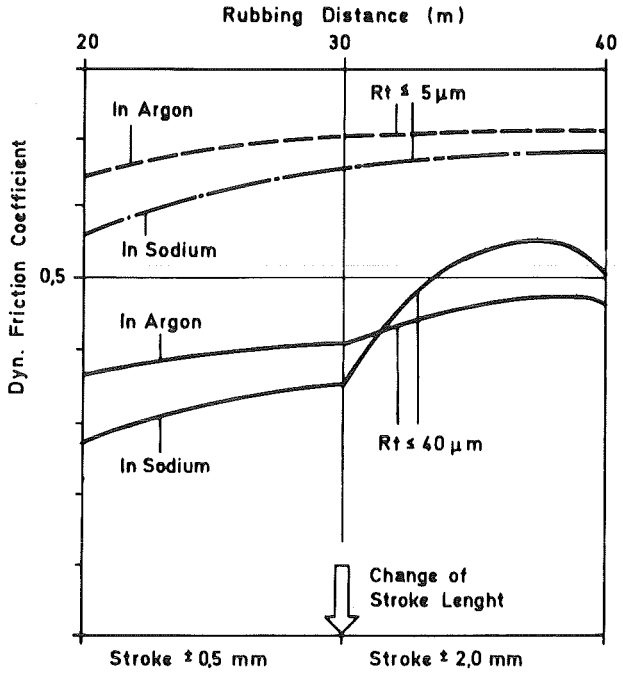

Fig. 84 Dynamic Friction Coefficient of LC-1H (effect of rolling particles with change of stroke length)

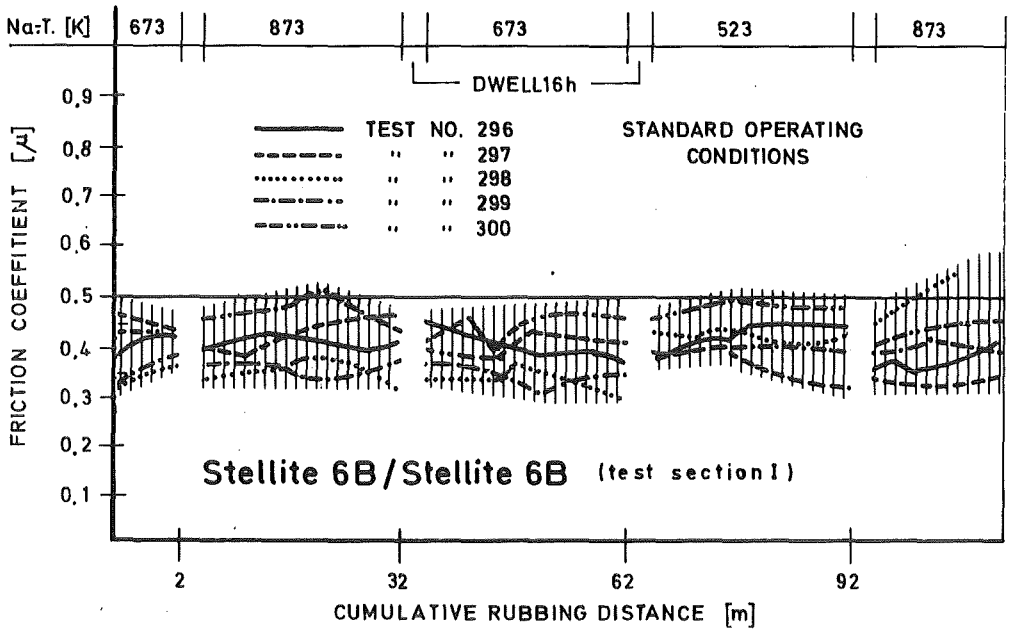

Fig. 85 Dynamic Friction Coefficient of Stellite B sheet material

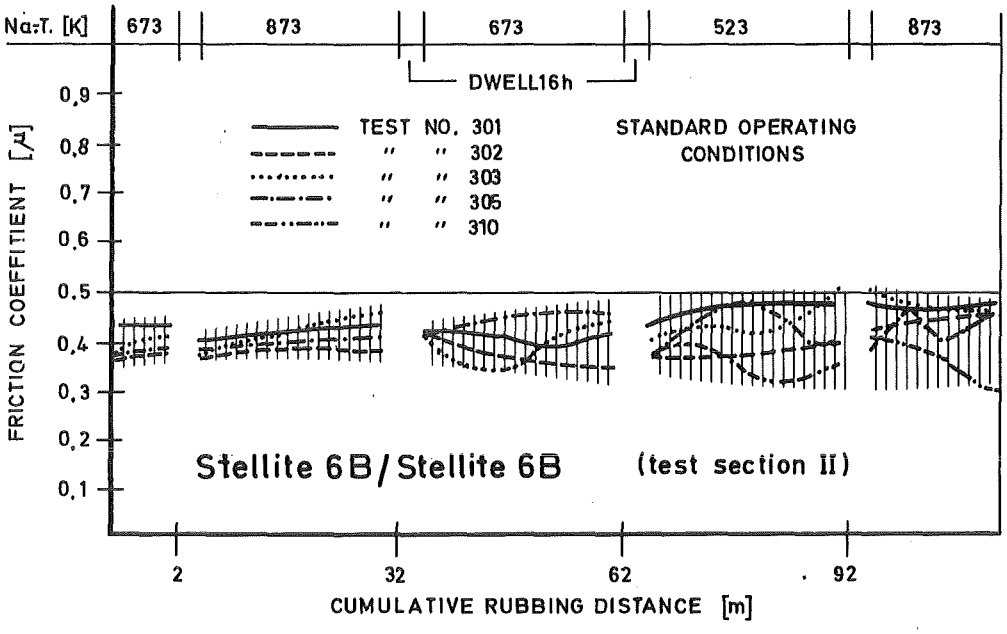

Fig. 86 Dynamic Friction Coefficient of Stellite 6 B sheet material

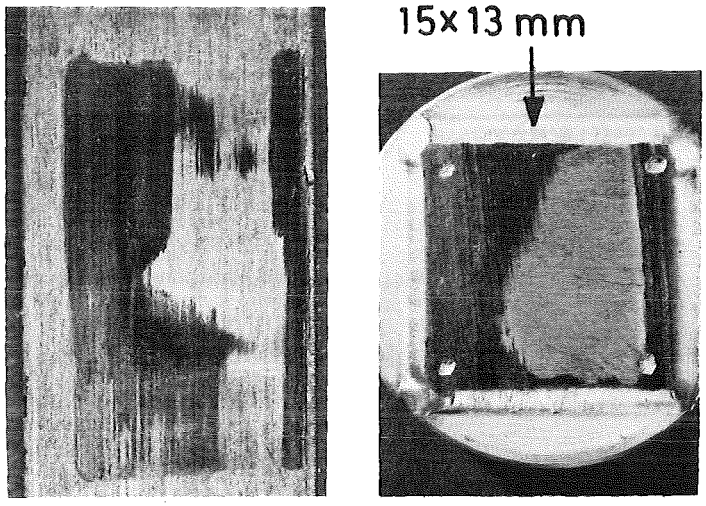

Fig. 87 WORN Surfaces of Test Specimens (Stellite 6 B)

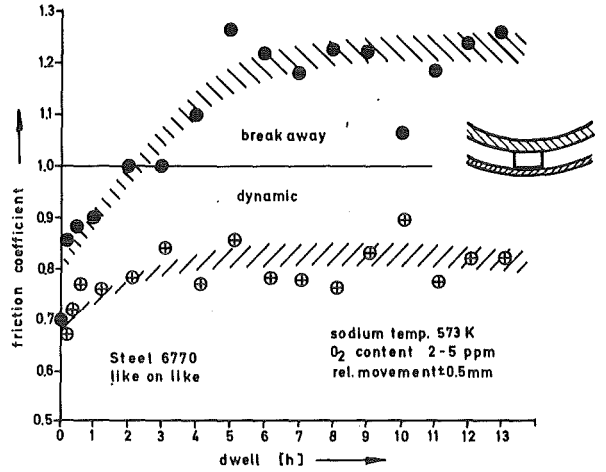

Fig. 88 Friction Coefficients of a Centering Knub System (function of dwell time)

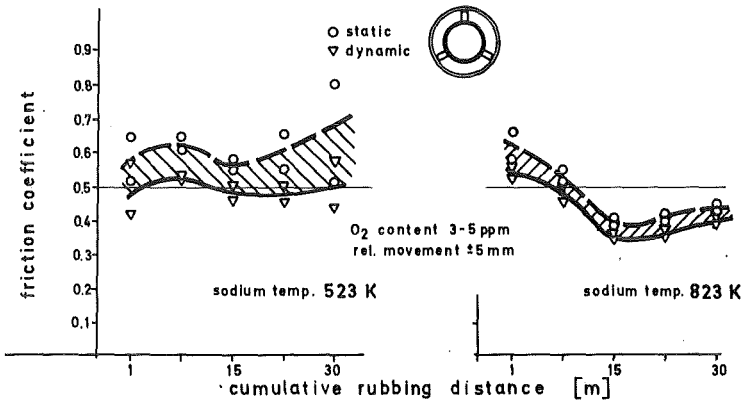

Fig. 89 Friction Coefficients of HTX Concentric Pipes (steel 6770 - Colmonoy 5)

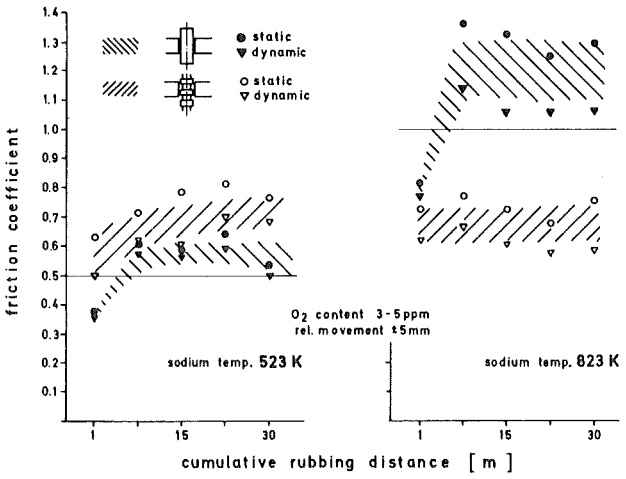

Fig. 90 Friction Coefficients of a HTX-Tube Support System (steel 6770 - Colmonoy 5)

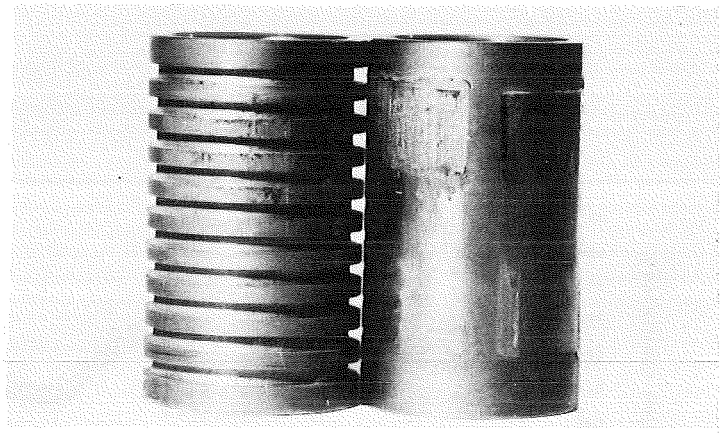

Fig. 91 HTX Tube Specimens after Friction Experiment

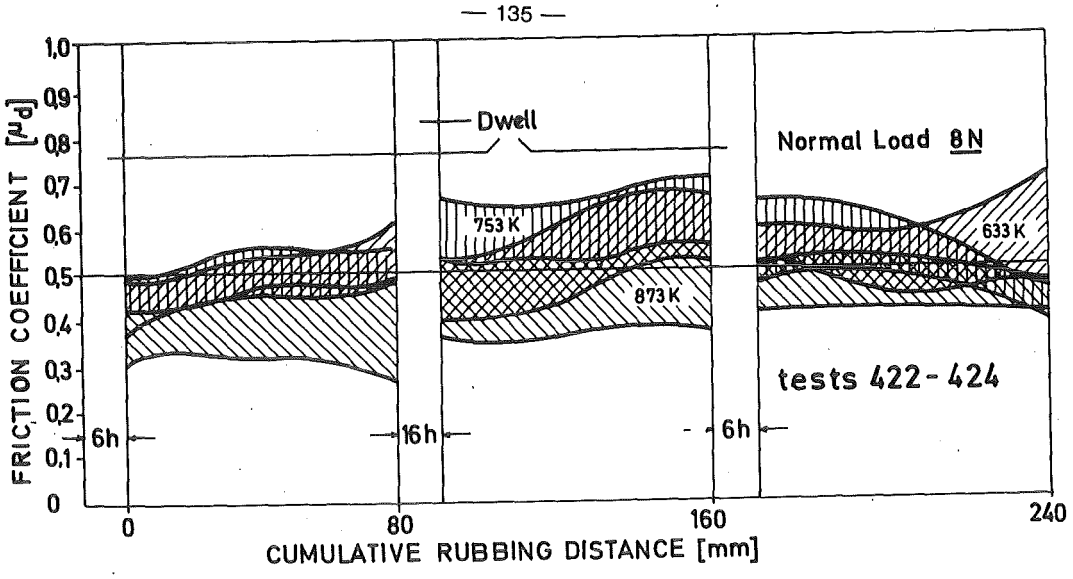

Fig. 92 Dynamic Friction Coefficients of a Cladding Tube/Spacer System (1.4970/1.4981)

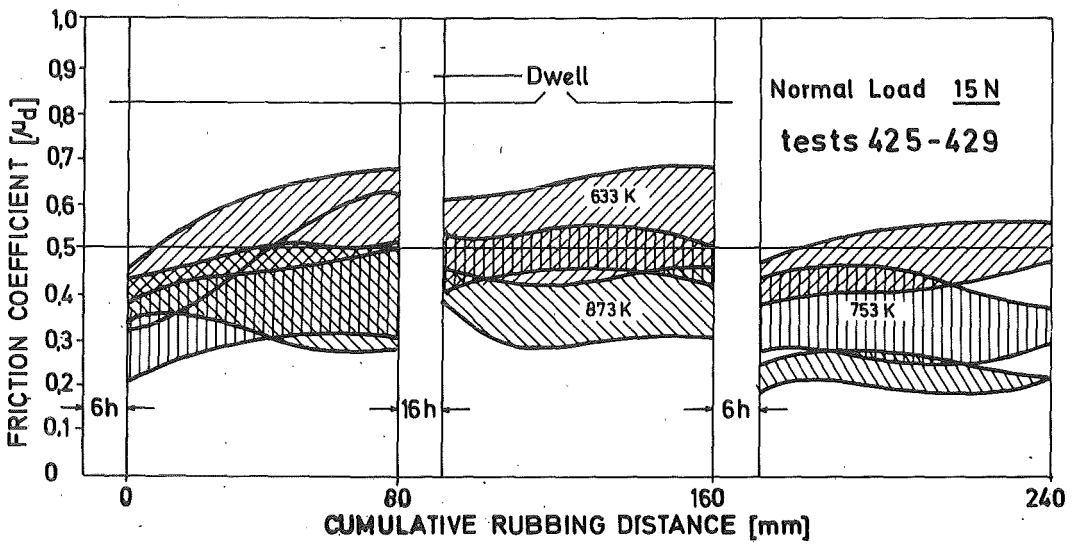

Fig. 93 Dynamic Friction Coefficients of a Cladding Tube/Spacer System (1.4970/1.4981)

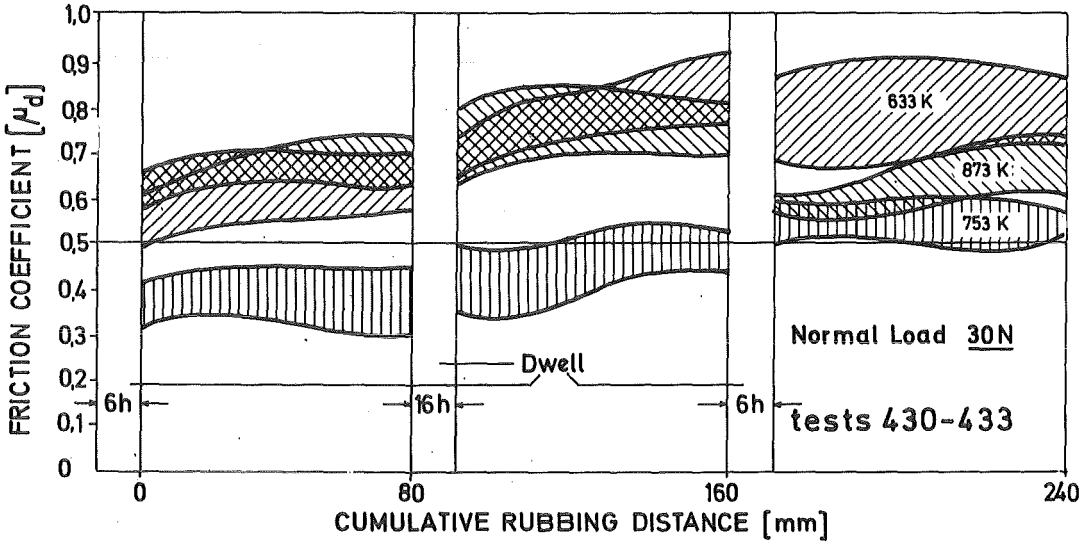

Fig. 94 Dynamic Friction Coefficients of a Cladding Tube/Spacer System (1.4970/1.4981)

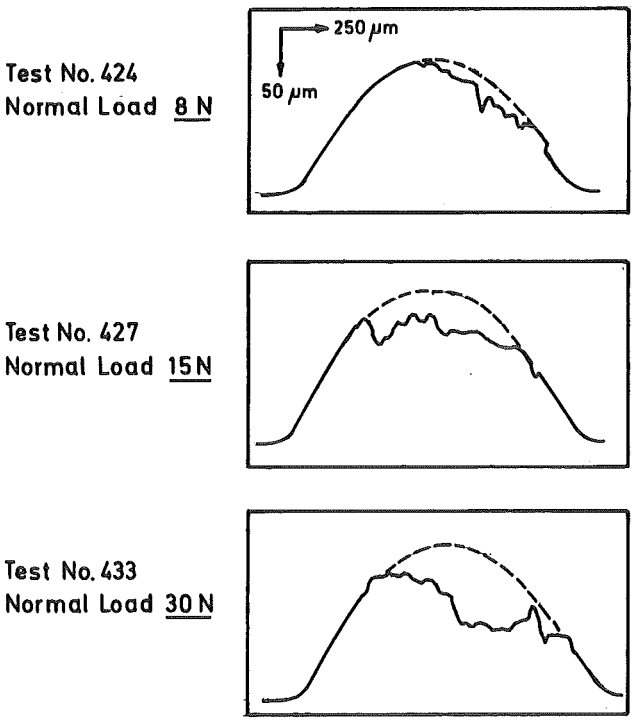

Fig. 95 Wear Scars on 1.4970 Cladding Tubes

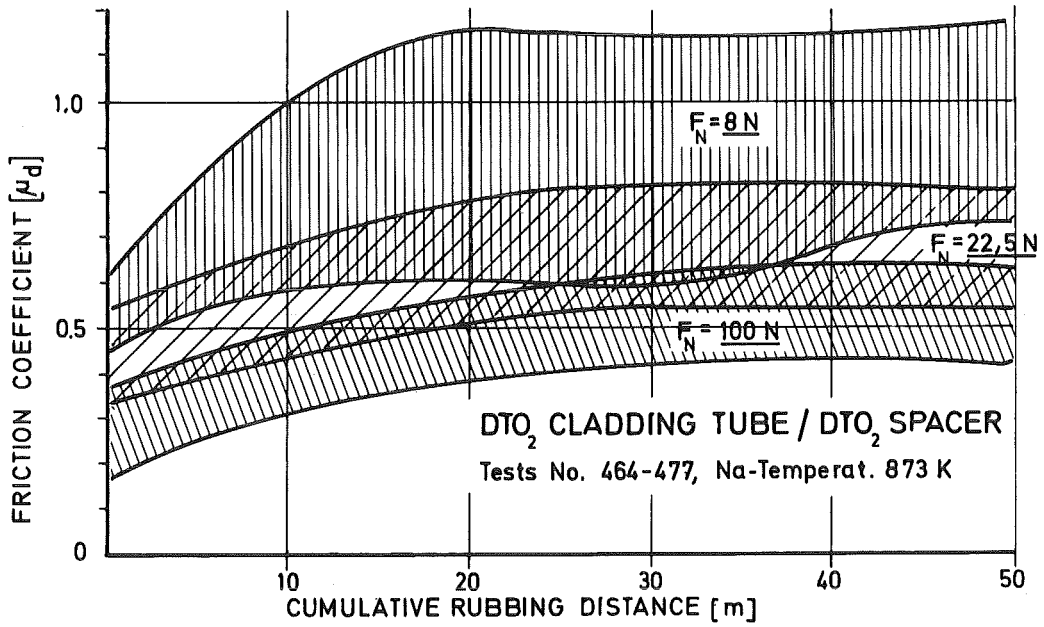

Fig. 96 Dynamic Friction Coefficients of a Cladding Tube/Spacer System (DTO_2/DTO_2)

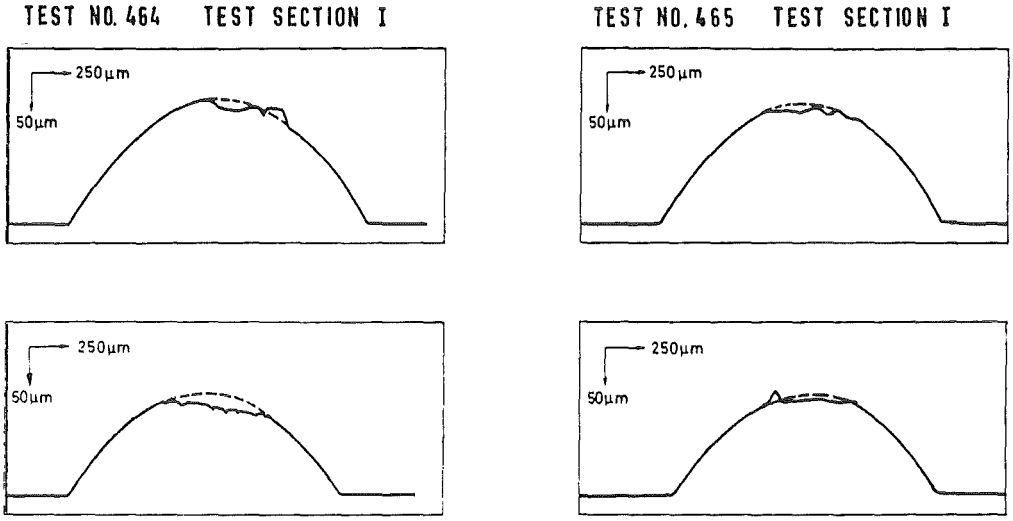

Fig. 97 Profile Traces Across Wear Scars On DTO_2

(F_N = 8 N)

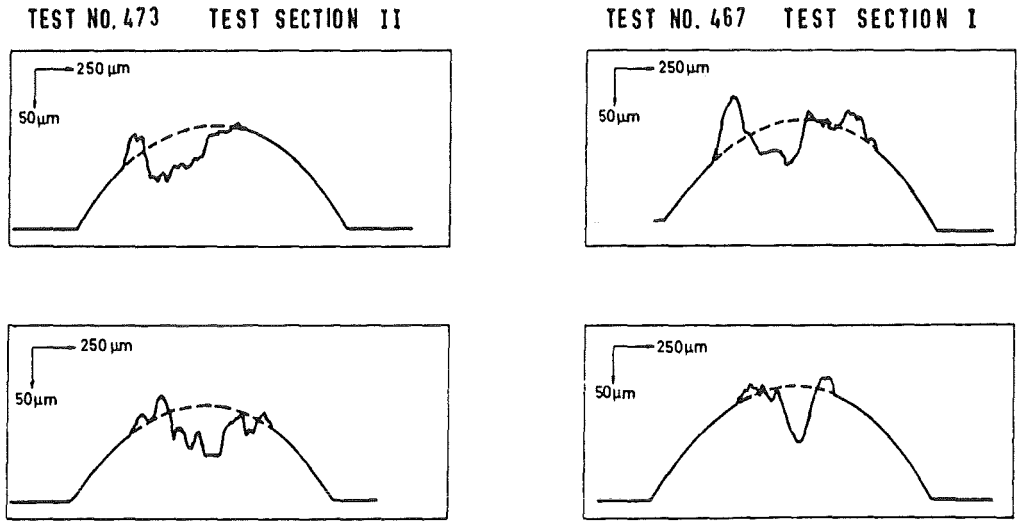

Fig. 98 Profile Traces Across Wear Scars On DTO_2

(F_N = 22,5 N)

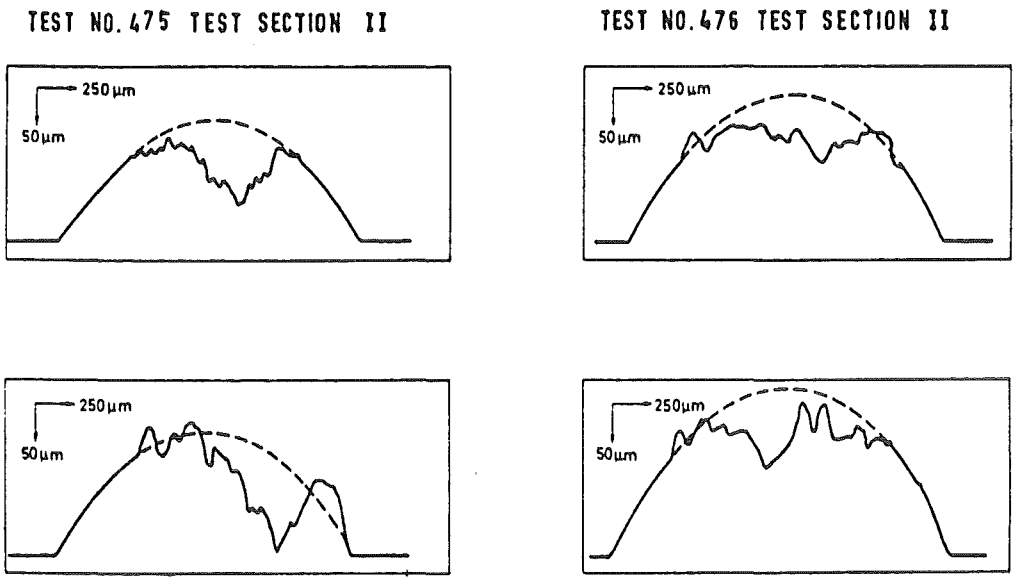

Fig. 99 Profile Traces Across Wear Scars On DTO_2
(F_N = 100N)

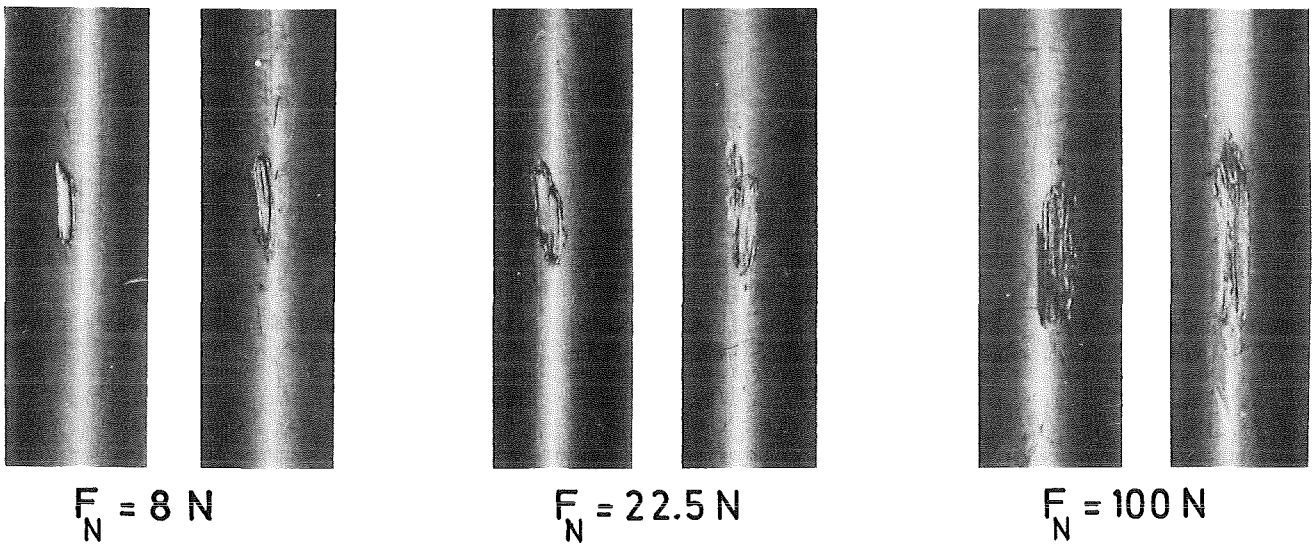

Fig. 100 Wear Scars on DTO_2 Cladding Tubes

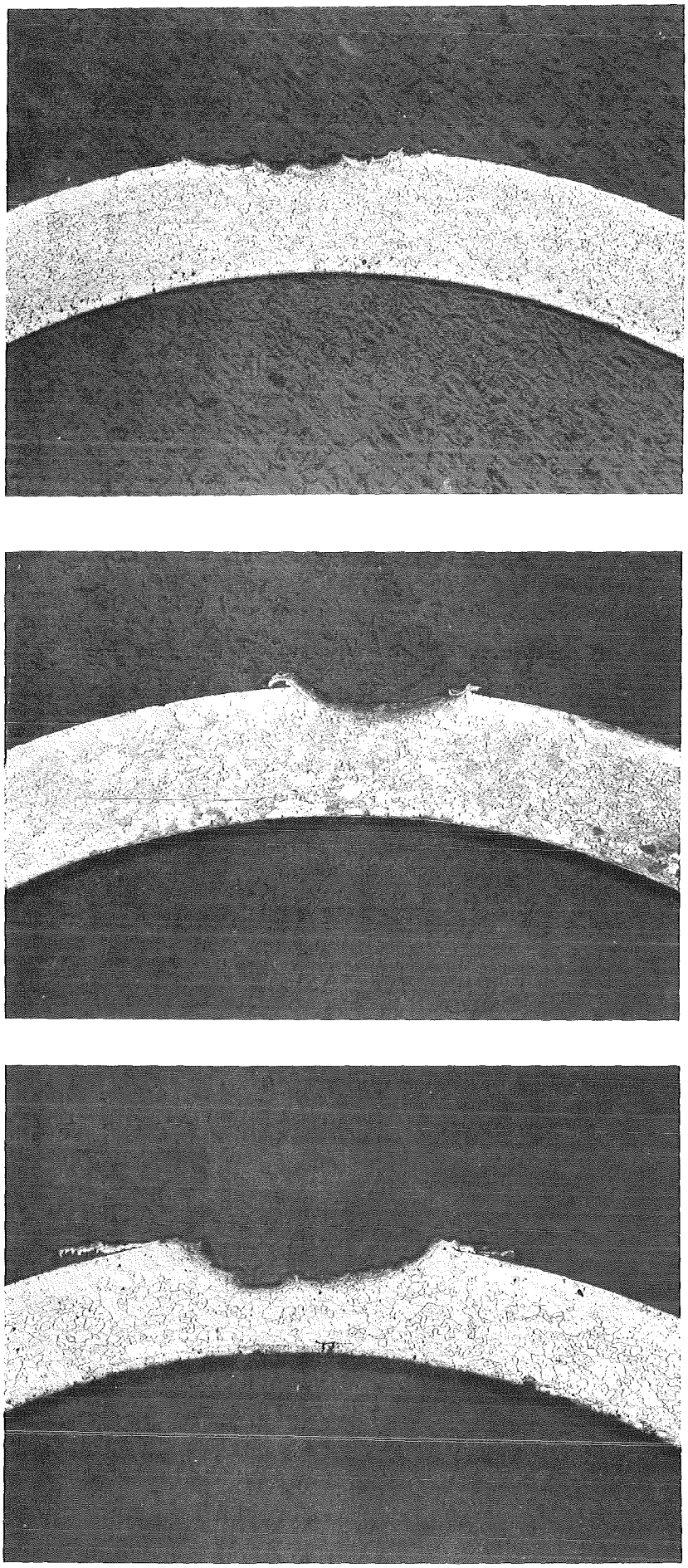

Fig. 101 Cross-sectional Micro Structure of DTO_2 Cladding Tubes

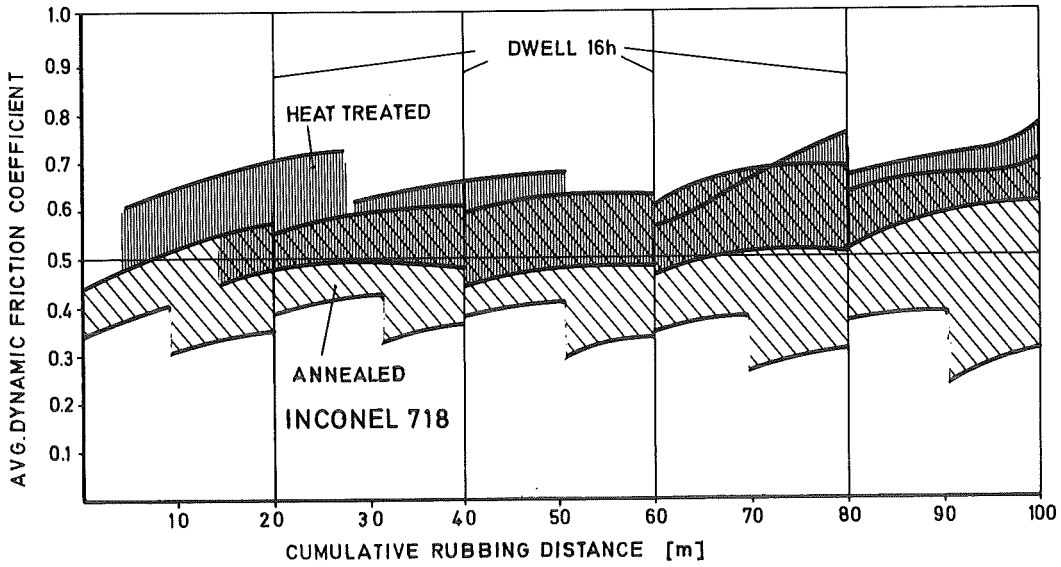

Fig. 102 Average Dynamic Friction Coefficient of Inconel 718

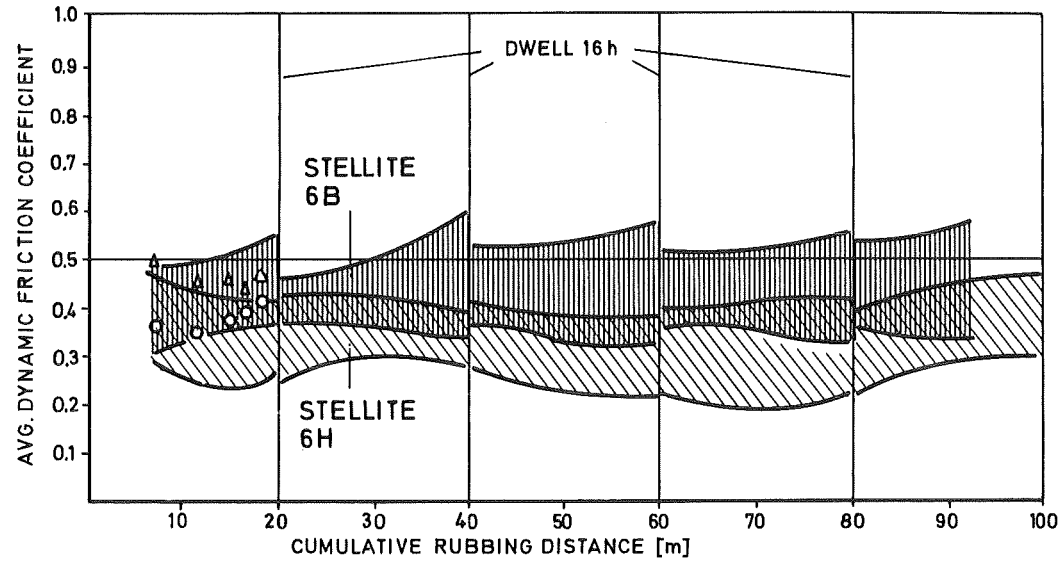

Fig. 103 Average Dynamic Friction Coefficients of Stellite 6

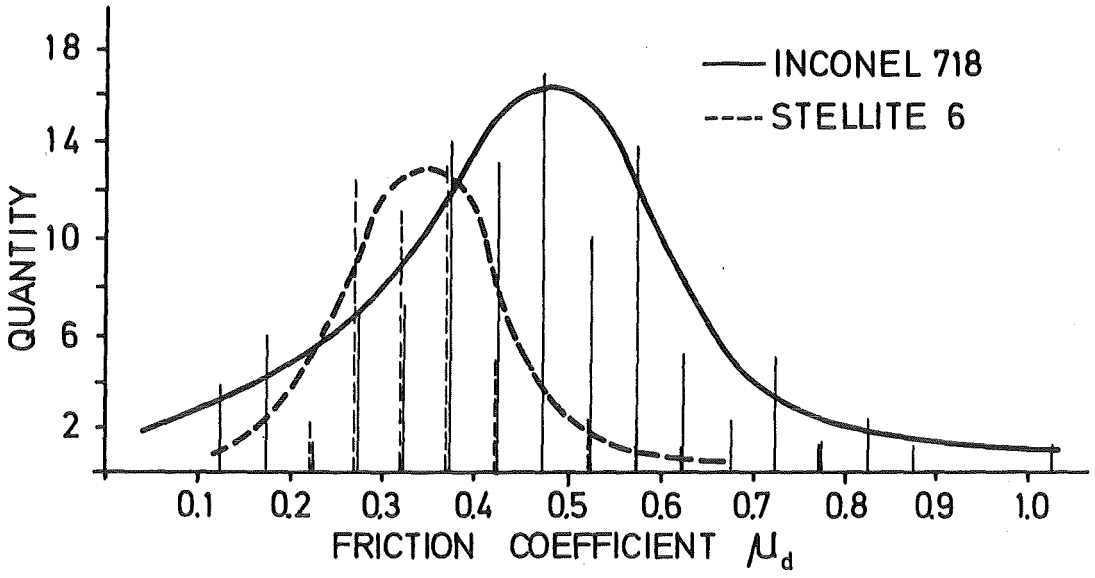

Fig. 104 Statistical Distribution of Friction Coefficients (for typical spacer pad operating conditions)

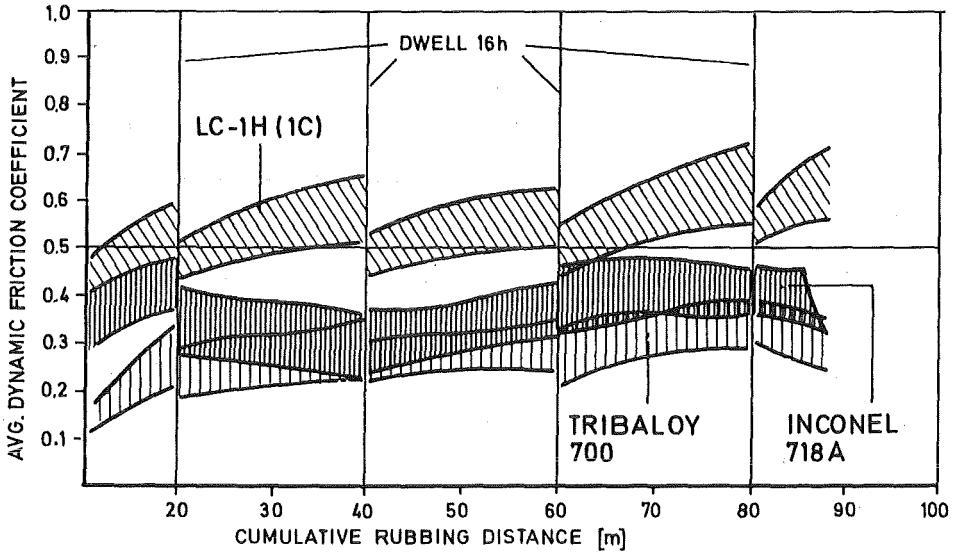

Fig. 105 Average Dynamic Friction Coefficients of Co-free Alternative Duct Pad Materials

11. APPENDIX

Test Materials

A multitude of publications is available concerning the different materials under tribological investigation. Hence, only the "SNR 300 Reference Materials" and their alternatives are described more deeply.

Inconel 718

The nickel-base alloy Inconel 718 was subjected to tribological experiments
- in the solution-annealed condition (718 (an))
- in the heat treated condition (718 (ht))
- in the alitized condition (718 (A)).

This material is a refractory, ageable nickel-chromium-iron-molybdenum alloy with particularly high strength and creep rupture properties up to about 1000 K. Its mechanical properties at room temperature are evident from Table A III, the physical properties from Table A IV.

The material was subjected to metallurgical examinations both in the as-delivered condition and after exposures of various durations to liquid sodium /62,64/. The characteristic grain structure is evident from the transverse micrograph in Fig. A 1. The surface structure of a sheet metal specimen which is interesting from the tribological point of view is shown in Fig. A 2. Also in an AES-diagram the distribution of constituents is given for the outermost layer of 1 μm thickness (Fig. A 3). Heat treating was performed in conformity with Table A V. The hardness at room temperature was thus increased from approximately 18 HR_C to approximately 45 HR_c.

In development work performed to improve the sliding properties of Inconel 718 several techniques were used. The most favorable results were obtained by surface "alitization". This process is described more thoroughly by Whitlow /65/. Essentially, a nickel aluminide coating of some few μm thickness is formed which partly penetrates into the base material whilst the major portion forms a layer on the surface. This is clearly visible in Fig. A 4.

The surface resulting from the coating (diffusion) process is shown in Fig. A. 5.

With the 1:100 magnification the machined surface profile (turning) is still recognizable. The AES-profile diagram for the alitized version of Inconel 718 is plotted in Fig. A 6 for comparison.

The attempt to apply NiAl powder by the flame spray technique was less successful. Although good bonding to the base material was achieved, numerous transverse cracks were detected in the NiAl layer which is a drawback of this technique (Fig. A 7).

Stellite 6

The alloy is applied to wearing surfaces by various welding processes, possessing excellent corrosion resistance and high temperature strength together with good ductility and excellent resistance to thermal shock. Its physical and mechanical properties are presented in Tabs. A VI and Tab. A VII respectively.

For characterisation of this material numerous metallurgical experiments were realized /66,67/. Its typical dentritic structure is shown in Fig. A 8 for a hardfacing brought about by T.I.G.-welding. Its surface has been finished by grinding for friction experiments (Fig. A 9). Also an AES-profile diagram has been provided to enable tribologists assigning friction data to material criteria (Fig. A 10).

Also in a sheet version (d = 0,9 mm) Stellite 6B has been spot welded to the 1.4961 bulk material. These surfaces were not ground but operated with the genuine surface structure (Fig. A 11). Nevertheless, this looks nearly similar to the ground Stellite 6H surface shown in Fig. A 9. Both, grain structure and distribution of constituents appear slightly different from the 6H-material. (Please compare Figs. A 8/A 12 and A 10/A 13 respectively).

For experiments with certain preconditioning as the parameter, Stellite 6 - surfaces have been exposed to 873 K - sodium far up to 6500 h. Analysis of both, surface morphology and composition showed a significant change no longer corresponding with the original conditions. According to the diagram of the AES-profiling analysis (Fig. A 14) iron is enriched up to more than 20 % and oxygen is about 15 % on the surface. Evidently cobalt and chromium were exchanged for iron, the resulting surface morphology being very rough and

rugged (Fig. A 15).

Tribaloy 700 (LDT 700)

Tribaloy 700 is a Nickel-base hardsurfacing alloy with 32 % content of Mo /68/. Its freedom from cobalt makes it particularly attractive for nuclear applications. It typically consists of a hard, intermetallic Laves-phase disposed in a softer matrix of eutectic or solid solution. The matrix phase is facecentred cubic. Mechanical property data are still limited to hardness tests, while physical property information was available from UCE especially for LDT-700 detonation-gun plated (Tab. A VIII). Figure A 16 shows the microstructure of such a layer and Fig. A 17 exhibits its surface character (a) as received after D-gun-process, (b) after brushfinish. A respective AES-diagram is given in Fig. A 18 especially as a proof for the high Mo-content in a Ni-base alloy.

LC-1H (LC-1C)

LC-1H, a chromium carbide coating with nickel-chromium binder, especially developed for application for friction systems operated in Liquid Metal Cooled Fast Breeder Reactors. This coating applied by the D-gun process provides resistance for galling wear for the contacting surfaces /69,70/. However, efforts were continuing to develope improved coating for advanced reactor applications. As one result LC-1H was provided which is very similar to LC-1C but with a smaller carbide powder particle size (40-100 micron) before D-gun process. This material has been examined intensively in the Institut für Materialforschung und Festkörperphysik (IMF) /71/.

Its physical characteristics are shown in Tab. A IX. It does not contain cobalt and is suitable for applications also in irradiated environments. For evaluation of the LC-1H layer cross sectional microstructures were photographed as shown in Figs. A 19 and A 20. Its surface structure after D-gun processing (Fig. A 21) proved to be of special interest for liquid sodium application.

Also the surface layer composition was determined using Auger electron spectros copy-profiling analysis. Fig. A 22 shows a diagram for a brush finished surface. No significant difference was found concerning the diagrams for

ground or lapped surfaces. By INTERATOM a special "Coating process Specification for SODIUM REACTOR COMPONENTS" has been provided for this material.

	C	Si	Mn	P	S	Cr	Mo	Ni	Al	B	Nb	W	Fe	Ti	Co	hot hardness at 873 K
1.4961	0,08	0,4	1,25	0,008	0,013	16,0		13,0			10X%C		balance		0,015	HR_B 40 - 50
1.4981	0,08	0,05	1,24	0,018	0,006	16,5	1,66	16,6			0,8		balance			HR_B 40 - 50
Inconel 718	0,05	0,03	0,01	0,005	0,003	18,85	3,06	53,1	0,72	0,0061	5,45		18,85	1,13		HR_C 35 - 38
Inconel 750	0,55	0,23	0,10	0,008	0,005	14,3			0,68	0,0045	0,76		8,20	2,62	0,82	HR_C 28 - 30
Nimonic 80	0,06					20,0		balance	1,4				5,0	2,4		HR_C 37 - 40
Hastelloy C	0,08	0,03	1,0	0,04		14,5	15-17	54,0				4,0	6,2		2,5	HR_B 87 - 90
TZM	0,025						99,4	0,002					0,01	0,50		HR_B 95 - 97
Colmonoy	1-2					10-17		71-87		2			7-10			HR_C 41 - 44
Stellit 6 H	1,0					27,0						4,5			balance	HR_C 27 - 30
Colmonoy 6	2,6					16,5		70,0		3,75		Fe + Si + C 10 % max.				HR_C 43 - 45
Akrit Co 50						27,0							balance			HR_C 40 - 42
Ferro TiC U	<0,1	TiC 32,5				12		8,5					46,5	0,5		HR_C 45 - 47
Tribaloy 700		3				15	32	50								HR_C 52 - 58
LC-1H	80 % Cr_3C_2 (80 Ni - 20 Cr)															

Tab. A I: CONSTITUENTS OF MATERIALS UNDER INVESTIGATION

Analysis No.	H	O	N	H_2O
1	-	5	60	15
2	165	<1	75	15
3	57	<1	73	5
4	36	<1	47	<1
5	23	<1	27	20

Tab. A II : RESULTS OF ARGON GAS ANALYSA [vpm]

0,2 Proof Strength	kg/mm^2		115
Tensile Strength	kg/mm^2		140
Elongation	%		15
Modulus of Elasticity	kp/mm^2		20800
873 K, Time h	100	1000	10000
Creep Strength kg/mm^2	87	70	50

Tab. A III | MECHANICAL PROPERTIES OF INCONEL 718

Temperature K	Room	473	673	873
Thermal Exp. $x10^{-6}$ m/m·K	12.9	13.5	14.1	14.7
Thermal conduct. cal/cm·sec·K	0.027	0.034	0.041	0.049
Hot Hardness R_c	∿ 40	∿ 38	∿ 36	∿ 34
Specific Gravity $x10^3 kg/m^3$				8.34

Tab. A IV PHYSICAL PROPERTIES OF INCONEL 718

Annealing		1230 K	1 h
air cooling			
heat treating		993 K	8 h
stove cooling	→	890 K	
air cooling	→	room temperature	

Tab. A V HEAT TREATING OF INCONEL 718

0,1 Proof Strength	kp/mm^2	55
Tensile Strength	"	91
Elongation	%	1
Elasticity Modulus	kg/mm^2	21100
Hardness	Rc	39-43

Tab. A VI: MECHANICAL PROPERTIES OF STELLITE 6 (ROOM TEMPERATURE)

Melting Range	^oC				1285-1395
Specific Gravity $x10^3 kg/m^3$					831
Temperature ^oC		Room	200	400	600
Thermal Exp. Coefficient	$^oCx10^6$	11,35	12,95	13,9	14,5
Hot Hardness	DHN	457	356	334	235

Tab. A VII: PHYSICAL PROPERTIES OF STELLITE 6

Temperature K		Room	473	673	873
Ultim. Tensile Strength	kp/mm^2	69	-	-	63
Coeff.of Therm. Exp.	$x10^{-6}m/m \cdot K$	5,0	5.4	5.8	6,3
Modulus of Elasticity	kg/mm^2			24000	
Hardness	Rc			52-58	
Melting Range	K			1500 - 1800	
Specific Gravity	$x10^3 kg/m^3$			9,0	
Heat Capacity	joules/kg·K			500	

Tab. A VIII MATERIAL PROPERTIES OF TRIBALOY 700

Temperature K		Room	473	673	873
Coeff.of Therm.Exp.	$x10^{-6}m/m \cdot K$	4.4	5.2	5.6	6.1
Modulus of Elasticity	not available				
Bond Strength on Inconel 718	kp/mm^2				7
Cross-Sectional Hardness	VPN_{300}				750 - 850
Specific Gravity	$x10^3 kg/m^3$				6.3
Porosity	% max.				1.5

Tab. A IX MATERIAL PROPERTIES OF LC-1C (1 H)

DTO_2	Fe 13	Cr 1.5	Mo 3,5	Ti 2.0	TiO_2
B 3	Fe 13	Cr 2.7	Ti 2	Mo	

Tab. AX FERRITIC CLADDING MATERIALS

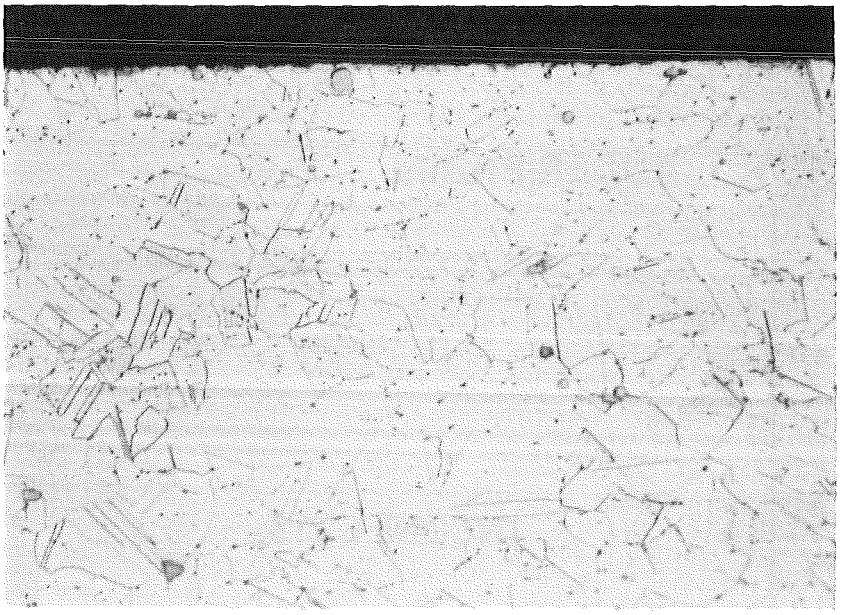

Fig. A 1 Typical microstructure of Inconel 718

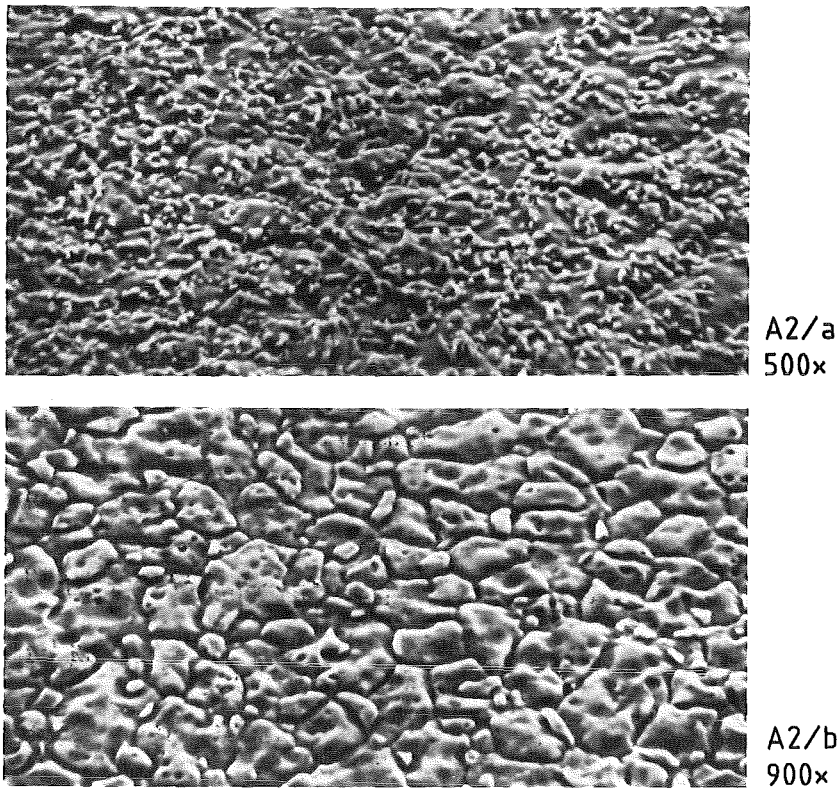

Fig. A 2 Surface Structure of an Inconel 718 specimen (sheet material)

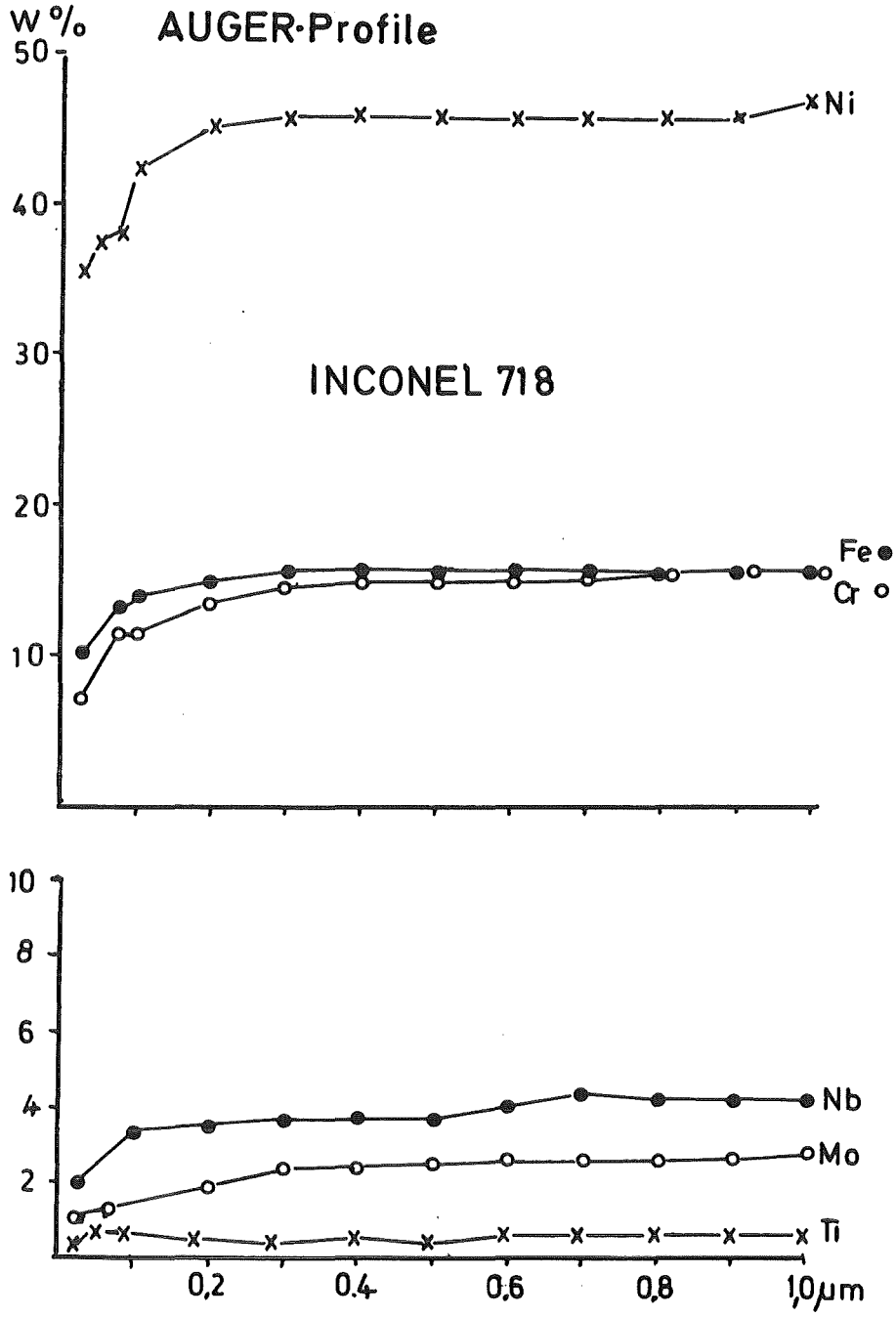

Fig. A 3 AES-profile of an Inconel 718 wear, specimen (annealed)

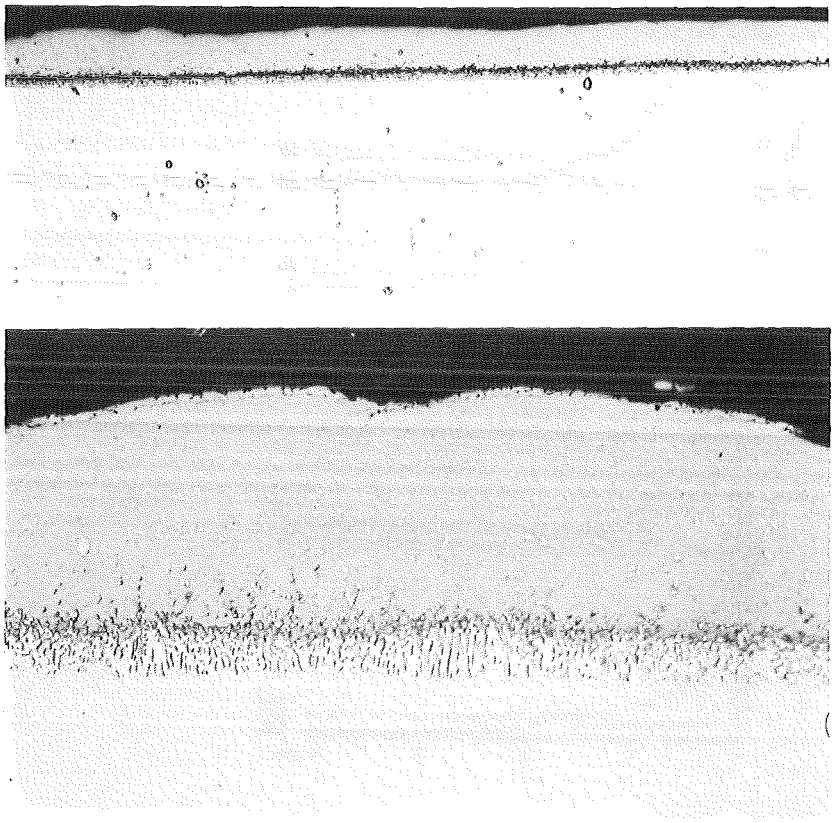

100 x

500 x

Fig. A 4 Micrograph of a NiAl coating on an Inconel 718 specimen surface

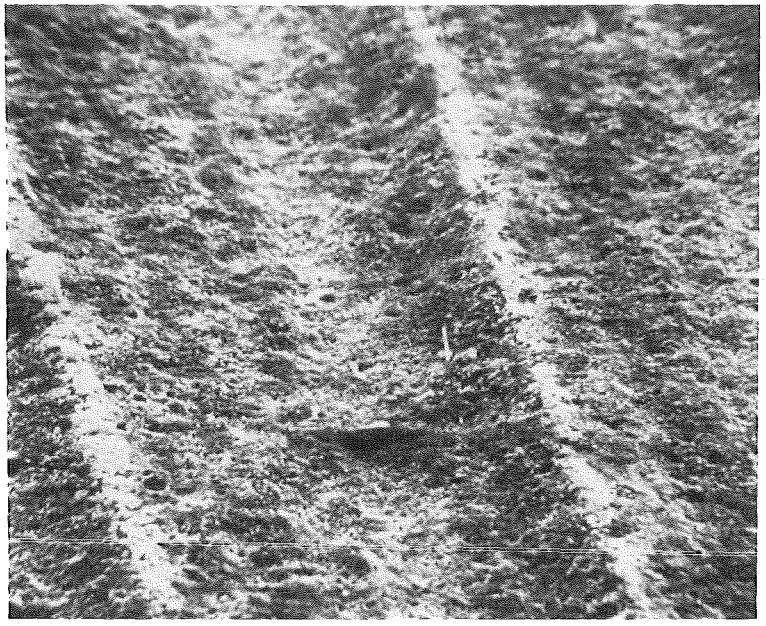

100 x

Fig. A 5 NiAl-surface on Inconel 718

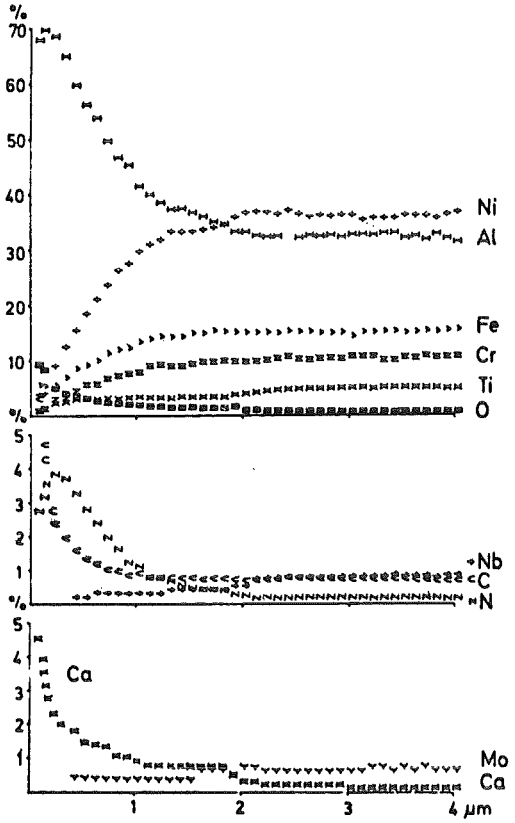

Fig. A 6 AES-profile diagram of an NiAl coating on Inconel 718

500 x

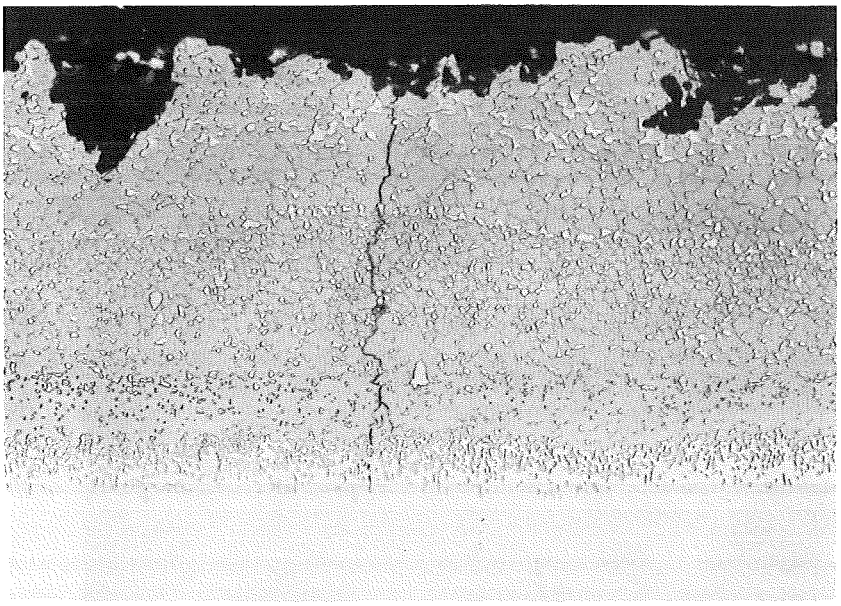

Fig. A 7 Cross-sectional micrograph of a NiAl flame spray coating

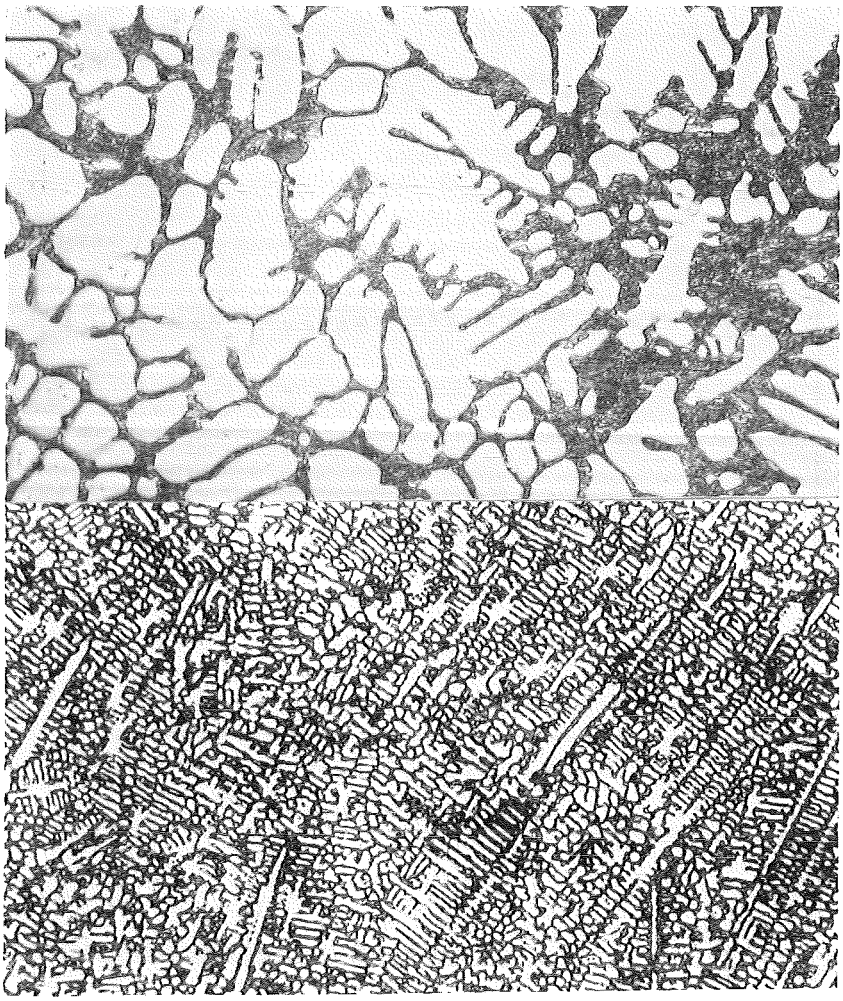

900 x

200 x

Fig. A 8 Cross-sectional micrograph of a Stellite 6 H coating

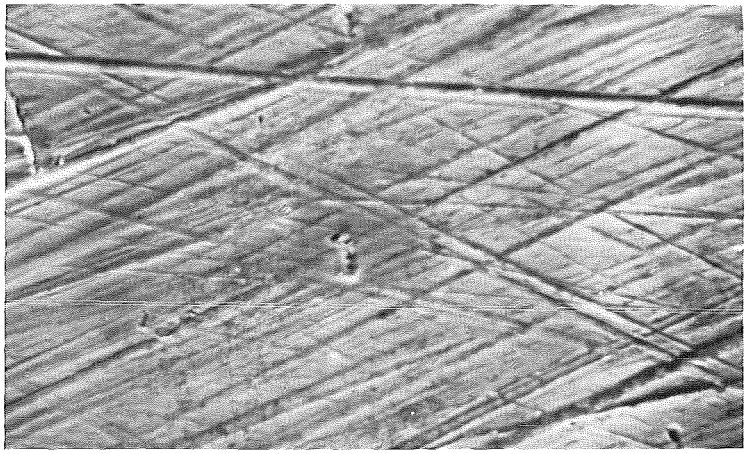

1000×

Fig. A 9 Typical surface appearance of as-received Stellite 6 H

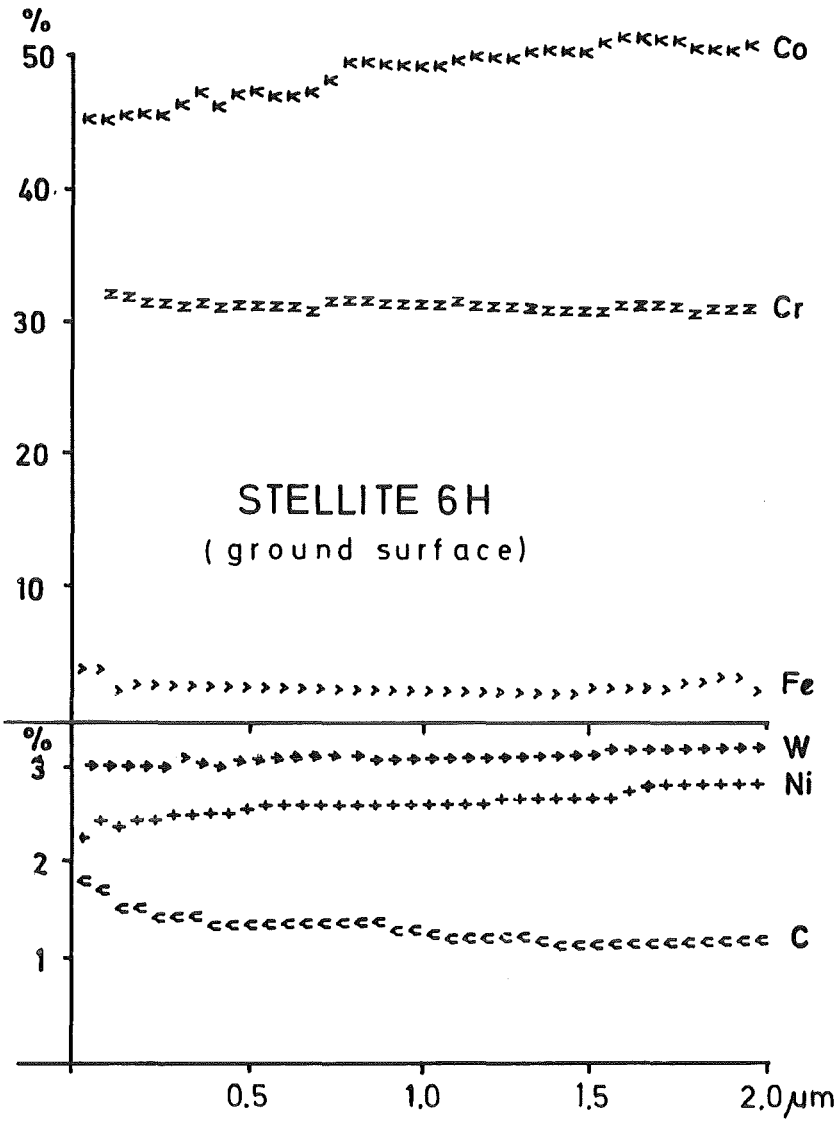

Fig. A 10 AES-profile diagram of a Stellite 6 H coating

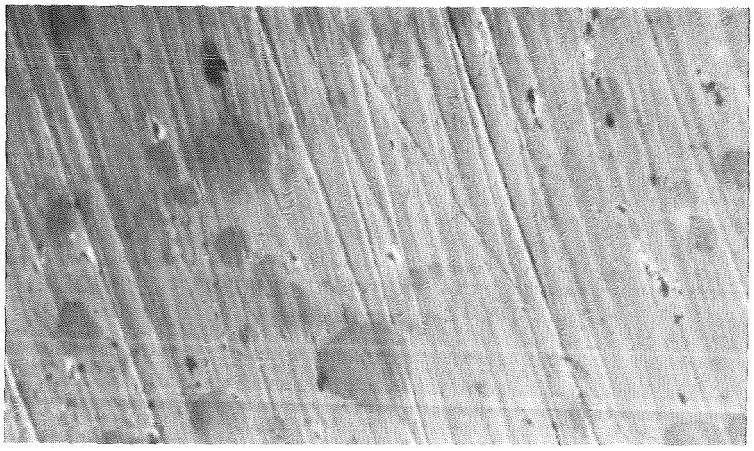

Fig. A 11 Stellite 6 B - surface (as received)

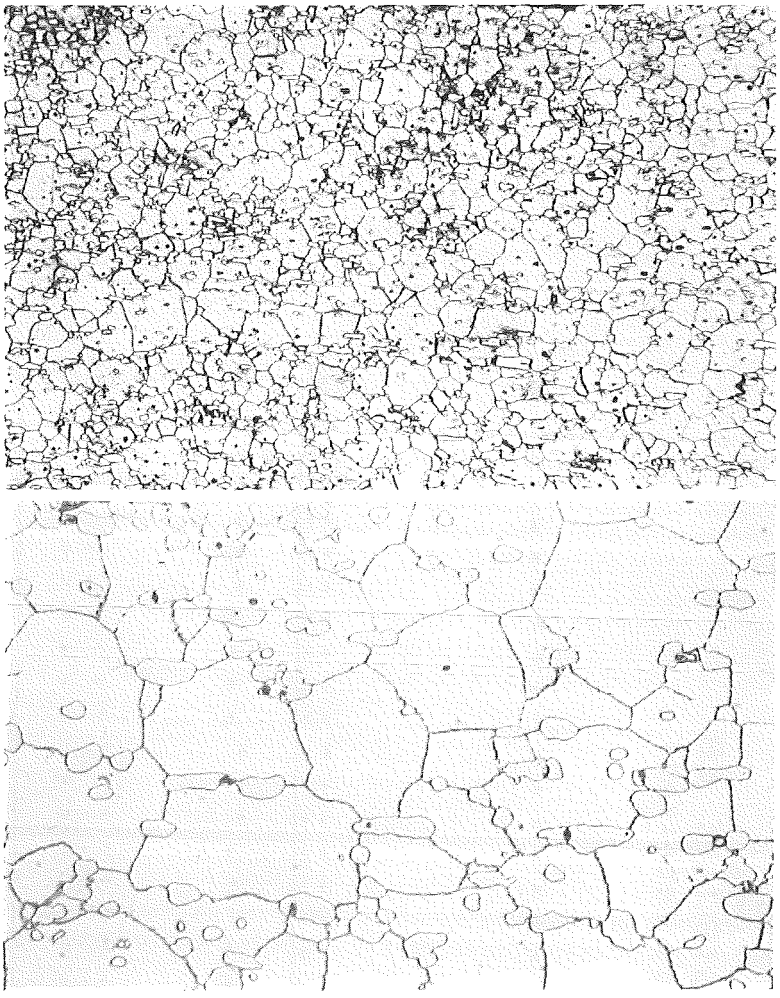

Fig. A 12 Typical grain structure of
Stellite 6 B (wrought)

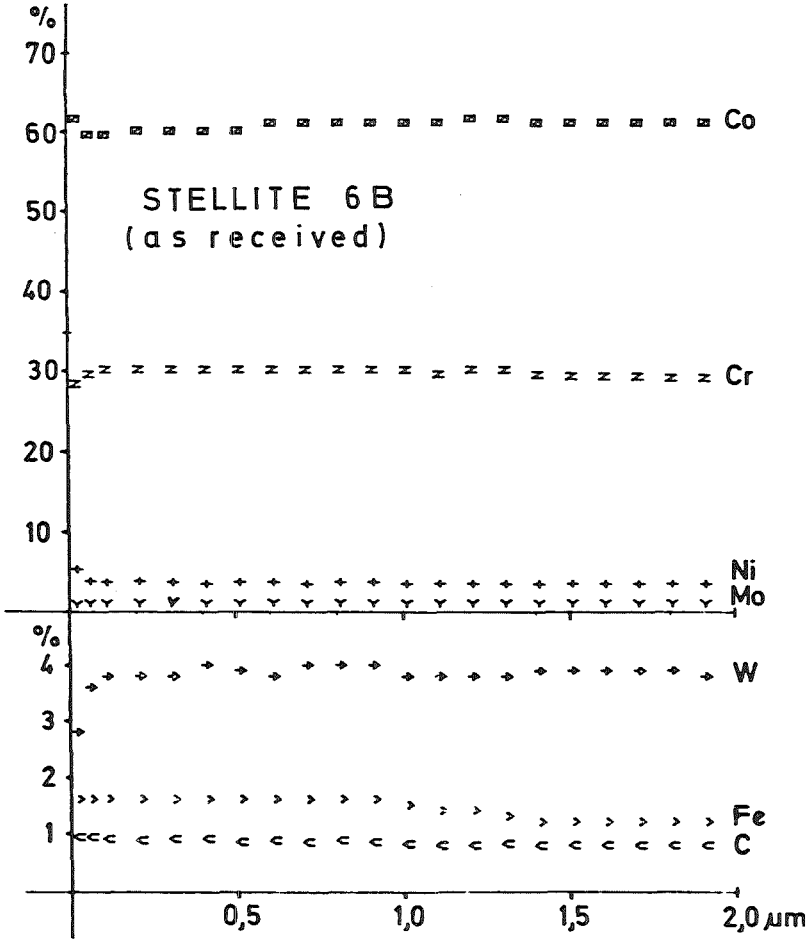

Fig. A 13 AES-Diagram of Stellite 6 B

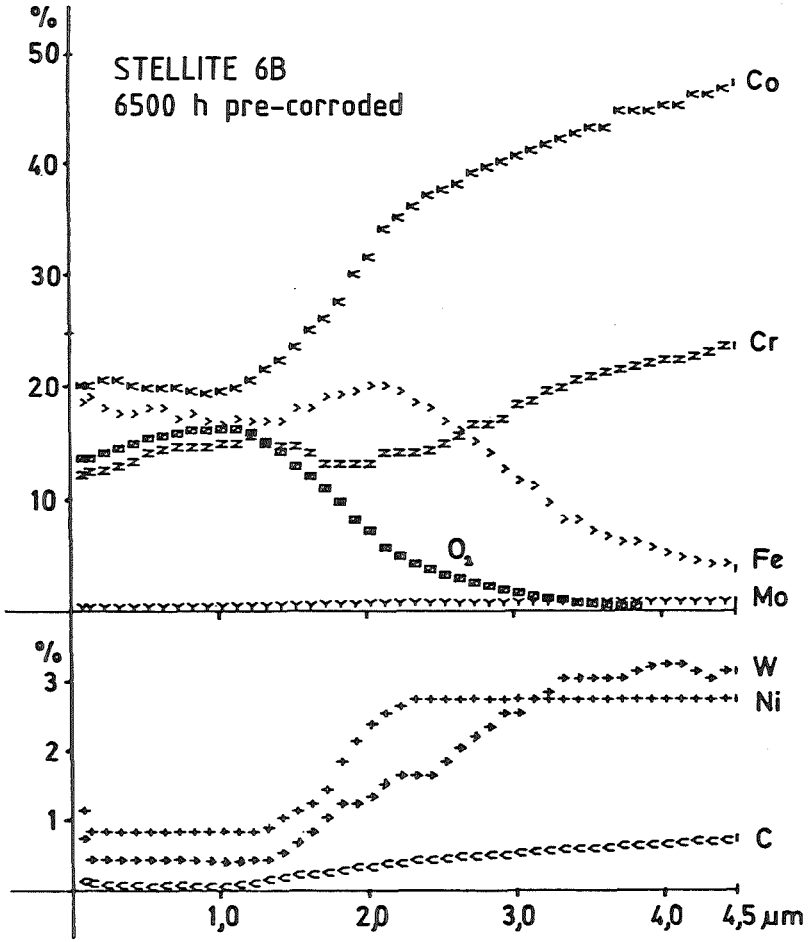

Fig. A 14 AES-Diagram of Stellite 6 H

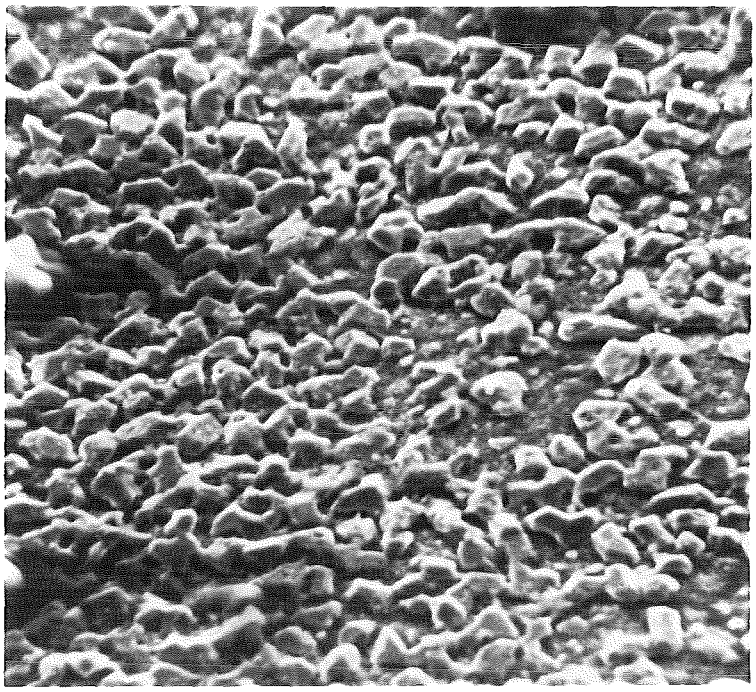

1000 x

Fig. A 15 Stellite 6 B surface after 6500 h of precorrosion (873 K)

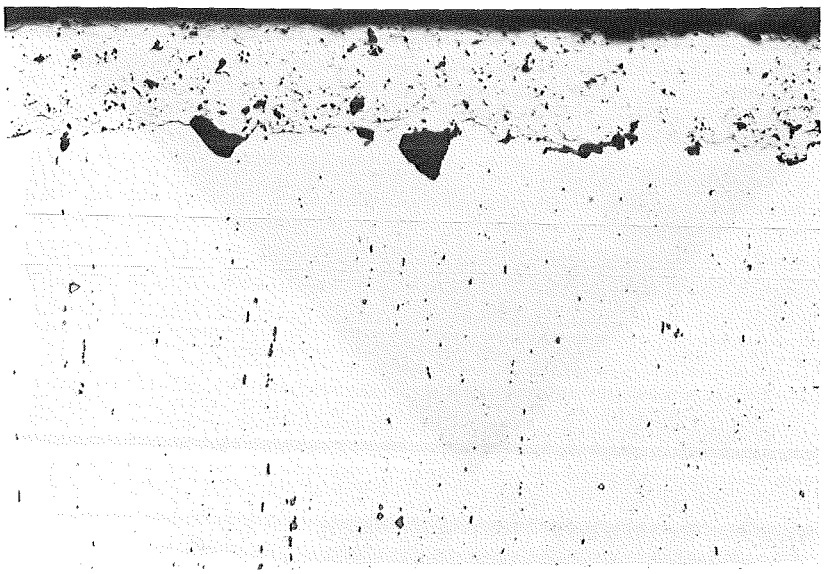

Fig. A 16 Micro structure of a Tribaloy 700 coating on Steel 1.4961

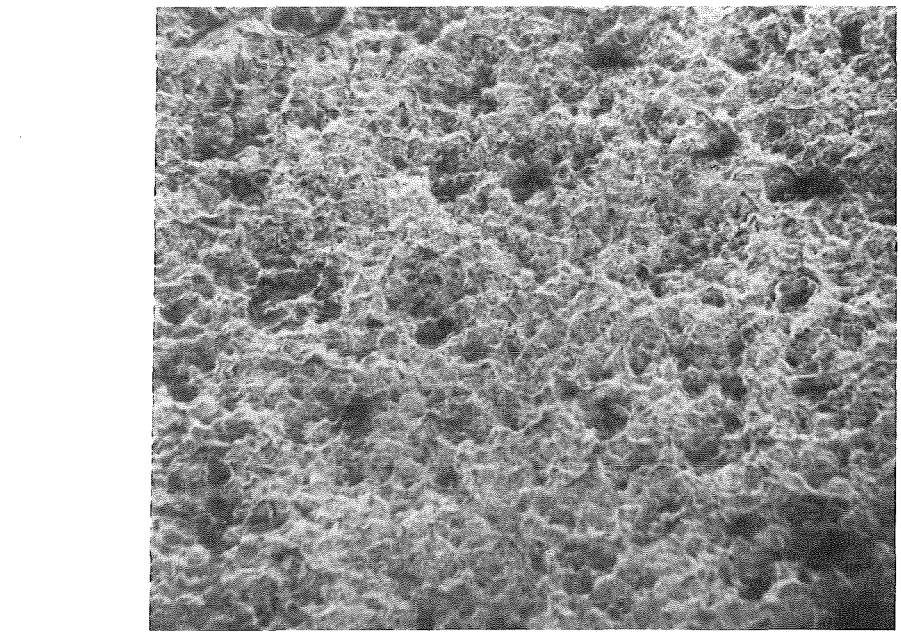

A 17 a
500 x

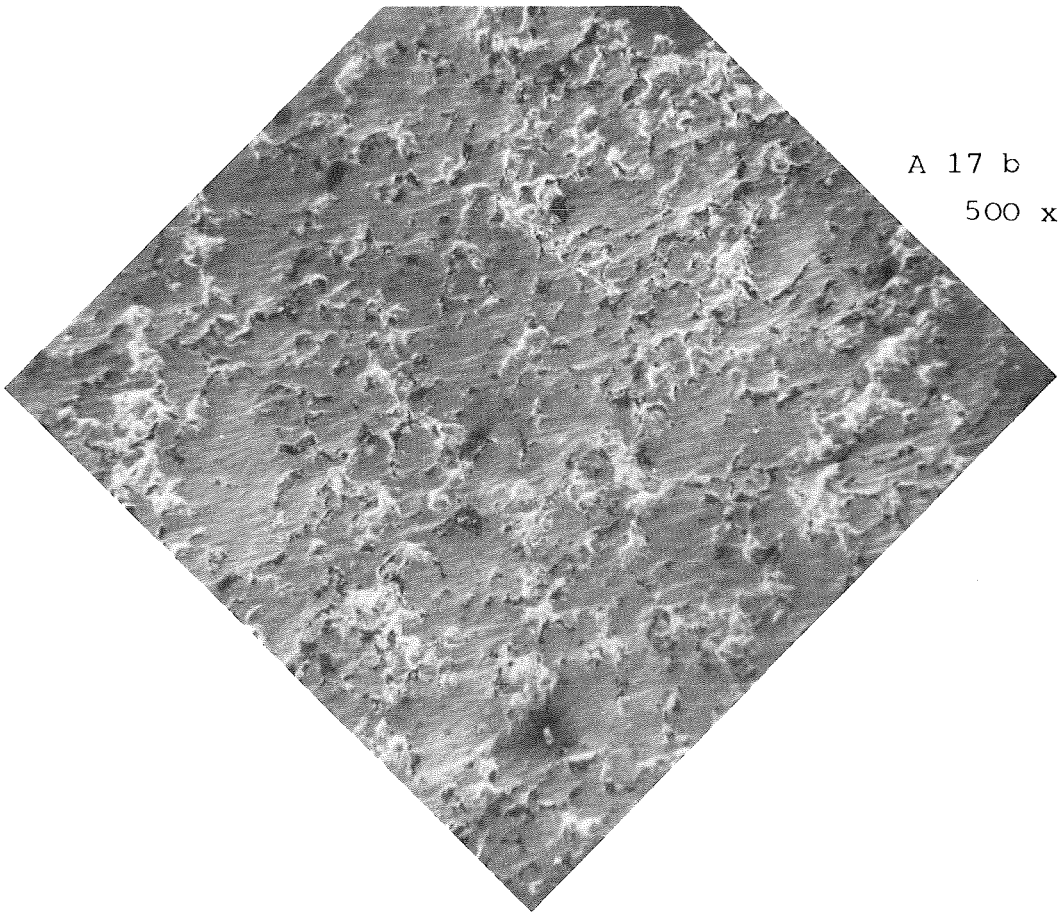

A 17 b
500 x

Fig. A 17 Tribaloy 700 surface
(a) D-gun coated (as received)
(b) after brush finish

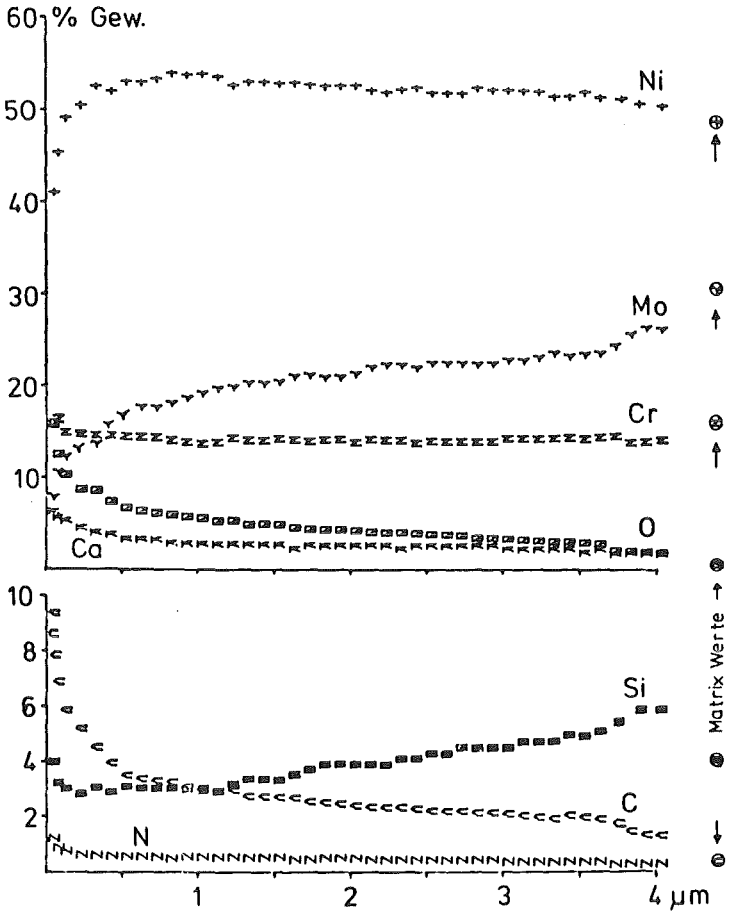

Fig. A 18 TRIBALOY 700 AES-Diagram
(as received)

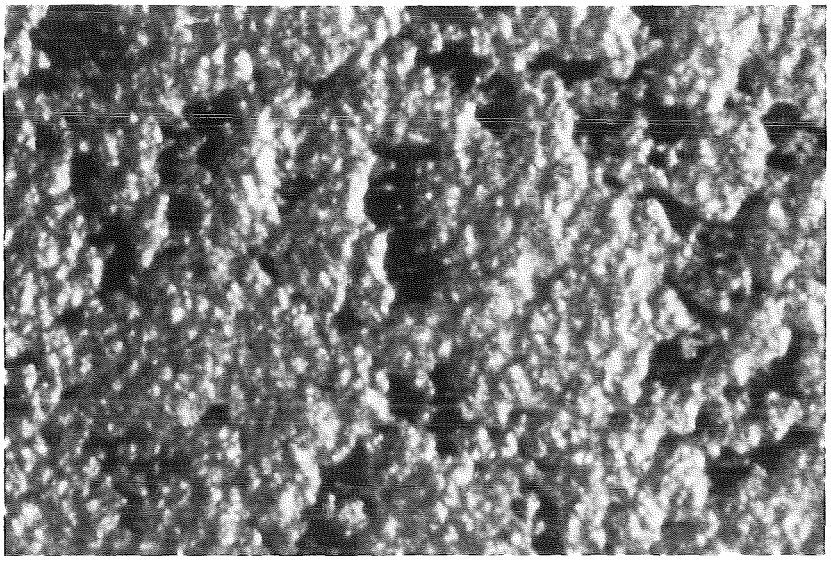

Fig. A 21 Brush finished surface of an LC-1 H coating

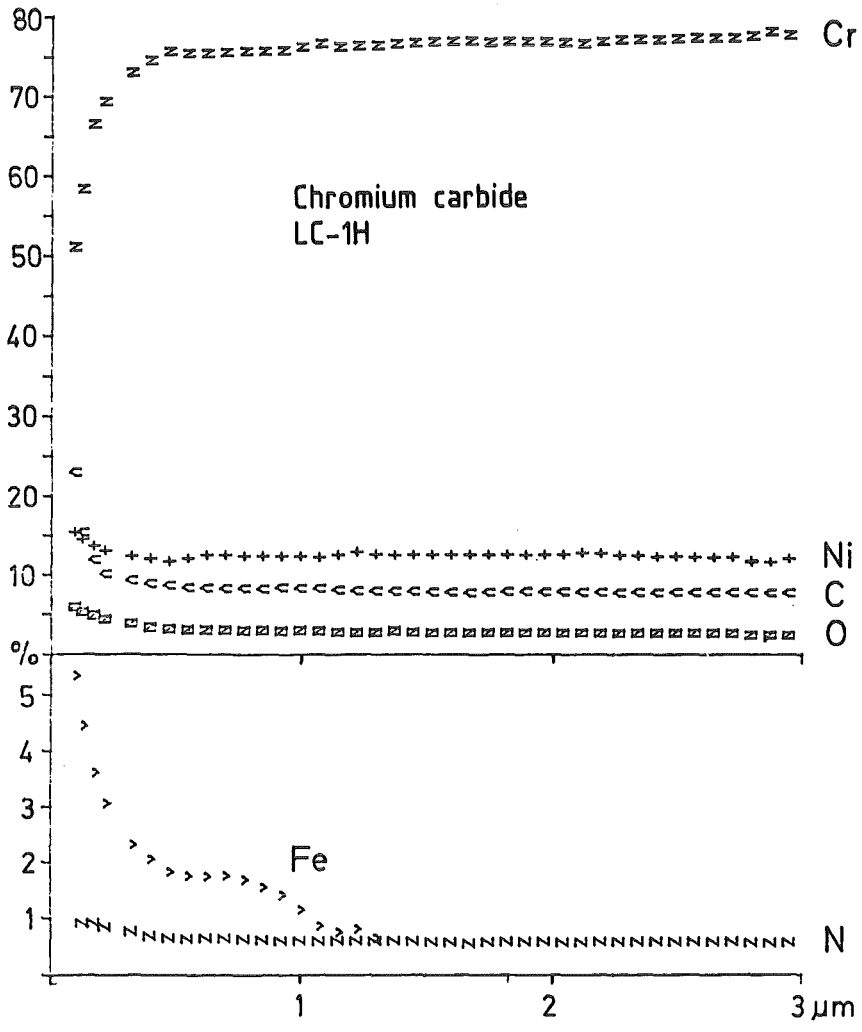

Fig. A 22 AES diagram of an LC-1 H coating
(brush finished)